

Time-averaging and nonergodicity of reset geometric Brownian motion with driftDeepak Vinod ^{1,*} Andrey G. Cherstvy ^{1,2,†} Ralf Metzler ^{1,‡} and Igor M. Sokolov ^{2,3,§}¹*Institute for Physics & Astronomy, University of Potsdam, Karl-Liebknecht-Straße 24/25, 14476 Potsdam-Golm, Germany*²*Institut für Physik, Humboldt-Universität zu Berlin, Newtonstraße 15, 12489 Berlin, Germany*³*IRIS Adlershof, Zum Großen Windkanal 6, 12489 Berlin, Germany*

(Received 18 April 2022; accepted 9 August 2022; published 29 September 2022)

How do near-bankruptcy events in the past affect the dynamics of stock-market prices in the future? Specifically, what are the long-time properties of a time-local exponential growth of stock-market prices under the influence of stochastically occurring economic crashes? Here, we derive the ensemble- and time-averaged properties of the respective “economic” or geometric Brownian motion (GBM) with a nonzero drift exposed to a Poissonian constant-rate price-restarting process of “resetting.” We examine—based both on thorough analytical calculations and on findings from systematic stochastic computer simulations—the general situation of reset GBM with a nonzero [positive] drift and for all special cases emerging for varying parameters of drift, volatility, and reset rate in the model. We derive and summarize all short- and long-time dependencies for the mean-squared displacement (MSD), the variance, and the mean time-averaged MSD (TAMSD) of the process of Poisson-reset GBM under the conditions of both rare and frequent resetting. We consider three main regions of model parameters and categorize the crossovers between different functional behaviors of the statistical quantifiers of this process. The analytical relations are fully supported by the results of computer simulations. In particular, we obtain that Poisson-reset GBM is a nonergodic stochastic process, with generally $\text{MSD}(\Delta) \neq \text{TAMSD}(\Delta)$ and $\text{Variance}(\Delta) \neq \text{TAMSD}(\Delta)$ at short lag times Δ and for long trajectory lengths T . We investigate the behavior of the ergodicity-breaking parameter in each of the three regions of parameters and examine its dependence on the rate of reset at $\Delta/T \ll 1$. Applications of these theoretical results to the analysis of prices of reset-containing options are pertinent.

DOI: [10.1103/PhysRevE.106.034137](https://doi.org/10.1103/PhysRevE.106.034137)**I. INTRODUCTION**

The introduction of this elaborate study is structured as follows. We start with a motivation for applying multiplicative exponentially growing processes in the presence of resetting for pricing of certain jump-containing options in Sec. **IA**. We continue by presenting an overview of (both the standard recent and some relevant older) stochastic-resetting-devoted studies for both arithmetic and multiplicative processes as well as by overviewing some reset-containing physical phenomena in Sec. **IB**. In Sec. **IC** we discuss shortly the aspect of ergodicity in the standard sense of the equivalence of the ensemble and time averages, our main tools in the following analysis. Finally, in Sec. **ID** we present the detailed sectioned plan of the whole paper. This study extends and generalizes the results of our recent brief communication [1] to reset geometric Brownian motion (GBM) with a nonzero drift.

A. Path-dependent and reset options

In contrast to standard path-independent options, the prices of some “exotic” options innately depend on their actual path

being, thus, inherently non-Markovian. The prices of such lookback-, barrier-, double-barrier-, reset-, and range-type options [2–26] are sensitive, e.g., to “extreme values” of the underlying asset and can depend on minimal and maximal prices in the past (for lookback- and barrier-type options), on being in certain ranges at certain preset time instances (for discrete-type path-dependent options), on the entire history of a time series (for continuous-type options), as well as on other path-dependent characteristics (such as, e.g., certain moving averages or preset thresholds).

The two most popular path-dependent options are the lookback- and barrier-type options. The owner of a lookback option, e.g., has the right to buy a given asset at a minimum price it assumes over a certain preset period of time. For a barrier-type option, the payoff at expiration varies depending on whether or not the asset price has crossed a certain preset “barrier level” during its life-time [16]. For so-called “continuously deactivating” double-barrier options, the option “vanishes” once the underlying asset price crosses a preset upper or lower barrier [15]. For a knock-out European call option, e.g., the option behaves as a standard vanilla European call unless a preset upper barrier is crossed: the option “knocks-out” after that and the contract is zero. For such options, the derivative prices can be adjusted or partially “reset” either on specific dates, regularly, or upon exceeding certain threshold levels. Numerous modifications exist in definitions (including options on options, etc.), data-sampling frequencies, and execution strategies of exotic path-dependent options.

*ugdeepakv@gmail.com

†a.cherstvy@gmail.com

‡rmetzler@uni-potsdam.de

§igor.sokolov@physik.hu-berlin.de

The principles of price formation and new nontrivial features of such options necessitate “correction” of the available option-pricing mathematical models [2,27–34], with their predictions being based on the omnipresent multiplicative-noise GBM [30]. A mixture of continuous and jump processes were historically proposed [34–36] in some jump-diffusion models to compute the prices of certain path-dependent options, “sowing a seed” for the “modern” stochastic-resetting approaches. These models were developed for normal and later for double-exponential [17,19] distributions of price jumps [37,38]. For the latter, the market’s reaction to high-impact good or bad news—arriving as a Poissonian process and representing various types of uncertainties in the market behavior—yields a random response of the asset price [prescribed by the jump-size distribution] and also enables the analytical solution for lookback- and barrier-type options [17].

B. Examples of processes with resetting dynamics

These quick option-price adjustments for reset options are reminiscent of general approaches of resetting employed for various stochastic processes, including the multiplicative ones [39–43]. The subject of stochastic resetting has recently experienced a tsunami of new—both theoretical and experimental—developments (see, i.a., Refs. [1,43–104] for *classical* formulations and Refs. [57,105–110] for much-less studied stochastically reset *quantum* systems). Not to be repetitive here, we refer the reader to Ref. [71] where a number of physical and mathematical phenomena involving abrupt jumps addressable with resetting approaches were overviewed, with explicit literature sources. The excellent recent overview on stochastic resetting (including applications) was also presented in Ref. [57]. Rests, in addition to resets, were also considered in the literature [111].

From the “hard-reset” perspective, we can add here, e.g., revolutions and coup/Putsch-like changes of governing regimes exemplifying possible “resetting events” in political-societal sciences. From a “soft-reset” perspective, the so-called Kondratieff’s “K-waves” [112,113] characterizing long global business-activity cycles—with a period of ≈ 50 years, possibly with a rich substructure of higher harmonics [114]—can be mentioned. These waves reflect the level of technological innovations and of the (macro-)economic growth correlated therewith with the economic crises [115] and depression phases clustering at the downswing of the patterns of K-waves.

For selecting an optimal portfolio [116–118] containing multiple differently performing options or risky stocks, the tasks of performance optimization—aimed at achieving certain profit levels and goals—would involve selling and buying individual positions [119], acting as reset events for the whole set of such co-evolving GBM-like processes in a given portfolio.

As to reset-GBM processes specifically, (i) the accumulation of the mean wealth of a person in a society or an ensemble of “renewable” (retiring and dying [120]) individuals, (ii) the dynamics of stock-market prices of an “overheated” company collapsing at a “bubble”-point, (iii) the growth dynamics of a bacterial colony—exponentially proliferating provided the

abundance of necessary resources [121,122]—being shock-treated by antibiotics [123] can be mentioned as examples, as well as (iv) an uncontrolled growth of malignant tumors treated by anticancer drugs [124], and (v) of lipid-membrane-enveloped corona-like viruses after being treated by high-% alcohol mixtures [125].¹

We stress that the concept of “stochastic resetting” used in the statistical-physics literature [42] has similarities to some random-process approaches which are considerably older than one decade. Time series of random Poisson-distributed “events occurring haphazardly in space or time” were, e.g., considered already by Cox [128].² Intimately related to the problem of Poissonian stochastic-resetting setups, as emphasized in Ref. [130], and to reset GBM specifically, the established theories of catastrophe- or annihilation-like events [130–147]—much less-noticed by the community of contemporary “reset physicists”—were considered in the models of population extinction, with a Poissonian “killing” process being often implemented (with later resurrection of the population). The catastrophic disasters or “resets” distributed according to the paradigmatic Poissonian law were considered in a large corpus of mathematical papers, where, i.a., the explicit probability laws of the form (23) presented below were derived (see, e.g., Eq. (3) in Ref. [141], Eq. (2.2) in Ref. [144], and Eq. (6) in Ref. [130]). The time of population extinction for birth-death processes with catastrophes were found [66,135,136,141]. For example, the scenarios with random sudden population reductions with the magnitudes scaling with the process value itself [132,133,140], with the rate of catastrophes being proportional to the existing population [135,137,138], and for arbitrary distributions of the catastrophe magnitudes [135] were examined.

Specifically, the phenomenon of population extinction within a deterministic model of exponential growth caused by demographic variability, environmental stochasticity [148], and random catastrophes were developed [140]. The risks of population extinction in dependence on the population-growth rate as well as on the magnitude and frequency of catastrophic events were examined. As in many “contemporary” stochastic-resetting studies, a Poissonian process was often

¹Additional, broader-scope examples of processes involving a snowball-like, exponential growth and sudden termination are (i) the accumulation of the number of abstract submissions for participating in a conference as the deadline is approaching (acting as a reset point), (ii) increasing vibrations and audible frequency of the Euler’s disk prior to its stoppage [126], and (iii) the accumulation of the induced electric charges in droplets—created by the Rayleigh-Plateau instability—in the Kelvin’s water-dropping hydroelectric generator [127]. For the latter, the charge growth is exponential-like due to a self-amplifying feedback loop, with sparking events acting as [quasiperiodic] resets.

²The concept of a nonlocal—as compared to a blind and local types of search—and various approaches to optimization or extremization of multiparametric mathematical problems based on certain “learning algorithms” were developed in the Soviet mathematical literature by Gel’fand *et al.* already in the 1960s [129]. These latter approaches employ adaptively and jump-wise chosen starting positions for the facilitation of and time-reduction in gradient-based search problems.

used to govern the occurrence of catastrophes in these models, with a constant fraction of population being destroyed by each disaster [140].

Clear parallels exist between the models of exponential growth in the population dynamics and the GBM-based models of price growth in financial economics. For instance, the average time until extinction of a population because of catastrophic events is equivalent to the average survival time of a company prior to a bankruptcy event [149], occurring, i.a., because of financial crashes.

C. Ensemble- and time-based-averaging: Concept of ergodicity

For a time series of an arbitrary continuous stochastic process, $S(t)$, for a large ensemble of statistically indistinguishable trajectories the second moment is expressed through the probability-density function (PDF) $P(S, t)$ as the statistical average

$$\langle S^2(t) \rangle = \int S^2 P(S, t) dS, \quad (1)$$

characterizing the mean-squared displacement (MSD). As a complementary time-averaging-based definition, the single-trajectory-based quantifier of the time-averaged MSD (TAMSD, a random variable by itself) is commonly computed as [150–153]

$$\overline{\delta^2(\Delta)} = \frac{1}{T - \Delta} \int_0^{T-\Delta} [S(t + \Delta) - S(t)]^2 dt. \quad (2)$$

The TAMSD is, thus, defined as the average over the squared increments of a process along a trajectory. Here, Δ is the lag time and T is the total length of the trajectory. Hereafter, the angular brackets denote averaging over realizations of noise [driving the process $S(t)$], whereas the overline over a quantity indicates time-averaging in the sense (2). Further averaging over N statistically equivalent and independent TAMSD realizations of a process yields the mean TAMSD [151, 152],

$$\langle \overline{\delta^2(\Delta)} \rangle = \frac{1}{N} \sum_{i=1}^N \overline{\delta_i^2(\Delta)}. \quad (3)$$

We call below a diffusion process ergodic—we refer the reader here to the original historical/classical studies on ergodicity [154–159] and to some recent developments, reviews and viewpoints [151, 152, 160–163]—if (for the vanishing first moment and zero initial position) the MSD and the mean TAMSD are equivalent in the limit of short lag times and long trajectories, $\Delta/T \ll 1$, namely,

$$\text{MSD}(\Delta) \approx \text{TAMSD}(\Delta). \quad (4)$$

D. Plan of the paper

The rest of the paper is organized in the following manner. We start via presenting the known results for nonreset GBM in Sec. II. Then we move to the results for the PDF in Sec. III, the MSD and variance in Sec. IV, and the mean TAMSD in Sec. IV D for a random walk of Poisson-reset GBM. The findings of stochastic simulations (with the numerical algorithm described in Sec. V) are favorably consistent with the theoretical expectations, as we demonstrate for three different

domains/regions of the model parameters. The latter are the drift magnitude μ , the strength of randomness σ^2 , and the reset rate r . The functional regimes and the asymptotic behaviors of the statistical quantifiers are thoroughly described in Sec. VI, namely, in Secs. VI A, VI B, VI C, and VI D for the first moment, second moment, variance, and TAMSD, correspondingly. The auxiliary Tables I, II, III, and IV presenting the main asymptotic behaviors can be found in Sec. VI E. A comparative analysis of the main results of Ref. [1] for a simpler process of drift-free reset GBM and a number of new results of the current study are summarized in Table V. The nonergodicity is discussed in Secs. VII A and VII B. The discussion and conclusions are presented in Sec. VII. The details of the TAMSD derivations—following and generalizing our short study [1] using the framework of Ref. [45]—are presented in Appendix A and supplementary Figs. 11–22 are collected in Appendix B.

II. RESULTS FOR GBM

The multiplicative-noise stochastic differential equation for standard or nonreset GBM, denoted as $X(t)$ below, is given by

$$dX(t) = \mu X(t) dt + \sigma X(t) dW(t), \quad (5)$$

where μ and σ are the constant parameters of drift and volatility.³ The increments of the Wiener process, $dW(t)$, represent random realizations of white Gaussian zero-mean noise. We consider Eq. (5) in the Itô representation [182] that gives rise to exponentially growing GBM of the form (after using Itô's lemma) [1, 183, 184]

$$X(t) = X_0 e^{(\mu - \sigma^2/2)t + \sigma W(t)}. \quad (6)$$

Here, the initial value of the process defines the prefactor of the entire price variation, $X_0 = X(0) > 0$.

The log-normal PDF of price fluctuations associated with GBM has the form

$$P(X, t) = \frac{\exp\{-(2\sigma^2 t)^{-1} [\log(X/X_0) - (\mu - \sigma^2/2)t]^2\}}{\sqrt{2\pi\sigma^2 t X^2}}. \quad (7)$$

This expression gives for the first and second moments as well as for the variance of GBM the corresponding results

$$\langle X(t) \rangle = X_0 e^{\mu t}, \quad (8)$$

$$\langle X^2(t) \rangle = X_0^2 e^{(2\mu + \sigma^2)t}, \quad (9)$$

³Numerous generalizations of Eq. (5) with, e.g., fluctuating and variable volatilities exist in the financial-mathematics literature, including those using the concept of “stochastic volatility” [143, 164–174] laying (yet again) the foundation of the “diffusing-diffusivity” approach “reincarnated” recently in the physics literature for the modified Langevin equation [175–178]. Note that similar mathematical “superstatistical” concepts of population-distribution parameters were also formerly utilized for modeling heterogeneous dispersion of animals to rationalize movement-ecology data (see, i.a., Refs. [179–181]). Note that certain models of optimal portfolios with a known diffusivity—but with unknown random drift coefficients—also exist [118].

and

$$\langle (X(t) - \langle X(t) \rangle)^2 \rangle = X_0^2 e^{2\mu t} (e^{\sigma^2 t} - 1). \quad (10)$$

For the multiplicative price dynamics governed by Eq. (5) the value of the process both at the initial time moment as well as after each resetting event should be positive.⁴ As a result of $S_0 \neq 0$, the second moment of the process is not exactly equal to the MSD defined as $\langle [S(t) - S_0]^2 \rangle$. As the first moments of both pure and reset GBM are also nonzero [and positively defined], we are also interested in the second central moment or the variance. For a standard exponentially growing GBM its leading-order long-time growth is the same for the second moment, MSD, and variance: it is defined by the exponential function with the largest growth rate, see below.

The mean TAMSD of GBM for the situation $\mu \neq 0$ —the general case considered below—is given by

$$\langle \overline{\delta^2(\Delta)} \rangle = \frac{X_0^2 (1 - 2e^{\mu\Delta} + e^{(\sigma^2 + 2\mu)\Delta})}{(T - \Delta)(\sigma^2 + 2\mu)} [e^{(\sigma^2 + 2\mu)(T - \Delta)} - 1] \quad (11)$$

and behaves at short lag times and for long trajectories as [1,183–185]

$$\langle \overline{\delta^2(\Delta)} \rangle \approx \langle X^2(T) \rangle \times \Delta/T \approx \langle (X(T) - \langle X(T) \rangle)^2 \rangle \times \Delta/T. \quad (12)$$

The mean TAMSD for GBM [1,183,185] and scaled GBM [184] were obtained recently.

The concepts of time-averaging and nonergodicity for the resetting dynamics were first applied by us to reset fractional Brownian motion (FBM) and heterogeneous-diffusion processes in Ref. [71]. The reader is also referred to our recent data-driven studies where the concepts of TAMSD and nonergodicity were first applied to the financial time series and GBM [183,185] and to drift-free GBM in the presence of Poisson resetting [1]. These studies formed the foundation for the current analysis. Some models of anomalous diffusion with drift [186] were recently considered in the literature [187–190], but—to the best of our knowledge—never in terms of both the MSD and the TAMSD for an exponentially growing process with drift and resetting, as we examine below for reset GBM with $\mu > 0$.

III. PDF OF RESET GBM

A. Derivation of the reset PDF

Our main focus here is to consider the process of GBM in the presence of constant-rate, Poissonian resetting, denoted as $S(t)$ below. For this simple and ubiquitously employed protocol of stochastic resetting, the waiting-time distribution between the consecutive resetting events is

⁴Only under this condition the so-called economic Brownian motion or GBM will enter the cycle of multiplying the already existing money. Starting with a zero initial capital cannot bring any profits. Note, however, that although negative prices *per se* sound irrational, these scenarios are not utterly impossible (as, e.g., the WTI crude-oil negative-price run in April 2020 triggered by the first lockdown during the current covid-19 pandemic).

exponential,

$$\psi(t) = re^{-rt}. \quad (13)$$

For the Poissonian resetting strategy, the average time between the recurrent events of resetting is the reciprocal rate of reset,

$$\langle t_{\text{reset}} \rangle = \int_0^\infty t' \psi(t') dt' = 1/r. \quad (14)$$

Under these conditions, an instantaneous price-reduction event or reset to a price value S_0 takes place with a constant rate r at each time-step, reminding thus a Sisyphus-type [82,191] random walk. We consider below the simplest scenario of a memoryless reset to a single position,

$$S_{\text{reset}} = S_0 = X_0. \quad (15)$$

This price level is set relatively small: such GBM interruptions are then associable with economic crashes [25,115,192] occurring at the time instances of resets.⁵

The first-principle derivation of the well-known [42,57] Eq. (20) is presented below mainly for pedagogical purposes, completing the presentation and also defining the scope for some later derivations. A stochastic process with constant-rate resetting at each step goes back to S_0 with the probability $r\Delta t$ or proceeds forward unchanged (according to its predefined rules) with the probability $(1 - r\Delta t)$, namely,

$$S(t_{n+1}) = \begin{cases} S_0, & p_{\text{reset}} = r\Delta t, \\ S(t_n) + \Delta S(t_n), & p_{\text{nonreset}} = 1 - r\Delta t. \end{cases} \quad (16)$$

Let $P_0(S, t)$ be the PDF of the nonreset parent process with a starting point S_0 at time $t = 0$. To derive the PDF of the reset process at time t , we look at different classes of trajectories for which the resetting events occur at different times. First, the trajectories for which no reset event occurred within the time interval $[0, t]$ give the PDF contribution

$$F(s, t) = \lim_{n \rightarrow \infty} P_0(s, t) (1 - rt/n)^n = P_0(s, t) e^{-rt}. \quad (17)$$

Here, n is the number of steps of the walk. Next, we consider the trajectories where the last reset event occurs at $(T - \tau)$ and no later; no reset events occur in the remaining time τ .

⁵Note that numerous modifications of this simplistic setup for, e.g., (i) distributed reset positions $P(S_{\text{reset}})$ (like in the jump-diffusion models [17]), (ii) a discrete set of different $S_{\text{reset},i}$ values with respective occurrence probabilities [39], (iii) a time-variable reset position $S_0(t)$, (iv) noninstantaneous or “soft” return events [62,88,94,101] according to a certain law (constant velocity, constant acceleration, etc.), (v) various types of reset strategies (including those with nonconstant and time-varying reset rates), (vi) relocation of the walker to certain path-history-dependent positions (such as, e.g., in the preferential-relocation models [193]), (vii) returns to the so-far achieved maximum position [194], or (viii) the construction of certain “elephant”-like [195–197] random walks) are possible. Models of resetting to multiple distributed prices $p(S_0)$ can be important for modeling of real reset options and also for some models of wealth- and tax-reallocation-dynamics in a collective of individuals, known also to be describable by a modified GBM [102,198–200].

Their contribution to the PDF is

$$F(s, \tau) = P_0(s, \tau) \lim_{\Delta\tau \rightarrow 0} r\Delta\tau(1 - r\Delta\tau)^{\frac{\tau}{\Delta\tau}}. \quad (18)$$

To obtain the entire PDF, we account for all such trajectories with different times of the last reset, $\tau \in [0, t]$, so that

$$\begin{aligned} \int_0^t F(s, \tau) d\tau &= \int_0^t P_0(s, \tau) \lim_{\Delta\tau \rightarrow 0} r\Delta\tau(1 - r\Delta\tau)^{\frac{\tau}{\Delta\tau}} d\tau \\ &= \int_0^t P_0(s, \tau) r e^{-r\tau} d\tau. \end{aligned} \quad (19)$$

Adding (17) and (19) yields the PDF of the reset process in the well-known form [1,42,57,60,71]

$$P(s, t) = P_0(s, t)e^{-rt} + \int_0^t P_0(s, \tau) r e^{-r\tau} d\tau. \quad (20)$$

The “mapping” of the nonreset PDF to the reset PDF (20) can be used to find expectation values: for an arbitrary function of a reset random variable $f(s)$ (with no explicit time dependence) the mean can be written as

$$\langle f(S; t) \rangle = \int f(s) P(s, t) ds. \quad (21)$$

Substituting here the PDF expression (20) yields

$$\begin{aligned} \langle f(S; t) \rangle &= e^{-rt} \int f(s) P_0(s, t) ds \\ &+ \int ds \int_0^t f(s) P_0(s, \tau) r e^{-r\tau} d\tau. \end{aligned} \quad (22)$$

Exchanging the order of integration in the second term—for reasonably well-behaving functions—and realizing that $\int f(s) P_0(s, t) ds$ is the expectation value with respect to the nonreset variable $X(t)$ —we obtain

$$\langle f(S; t) \rangle = e^{-rt} \langle f(X; t) \rangle + \int_0^t \langle f(X; \tau) \rangle r e^{-r\tau} d\tau. \quad (23)$$

B. Long-time PDF: The NESS

The general expression for the PDF of reset GBM is obtained below. We are interested in obtaining the PDFs under certain special conditions (called below the first, the second, and the third regime of behavior of important quantifiers), and, in particular, in the long-time limit of a frequently reset GBM where the so-called nonequilibrium stationary state (NESS) can realize. In the NESS—where the PDF is stationary, but the probability current is still nonzero [57]—the PDF is obtainable via the mapping (20), where the PDF P_0 of nonreset GBM is given by Eq. (7), namely,

$$P(S) = \lim_{t \rightarrow \infty} \int_0^t P_0(S, \tau) r e^{-r\tau} d\tau. \quad (24)$$

This integral can be computed analytically for $\{\sigma, r\} > 0$ to yield the power-law steady-state PDF,

$$P_{\mp}(S) = \frac{r(S/S_0)^{\mp\sqrt{(\mu-\sigma^2/2)^2+2r\sigma^2/\sigma^2-3/2+\mu/\sigma^2}}}{S_0\sigma\sqrt{(\mu-\sigma^2/2)^2+2r\sigma^2}}, \quad (25)$$

where the negative and positive signs correspond to the case $S > S_0$ and $S < S_0$, respectively. The transition between these

two different PDF forms gives rise to a sharp cusp at $S = S_0$. Note that Eq. (25) corrects erroneous expressions for the PDFs of reset GBM given by Eq. (B3) of Ref. [73] and Eq. (7) of Ref. [74].

The values of the first moment, the second moment, and the variance obtained with the NESS-related PDF (25) are the plateaus given by Eqs. (100), (116), and (140) below, as expected. The condition for the existence of a nondivergent p th moment of the PDF (25)—see also Refs. [73,201]—defines the frequency of necessary resetting events as

$$r > p(\mu - \sigma^2/2) + p^2\sigma^2/2. \quad (26)$$

Consistent with our physical intuition, the higher the order p of the moment is, the larger the rate of resetting r should be to ensure a stagnating NESS-related plateau for the p th moment. The strong- or frequent-resetting region of parameters is realized for sufficiently large r magnitudes, such that all (relevant) moments saturate to a stationary value. The critical reset rates following from Eq. (26) for $p = 1$ and $p = 2$ define the boundaries of the respective parameter regions as

$$r = \mu \quad (27)$$

and

$$r = 2\mu + \sigma^2. \quad (28)$$

For the first region, at $\mu = r$, a normalized PDF can be obtained from the general expression (25), but already the first moment—and, naturally, all higher moments—do not converge, as Eqs. (86) and (102) indicate. This fact—again, consistent with the condition (26)—indicates that the NESS—typically characterized by the plateaus of all (relevant) moments and time-independent, steady-state PDF—does not exist in this region of model parameters. The NESS is not expected when the moments do not converge at long times.

For $\sigma^2 + 2\mu = r$ —the condition of the second region of model parameters—the PDF (25) simplifies to

$$P(S) = \frac{2r}{S_0(r + 2\sigma^2)} \begin{cases} (S/S_0)^{r/\sigma^2-1}, & S < S_0, \\ (S/S_0)^{-3}, & S > S_0, \end{cases} \quad (29)$$

that produces a plateau for the first moment with the height (90) but gives a divergent second moment and variance, consistent with expression (26), indicating a partial NESS in this region as far as the first two moments are considered.

For the third—or the general—region of model parameters the reset rate should exceed $r > 2\mu + \sigma^2$ in order for the first and second moments to converge. Such plateau-like behavior of these moments then ensures the existence of the NESS in this case. For the situations when the moments of higher order (such as skewness and kurtosis) matter, the reset rate should exceed the thresholds given by the $p = 3$ and $p = 4$ solutions of Eq. (26), respectively. The NESS is then realized up to the 4th order in the moment-containing observables in displacement, characterizing the stochastic dynamics.

In the absence of drift, from Eq. (25) we recover the PDF result of Ref. [1],

$$P(S) = \frac{2r(S/S_0)^{\mp\sqrt{\sigma^2+8r}/(2\sigma)-3/2}}{S_0\sigma\sqrt{\sigma^2+8r}}, \quad (30)$$

that produces the expressions (34), (38), and (64) for the first moment, the second moment, and the variance in the NESS for a drift-free reset GBM.

To shorten the paper, we skip here the theory-versus-simulations comparison for the PDFs of reset GBM (for the general and each of the special cases or region of parameters). We refer the interested reader to the quantitative PDF analysis performed for the case of drift-free reset GBM in Ref. [1].

IV. MOMENTS, VARIANCE, AND TAMSD OF RESET GBM

A. First moment

The first moment of reset GBM is found from Eq. (23) as

$$\langle S(t) \rangle = e^{-rt} \langle X(t) \rangle + \int_0^t d\tau r e^{-r\tau} \langle X(\tau) \rangle, \quad (31)$$

where $\langle X(t) \rangle$ is the first moment of GBM (8), that gives

$$\langle S(t) \rangle = S_0 \left(e^{-rt} e^{\mu t} + \int_0^t d\tau r e^{-r\tau} e^{\mu\tau} \right). \quad (32)$$

Two region of parameters in expression (32) are possible, namely, $\mu = r$ and $\mu \neq r$. Performing the integration in both cases yields the general expression for the first moment

$$\langle S(t) \rangle = S_0 \begin{cases} 1 + rt, & \mu = r, \\ \frac{2r + (\sigma^2 - r)e^{-\frac{(\sigma^2 + r)t}}}{\sigma^2 + r}, & \sigma^2 + 2\mu = r, \\ \frac{\mu e^{(\mu - r)t} - r}{\mu - r}, & \sigma^2 + 2\mu \neq r, \mu \neq r. \end{cases} \quad (33)$$

Substituting $\mu = 0$ in the last, general expression of Eq. (33) yields

$$\langle S(t) \rangle = S_0. \quad (34)$$

As expected, at $r = 0$ from Eq. (33) the first moment of nonreset GBM (8) is obtained.

B. Second moment

Similarly, the calculation of the second moment—using the second moment of nonreset GBM (9) and Eq. (23)—yields

$$\langle S^2(t) \rangle = S_0^2 e^{-rt} e^{(\sigma^2 + 2\mu)t} + S_0^2 \int_0^t d\tau r e^{-r\tau} e^{(\sigma^2 + 2\mu)\tau}. \quad (35)$$

Here, again, two possible—but different—region of model parameters arise, namely, $\sigma^2 + 2\mu = r$ and $\sigma^2 + 2\mu \neq r$. Calculating the elementary integral in Eq. (35) we get

$$\langle S^2(t) \rangle = S_0^2 \begin{cases} \frac{(\sigma^2 + 2r)e^{(\sigma^2 + r)t} - r}{\sigma^2 + r}, & \mu = r, \\ 1 + rt, & \sigma^2 + 2\mu = r, \\ \frac{(\sigma^2 + 2\mu)e^{(\sigma^2 + 2\mu - r)t} - r}{\sigma^2 + 2\mu - r}, & \sigma^2 + 2\mu \neq r, \mu \neq r. \end{cases} \quad (36)$$

Generally, when $\sigma^2 + 2\mu \neq r$, substituting in the last line of this expression $\mu = 0$ gives the special case of Ref. [1],

$$\langle S^2(t) \rangle = S_0^2 \frac{\sigma^2 e^{(\sigma^2 - r)t} - r}{\sigma^2 - r}. \quad (37)$$

In the limit of frequent resetting $r \gg \sigma^2$ and at long times expression (37) yields the plateau value

$$\langle S^2(t) \rangle = S_0^2 r / (r - \sigma^2). \quad (38)$$

At $r = 0$, when the resetting process is switched off, as expected, from the first expression of Eq. (36) we recover Eq. (9) for nonreset drift-free GBM. For the first moment (33) and the second moment (36) we added for completeness the expressions for $\sigma^2 + 2\mu = r$ and $\mu = r$, used later as separate branches of the asymptotes for the variance and mean TAMSD.

C. Variance

To compute the variance of reset GBM, generally given by

$$(\langle S(t) \rangle - \langle S(t) \rangle)^2 = \langle S^2(t) \rangle - \langle S(t) \rangle^2, \quad (39)$$

we use the first and second moments from Eqs. (33) and (36). Interestingly, three mutually exclusive regions of parameters arise from combining the previous parameter regimes [for the case of positive drift, $\mu > 0$]. The first one is $\mu = r$ (which implies $\sigma^2 + 2\mu$ is not equal to r), the second one is $\sigma^2 + 2\mu = r$ (which implies μ is not equal to r), and the third one is $\sigma^2 + 2\mu \neq r$ and $\mu \neq r$. The variance of reset GBM in each of these three regions of model parameters is

$$\begin{aligned} & \langle (S(t) - \langle S(t) \rangle)^2 \rangle \\ &= S_0^2 \begin{cases} \frac{(\sigma^2 + 2r)e^{(\sigma^2 + r)t} - r}{\sigma^2 + r} - [1 + rt]^2, & \mu = r, \\ 1 + rt - \left[\frac{\mu e^{(\mu - r)t} - r}{\mu - r} \right]^2, & \sigma^2 + 2\mu = r, \\ \frac{(\sigma^2 + 2\mu)e^{(\sigma^2 + 2\mu - r)t} - r}{\sigma^2 + 2\mu - r} - \left[\frac{\mu e^{(\mu - r)t} - r}{\mu - r} \right]^2, & \sigma^2 + 2\mu \neq r, \mu \neq r. \end{cases} \end{aligned} \quad (40)$$

For the case $\sigma^2 + 2\mu \neq r$ and $\mu \neq r$, substituting $\mu = 0$, we get a simple expression [1],

$$\langle (S(t) - \langle S(t) \rangle)^2 \rangle = S_0^2 \frac{\sigma^2}{\sigma^2 - r} (e^{(\sigma^2 - r)t} - 1). \quad (41)$$

As expected, setting here $r = 0$ produces the standard result for nonreset GBM, Eq. (10).

D. TAMSD

The splitting procedure of the TAMSD of reset GBM is given by Eq. (A25), with the general analytical results for $\langle \delta^2(\Delta) \rangle_\mu$ and $\langle \delta^2(\Delta) \rangle_{\sigma^2 + 2\mu}$ given by expressions (A23) and (A24), respectively.

1. Regime 1: Region of parameters $\mu = r$

When $\mu = r$, combining the second expression of $\langle \delta^2(\Delta) \rangle_\mu$ and the first of $\langle \delta^2(\Delta) \rangle_{\sigma^2 + 2\mu}$ from Eqs. (A23) and

(A24), respectively, that after setting $\mu - r = 0$ yields

$$\overline{\langle \delta^2(\Delta) \rangle} = S_0^2 \left\{ \frac{(\sigma^2 + 2r)(e^{(\sigma^2+r)\Delta} - 1)(e^{(\sigma^2+r)(T-\Delta)} - 1)}{(\sigma^2 + r)^2(T - \Delta)} - 2r\Delta \left[1 + r \frac{(T - \Delta)}{2} \right] \right\}. \tag{42}$$

If we set $\mu = r = 0$, then expression (42) simplifies into the mean TAMSD of nonreset drift-free GBM, namely,

$$\overline{\langle \delta^2(\Delta) \rangle} = S_0^2 \frac{(e^{\sigma^2\Delta} - 1)(e^{\sigma^2(T-\Delta)} - 1)}{\sigma^2(T - \Delta)}, \tag{43}$$

in agreement with Eq. (11) evaluated at $\mu = 0$.

2. Regime 2: Region of parameters $\sigma^2 + 2\mu = r$

When $\sigma^2 + 2\mu = r$, we use the first expression of $\overline{\langle \delta^2(\Delta) \rangle}_\mu$ and the second of $\overline{\langle \delta^2(\Delta) \rangle}_{\sigma^2+2\mu}$ from Eqs. (A23) and (A24), respectively, while setting $\sigma^2 + 2\mu - r = 0$ gives rise to the mean TAMSD of reset GBM in the form

$$\overline{\langle \delta^2(\Delta) \rangle} = S_0^2 \left\{ (2 + rT)(1 - e^{(\mu-r)\Delta}) + e^{(\mu-r)\Delta} r\Delta - 2(e^{(\mu-r)\Delta} - 1) \frac{r[\mu(e^{(\mu-r)(T-\Delta)} - 1) - r(\mu - r)(T - \Delta)]}{(\mu - r)^3(T - \Delta)} \right\}, \tag{44}$$

that for $\mu = 0$ simplifies to

$$\overline{\langle \delta^2(\Delta) \rangle} = S_0^2 r [T - (T - \Delta)e^{-r\Delta}]. \tag{45}$$

3. Regime 3: Region of parameters $\mu \neq r$ & $\sigma^2 + 2\mu \neq r$

In the most general scenario $\sigma^2 + 2\mu \neq r$ and $\mu \neq r$ and, consequently, we utilize the first expression of $\overline{\langle \delta^2(\Delta) \rangle}_\mu$ and the first expression of $\overline{\langle \delta^2(\Delta) \rangle}_{\sigma^2+2\mu}$ from Eqs. (A23) and (A24), correspondingly, to obtain the general expression for the mean TAMSD of reset GBM as

$$\overline{\langle \delta^2(\Delta) \rangle} = S_0^2 \left\{ \frac{(\sigma^2 + 2\mu)(1 + e^{(\sigma^2+2\mu-r)\Delta} - 2e^{(\mu-r)\Delta})(e^{(\sigma^2+2\mu-r)(T-\Delta)} - 1)}{(\sigma^2 + 2\mu - r)^2(T - \Delta)} + \frac{2r[e^{(\mu-r)\Delta} - 1]}{\sigma^2 + 2\mu - r} - 2(e^{(\mu-r)\Delta} - 1) \frac{r[\mu(e^{(\mu-r)(T-\Delta)} - 1) - r(\mu - r)(T - \Delta)]}{(\mu - r)^3(T - \Delta)} \right\}. \tag{46}$$

If we set $\mu = 0$, this turns into [1]

$$\overline{\langle \delta^2(\Delta) \rangle} = S_0^2 \left\{ \frac{1}{T - \Delta} \frac{\sigma^2}{(\sigma^2 - r)^2} [(1 + e^{(\sigma^2-r)\Delta} - 2e^{-r\Delta})(e^{(\sigma^2-r)(T-\Delta)} - 1)] - 2(1 - e^{-r\Delta}) \left(1 + \frac{r}{\sigma^2 - r} \right) \right\}, \tag{47}$$

that, in turn, after switching off the resetting process via setting $r = 0$ yields the TAMSD result for nonreset driftless GBM.

4. Joining different TAMSD regimes

To get the full expression for the mean TAMSD for reset GBM, we combine all the regimes from Eqs. (42), (44), and (46) to get the main analytical result of the current study in a rather sophisticated form, namely,

$$\overline{\langle \delta^2(\Delta) \rangle} = S_0^2 \begin{cases} \frac{(\sigma^2+2r)[e^{(\sigma^2+r)\Delta}-1][e^{(\sigma^2+r)(T-\Delta)}-1]}{(\sigma^2+r)^2(T-\Delta)} - 2r\Delta \left[1 + r \frac{(T-\Delta)}{2} \right], & \mu = r, \\ (2 + rT)(1 - e^{(\mu-r)\Delta}) + e^{(\mu-r)\Delta} r\Delta & \sigma^2 + 2\mu = r, \\ -2[e^{(\mu-r)\Delta} - 1] \frac{r[\mu(e^{(\mu-r)(T-\Delta)} - 1) - r(\mu - r)(T - \Delta)]}{(\mu - r)^3(T - \Delta)}, & \\ \frac{(\sigma^2+2\mu)[1+e^{(\sigma^2+2\mu-r)\Delta}-2e^{(\mu-r)\Delta}][e^{(\sigma^2+2\mu-r)(T-\Delta)}-1]}{(\sigma^2+2\mu-r)^2(T-\Delta)} + \frac{2r(e^{(\mu-r)\Delta}-1)}{\sigma^2+2\mu-r} & \mu \neq r, \sigma^2 + 2\mu \neq r. \\ -2[e^{(\mu-r)\Delta} - 1] \frac{r[\mu(e^{(\mu-r)(T-\Delta)} - 1) - r(\mu - r)(T - \Delta)]}{(\mu - r)^3(T - \Delta)}, & \end{cases} \tag{48}$$

The particular expressions for $\langle S(t) \rangle$, $\langle S^2(t) \rangle$, $\langle (S(t) - \langle S(t) \rangle)^2 \rangle$, and $\overline{\langle \delta^2(\Delta) \rangle}$ in each of the region of parameters $\mu = r$ and $\sigma^2 + 2\mu = r$ follow—upon performing the Taylor expansions in terms of the small parameters $\delta r = \mu - r$ and $\delta r = \sigma^2 + 2\mu - r$ (to the necessary order)—from the

general expressions for the first moment (33), the second moment (36), the variance (40), and the mean TAMSD (48) of Poisson-reset GBM obtained for the general case $\mu \neq r$ and $\sigma^2 + 2\mu \neq r$. The drift-free $\mu = 0$ results for the moments [(33) and (37)], variance (41), and mean TAMSD (47) of Poisson-reset GBM were presented in our short study [1].

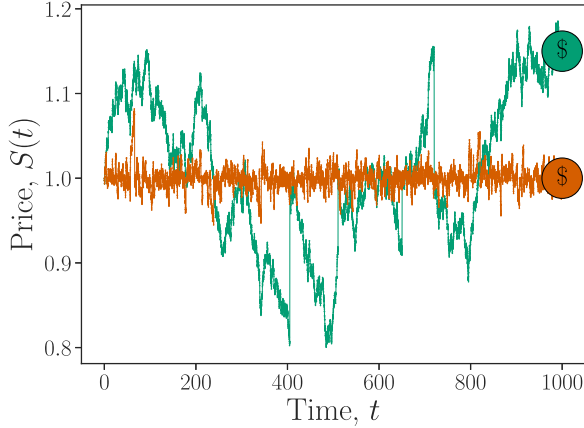


FIG. 1. Simulated Sysiphus-type random walk [82,191] trajectories of reset GBM for the case of rare ($r = 0.005$, green curve) and frequent ($r = 0.5$, red curve) resetting, computed for $\sigma = 10^{-2}$ and the initial-and-reset price $S_0 = 1$. The green-colored path [with larger reset jumps] is a process with potentially larger speculative “winning margins,” as compared to the red trajectory [with much smaller rises and drops of the price, both shown symbolically with \$ sign]. A low-saturation Morandi-like color palette is used in this and later plots. The figure is reproduced from Ref. [1], subject to APS 2022 copyright.

V. SIMULATION SCHEME

From Eq. (5), the time-evolution of reset GBM is driven by the increments $dW(t)$ modeled using the unit-variance and zero-mean normal distribution,

$$dW(t) \sim \mathcal{N}(0, 1) \times dt. \quad (49)$$

Within the Euler-Murayama simulation scheme, a stochastic differential equation of the form

$$dX(t) = f(X(t))dt + g(X(t))dW(t), \quad (50)$$

subject to the initial condition $X(0) = X(t = 0)$, can be numerically solved on an interval $[0, T]$ via splitting it into \bar{N} time steps

$$0 = t_0 < t_1 < t_2 < \dots < t_{\bar{N}} = T \quad (51)$$

or $t_i = t_0 + i \times \Delta t$, with the time-step given by

$$\Delta t = T/\bar{N}. \quad (52)$$

Applying this discrete scheme to Eq. (50), with the increments of the Wiener process

$$\Delta W_n = W(t_{n+1}) - W(t_n), \quad (53)$$

the recurrently used relation to generate GBM—consistent with the prepoint Itô interpretation [182] used in the analytical considerations above—becomes [1,183,184]

$$X_{n+1} = X_n + \mu X_n \Delta t + \sigma X_n \Delta W_n. \quad (54)$$

For reset GBM with a constant-rate resetting, at each step the random walk goes back to a fixed starting point with the probability $r\Delta t$, or alternatively it proceeds in accord with Eq. (54) with the probability $(1 - r\Delta t)$. Thus, the discretized

scheme to simulate Poissonian-reset GBM (see Fig. 1) is

$$S(t_{n+1}) = \begin{cases} S_0, & p_{\text{reset}} = r\Delta t, \\ S_n + \mu S_n \Delta t + \sigma S_n \Delta W_n, & p_{\text{nonreset}} = 1 - r\Delta t. \end{cases} \quad (55)$$

VI. ASYMPTOTIC BEHAVIORS OF THE MAIN OBSERVABLES

We present the results of the asymptotic expansions for the first moment, the second moment, the variance, and the mean TAMSD in Tables I, II, III, and IV, correspondingly. We outline below separately the regimes of behaviors in each of the three regions of the model parameters μ , σ^2 , and r from the above Secs. IV D 1, IV D 2, and IV D 3.

We are interested in the behavior of all quantifiers of Poisson-reset GBM from the derived analytical expressions at short and long (lag) times. The short-time limit is realized when the diffusion time is much shorter than the shortest timescale in the problem. The limit of long times is realized when the diffusion time is much longer than the longest timescale. The total length of the trajectory is, often, even longer than this longest timescale, at least in the limit of frequent resetting. In this case each trajectory contains a large number of resetting events.

The existence of three main model parameters—the nonzero drift μ (responsible for a deterministic growth of the drift-containing GBM process), the volatility-related parameter σ^2 (describing the fluctuations-related growth), and the rate of Poissonian resetting r (defining the average frequency of resetting events)—defines a number of possible scenarios or regimes for GBM-based diffusion in the presence of drift and resetting. In our short study [1] of the simplest case $\mu = 0$ the limits of rare and frequent resetting were defined as $r \ll \sigma^2$ and $r \gg \sigma^2$, respectively. The existence of a nonzero drift complicates the terminology for the drift-containing situation considered here: the rate of resetting should not only be compared to the diffusivity parameter σ^2 but also to the drift μ . This gives rise to different timescales in the evolution of the ensemble- and time-averaged statistical quantifiers of reset GBM determined by certain combinations of these three main model parameters, as we describe below.

A. First moment

In the main text the results for the third regime of model parameters for all relevant statistical quantifiers are presented, while Appendix B contains the auxiliary figures with the results of both computational and analytical analyses for the parameters regions 1 and 2. For each region of model parameters the comparison of analytical (as well as asymptotic predictions) with the results of computer simulation demonstrates good, quantitative agreement. The results of simulations and their comparison with the theoretical predictions for the first moment of drift-containing reset GBM are presented for regime 1, regime 2, and regime 3 of the model parameters in Figs. 11, 12, (Appendix B) and 2, correspondingly.

1. Regime 1

We start with the limit of long observation times, see Fig. 11(a). In the first region of model parameters, when $\mu = r$, the first expression in Eq. (33) is the asymptote by itself, with no limits to be considered, so that $\langle S(t) \rangle = S_0[1 + rt]$, as indicated in Eqs. (85) and (86) of Table I.

The condition $\sigma^2 + 2\mu = r$ provides a special subset of $\mu \neq r$ expression in Eq. (33) with an additional constraint on the allowed values of μ and r . The respective regime of the first-moment variation is of interest here because it emerges in the analysis of the variance and the mean TAMSD later. The timescale-variable then becomes $(\mu - r)T = -(\sigma^2 + r)T/2$. As both the volatility and rate of reset are positively defined, this imposes a constraint on the drift, namely, $\mu < r$.

The behaviors of the first moment of reset GBM in a wide range of times and at short times are demonstrated in supplementary Figs. 11(a) and 11(b), respectively. Note that μ and σ^2 were chosen here relatively small to reach satisfactory averaging statistics for the chosen number of trajectories in the set and their length. Larger drift and volatility parameters will surely enhance the exponential-like GBM growth and require [for a fixed trace length T] a larger ensemble of the trajectories to be generated *in silico*.

2. Regime 2

The results of simulations for the first moment in the second region of parameters are presented in Figs. 12(a) and 12(b), respectively, for the general as well as the short-time variation.

In the second region of model parameters we formally choose the second line in expression (33). We find that at short times, when $(\sigma^2 + r)t \ll 1$, the asymptotes are always linear in time, with the prefactors epitomizing the three essential characteristic rates in the problem, namely, μ , $r/2$, and $\sigma^2/2$.

At short times we find the the linear asymptote for the first moment of reset GBM, with these three parameters determining the prefactors in Eqs. (89), (91), and (93). We stress

here that the negative sign in Eq. (93) stems from effectively negative drift $\mu \approx -\sigma^2/2 < 0$ in the subsubcase $r \ll \sigma^2$ of the subcase $(r - \mu)T \gg 1$ of the second region of parameters. We do not address this subsubcase in the plots, limiting ourselves to the situation $\mu > 0$ to simplify the description.

In the limit of long times, at $(\sigma^2 + r)t \gg 1$, interestingly, under the conditions of frequent resetting with $r \gg \sigma^2$, $\langle S(t) \rangle$ tends to $2S_0$ (twice the intuitively expected value). This value for the subsubcase $r \gg \sigma^2$ stems from the fact that $(\mu - r) \approx -r/2 < 0$ so that in the general expression (33) the nonexponential factors give rise to the long-time limit

$$\langle S(t) \rangle \approx 2S_0. \quad (56)$$

Note that the fluctuations of the computed plateau heights of the first moment in this regime (as a function of time) stem from a finite number of trajectories used for ensemble-averaging. Under the conditions of weak or rare resetting—that means here $r \ll \sigma^2$ —we find that the long-time limit of $\langle S(t) \rangle$ becomes quite small, cf. Eqs. (90), (92), and (94). This trend is again opposite to expectations [once we realize that the two cases are the subsets of the $-(\mu - r)T \gg 1$ case in Table I]. The vanishing first moment in the subsubcase (94) is a consequence of effectively negative drift at these conditions, so that in the general expression (33) the exponential function can be neglected at long times and the constant factor gives $\langle S(t) \rangle \propto 2r/\sigma^2 \rightarrow 0$ at $r \ll \sigma^2$.

For the condition $|\mu - r|T \ll 1$ we detect two identical asymptotes for the short- and long-time behavior of the first moment, see Eqs. (87) and (88) in Table I.

3. Regime 3

Now we consider the third region of parameters: when $\mu \neq r$ and the third expression of the general Eq. (33) is to be taken. The general and short-time evolution of the first moment for this regime is presented in Figs. 2(a) and 2(b), respectively. The timescale variable that determines the behavior of $\langle S(t) \rangle$

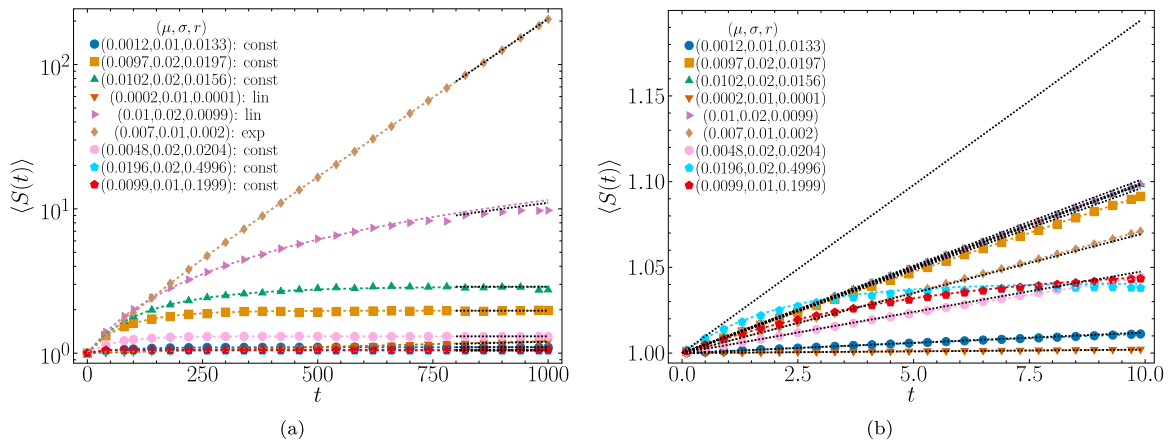


FIG. 2. The same as in Fig. 11, but for the third region of parameters (see Table I and the legend for the actual values of parameters). The colors and the styles of the data symbols for the specific values of drift, volatility, and reset rate stay the same in all the plots illustrating the behaviors of the moments, the variance, the TAMSD, the mean TAMSD, as well as the EB parameter for each region of parameters. (a) The colored curves are according to Eq. (33), while the dashed asymptotes are Eqs. (96), (98), and (100). Log-linear scale is chosen here to emphasize the exponential long-time growth of the fastest-growing curve (with the notation “exp” denoting this fact in the legend). (b) The same as in Fig. 2(a) shown for the same parameters at short times. The asymptotes from Eqs. (95), (97), and (99) are shown as the dashed lines.

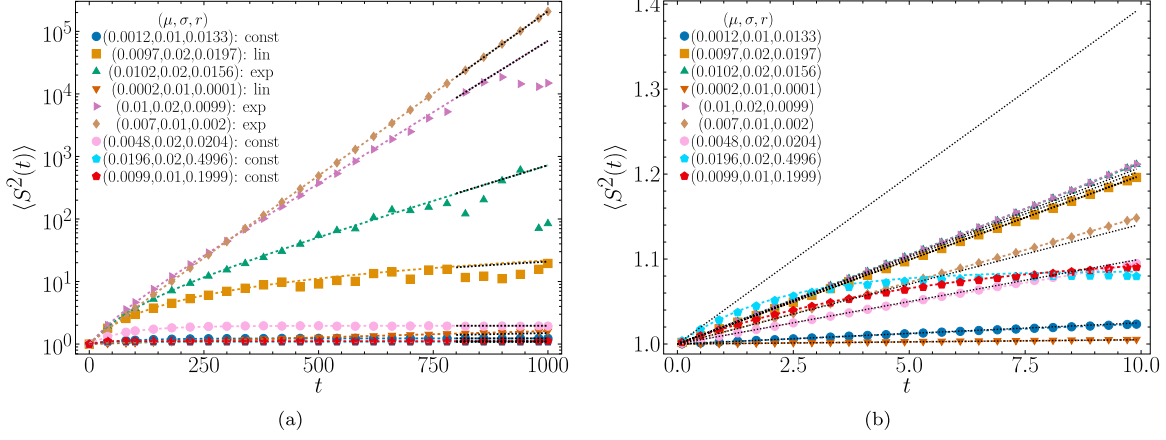


FIG. 3. The same as in Fig. 13 but the third region of parameters in Table II. The parameters are the same as in Fig. 2. (a) The colored curves are according to Eq. (36), while the dashed asymptotes are plotted according to Eqs. (112), (114), and (116). (b) The same as in Fig. 3(a), but shown as a zoom-in at short times, with the dashed asymptotes following Eqs. (111), (113), and (115).

in this regime is $(\mu - r)T$. Comparing the rate of resetting and the drift we can define the regimes of frequent and rare resetting in this regime as $\mu \ll r$ and $\mu \gg r$, correspondingly. The asymptotes of analytical expression (33) for $\langle S(t) \rangle$ at short and long times are listed in Table I as Eqs. (95), (97), (99) and (96), (98), (100), respectively.

The first moment of reset GBM given by Eq. (33) grows (naturally) slower in time as that of the nonreset process in the limit of long times, cf. Eqs. (96) and (8). It is also not surprising that for rare resetting, at $r \ll \mu$, the existing drift dominates resetting so that the behavior of the first moment resembles that of nonreset or pure GBM, but with a slower exponential growth. In a subregion of parameters, when for the entire time domain $|\mu - r|T \ll 1$, the first moment of reset GBM exhibits a linear-in-time growth, both at short and at long times. At long times, under the conditions of frequent resetting we get $S(t) \rightarrow S_0$, as intuitively expected; see Eq. (100).

B. Second moment

The asymptotic behaviors of the second moment of reset GBM are presented in Table II. These asymptotes for the first, second, and third regions of the above-mentioned model parameters in the limit of short and long times are favorably compared to the results of simulations in Figs. 13(b), 14(b), 3(b) and 13(a), 14(a), 3(a), correspondingly.

1. Regime 1

In the first region of parameters, at $\mu = r$ and for $\sigma^2 + 2\mu \neq r$, we find that in the limit $|\sigma^2 + 2\mu - r|T \ll 1$ the second moment develops linearly both at short and long times, according to Eqs. (107) and (108), respectively. In the opposite limit of $(\sigma^2 + 2\mu - r)T \gg 1$ the general short- and long-time expressions are given by Eqs. (101) and (102). The former one presents again a growth which is linear in time, whereas the latter exhibits an exponential growth slowed down by resetting. This one can judge via comparing (102) with the second moment of nonreset GBM (9). The behavior at $\mu = r$ can further be separated into the regimes characteriz-

ing the frequent- and rare-resetting protocols (established via comparing r to σ^2).

Namely, for frequent resetting ($r \gg \sigma^2$) the second moment of reset GBM features a linear behavior at short times and an exponential asymptotic growth at long times, both containing only the reset rate r as the essential parameter, cf. Eqs. (103) and (104). In the opposite limit of rare resetting, the diffusivity parameter σ^2 controls the linear short-time evolution of $\langle S^2(t) \rangle$ and the exponential long-time behavior of the second moment, as specified by Eqs. (105) and (106), see also Fig. 13. Naturally, only σ^2 is the essential parameter in this rare-resetting limit in the first region.

2. Regime 2

In the second region of model parameters, at $\sigma^2 + 2\mu = r$, the short- and long-time asymptotic laws of the second moment of reset GBM are identical to one another being linear in time, see Eqs. (109) and (110), as follows from Eq. (36). In this limit, the exponential growth stemming from the dependence on the parameter $(\sigma^2 + 2\mu)$ and the exponential decay of the second moment originating from the reset rate r cancel each other that yields an unexpectedly simple linear growth of $\langle S^2(t) \rangle$ of reset GBM in this situation, see also Fig. 14.

3. Regime 3

In the third region of model parameters, when $\mu \neq r$ and $\sigma^2 + 2\mu \neq r$, we describe the behaviors in this regime in the three different limiting situations. Their physical meaning is as follows. At short times all three subcases give the same linear asymptote for the second moment, see Eqs. (115), (113), and (111). In the limit of long time, however, depending on each specific condition chosen, we predict three different functional dependencies.

Namely, in the first subcase of the third regime, for the region of parameters when the resetting rate can be neglected, the long-time exponential growth of the second moment of reset GBM is similar to that of pure GBM (9), cf. Eq. (112).

For the second subcase of the third regime, the simplifications of Eq. (36) yields a linear dependence of the second

TABLE I. Asymptotes of the first moment of Poisson-reset GBM in the presence of nonzero drift. Each regime and subregime/subcase of functional behaviors is realized for a respective region and subregion of the model parameters, as indicated here and in the following Tables. The underlined and double-underlined results in regime 3 of this Table turn into the results of Ref. [1] in the limits of weak/rare and strong/frequent resetting, respectively.

$\langle S(t) \rangle / S_0$			Short time		Long time
Regime 1					
$\mu = r$			$1 + rt$ (85)		$1 + rt$ (86)
Regime 2	$ \mu - r T \ll 1$		$1 + \mu t$ (87)		$1 + \mu t$ (88)
$\sigma^2 + 2\mu = r$			$1 + \mu t$ (89)		$2r/(\sigma^2 + r)$ (90)
	$-(\mu - r)T \gg 1$	$\begin{cases} r \gg \sigma^2 \\ r \ll \sigma^2 \end{cases}$	$1 + rt/2$ (91)		2 (92)
			$1 - \sigma^2 t/2$ (93)		$2r/\sigma^2 \approx 0$ (94)
Regime 3	$+(\mu - r)T \gg 1$			$1 + \mu t$ (95)	
$\mu \neq r$	$ \mu - r T \ll 1$		<u>$1 + \mu t$</u> (97)		<u>$1 + \mu t$</u> (98)
$\sigma^2 + 2\mu \neq r$	$-(\mu - r)T \gg 1$		<u>$1 + \mu t$</u> (99)		<u>$r/(r - \mu) \approx 1$</u> (100)

moment of time, Eq. (114), both at short and long times, like in the second regime [see Eqs. (109) and (110)].

Lastly, for the third subcase of the third regime (frequent resetting), the process is interrupted so often that at long times we get for the second moment simply the square of the reset position, S_0^2 , see Eq. (116), see also Fig. 3.

C. Variance

As the variance involves the first and the second moments, see Eq. (39), the number of possible regions of parameters remains the same, but the number of different combinations of the subregions of parameters increases, see Table III. It is remarkable, however, that in the limit of short times all these different regions and subregions of model parameters give rise

to the same asymptotic growth of the variance, namely,

$$\langle (S(t) - \langle S(t) \rangle)^2 \rangle \approx S_0^2 \sigma^2 t. \tag{57}$$

We mention here also that, effectively, the short-time asymptotic behaviors of the first and second moments are also the same, as detailed in Tables I and II. In the limit of long times, however, the different regimes yield functionally diverse asymptotic forms of the variance, as described for each of the regimes and subcases below.

These asymptotic behaviors for the first, second, and third regimes in the respective regions of parameters, both at short and long times, are in good, quantitative agreement with the results of computer simulations. Both theoretical and simulational results for $\langle (S(t) - \langle S(t) \rangle)^2 \rangle$ are presented in

TABLE II. Asymptotes of the second moment of reset GBM. The underlined and double-underlined results in regime 3 in Tables II, III, and IV turn at $\mu = 0$ into the findings of Ref. [1] for a simpler drift-less reset GBM, see also Table V.

$\langle S^2(t) \rangle / S_0^2$			Short time		Long time
Regime 1					
$\mu = r$	$+(\sigma^2 + r)T \gg 1$	$\begin{cases} r \gg \sigma^2 \\ r \ll \sigma^2 \end{cases}$	$1 + (\sigma^2 + 2r)t$ (101)		$\frac{(\sigma^2 + 2r)e^{(\sigma^2 + r)t}}{\sigma^2 + r}$ (102)
			$1 + 2rt$ (103)		$2e^{rt}$ (104)
			$1 + \sigma^2 t$ (105)		$e^{\sigma^2 t}$ (106)
	$ \sigma^2 + r T \ll 1$		$1 + (\sigma^2 + 2r)t$ (107)		$1 + (\sigma^2 + 2r)t$ (108)
Regime 2					
$\sigma^2 + 2\mu = r$			$1 + rt$ (109)		$1 + rt$ (110)
Regime 3	$+(\sigma^2 + 2\mu - r)T \gg 1$		<u>$1 + (\sigma^2 + 2\mu)t$</u> (111)		<u>$\frac{(\sigma^2 + 2\mu)e^{(\sigma^2 + 2\mu - r)t}}{\sigma^2 + 2\mu - r}$</u> (112)
$\mu \neq r$	$ \sigma^2 + 2\mu - r T \ll 1$		$1 + (\sigma^2 + 2\mu)t$ (113)		$1 + (\sigma^2 + 2\mu)t$ (114)
$\sigma^2 + 2\mu \neq r$	$-(\sigma^2 + 2\mu - r)T \gg 1$		<u>$1 + (\sigma^2 + 2\mu)t$</u> (115)		<u>$\frac{r}{r - \sigma^2 - 2\mu} \approx 1$</u> (116)

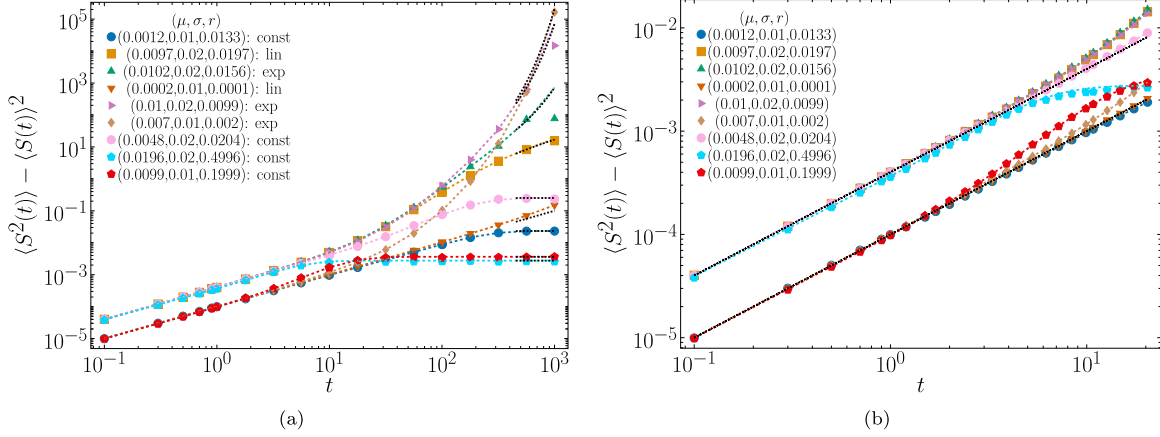


FIG. 4. The same as in Fig. 15 but the third region of parameters in Table III. The parameters are the same as in Fig. 2. (a) The colored curves represent Eq. (40), while the dashed asymptotes are according to Eqs. (130), (132), (134), (136), (138), and (140). All three different functional forms of the long-time asymptotes—the exponential growth, the linear increase, and the saturation to the NESS-like plateau—are indicated in the legend. (b) The same as in Fig. 4(a), with the behavior at short times being illustrated. The dashed lines follow Eqs. (129), (131), (133), (135), (137), and (139).

Figs. 15(a), 16(a), 4(a) and 15(b), 16(b), 4(b), correspondingly. Log-log scale in all these figures properly represents the power-law growth of the variance at short times in all the regimes (and also at long times in some of them).

1. Regime 1

For the first region of parameters, at $\mu = r$, as given by the first line in Eq. (40), for the subcase $(\sigma^2 + r)T \gg 1$ (that is the characteristic parameter) the exponential growth at long time is detected, Eq. (118), namely

$$\langle (S(t) - \langle S(t) \rangle)^2 \rangle \approx S_0^2 \frac{(\sigma^2 + 2r)e^{(\sigma^2 + r)t}}{\sigma^2 + r}. \quad (58)$$

This result in the case of rare resetting, $r \ll \sigma^2$, yields that $\langle (S(t) - \langle S(t) \rangle)^2 \rangle \approx S_0^2 \times e^{\sigma^2 t}$ [see Eq. (122)], as for nonreset GBM, as intuitively expected. For the situation of frequent resetting, when $r \gg \sigma^2$, the asymptotic behavior of the variance is determined solely by the reset rate, namely, $\langle (S(t) - \langle S(t) \rangle)^2 \rangle \approx S_0^2 \times 2e^{rt}$; see Eq. (120).

Similar to the long-time asymptotics of the second moment given by expression (104), we obtain in this region of parameters the exponential growth of variance of reset GBM at long times. The reason for such a growth for both $\langle S^2(t) \rangle$ and $\langle (S(t) - \langle S(t) \rangle)^2 \rangle$ for the case of frequent resetting $r \gg \sigma^2$ —where for a drift-free scenario one expects and observes the respective NESS plateaus [1]—is the argument of the exponential function in the general drift-containing case, see the third lines in expressions (36) and (40), correspondingly.

Namely, in the case of GBM with a nonzero drift considered here, at $\mu = r$ the leading dependencies for the second moment and of the variance given by $\propto e^{(2\mu - r)t}$ turn into $\propto e^{rt}$, as described. The NESS plateau is only detected when both conditions

$$r \gg \sigma^2 \quad \text{and} \quad r \gg \mu \quad (59)$$

are satisfied. These plateaus are described by expressions (116) and (140) for the second moment and variance, respectively (see the third subcase in Sec. VIB 3 and the sixth subcase in Sec. VIC 3).

In the second subregion of model parameters, at $|\sigma^2 + r|T \ll 1$, both exponential functions in the general solution for the variance (40) can be expanded (due to the smallness of their arguments at all times). Therefore, the long-time result in this subcase is the same as the short-time one, see Eq. (124),

$$\langle (S(t) - \langle S(t) \rangle)^2 \rangle \approx S_0^2 \sigma^2 t, \quad (60)$$

see also the results of Fig. 15.

2. Regime 2

In the second region of model parameters, when $\sigma^2 + 2\mu = r$, $(\mu - r)T$ is the behavior-determining parameter, as follows from the second line in Eq. (40). In this regime, we observe at long times the linear-in-time evolution of the variance of reset GBM. Namely, the behavior (57) listed in Eq. (126) for the first subcase $|\mu - r|T \ll 1$ is obtained.

For the second subregion of this parameter region, at $-(\mu - r)T \gg 1$, the growth law of the variance

$$\langle (S(t) - \langle S(t) \rangle)^2 \rangle \sim S_0^2 \times rt \quad (61)$$

follows from expression (126) at $rt \gg 1$ and for $r \gg \sigma^2$. The results for this regime are shown in Fig. 16.

3. Regime 3

In the third regime of parameters, when $\mu \neq r$ and $\sigma^2 + 2\mu \neq r$, the general expression (40) should be used. For all the subregimes of this regime we obtain the linear-in-time growth given by Eq. (57), whereas at long times the exponential growth of the variance at rare resetting, the linear-in-time growth at intermediate resetting, as well as a plateau-like stagnating behavior of the variance at frequent resetting are detected. We describe these behaviors one by one below and illustrate them in Fig. 4.

For the first subcase of the third regime, at $(\mu - r)T \gg 1$ and $(\sigma^2 + 2\mu - r)T \gg 1$, the exponential growth of GBM is only weakly perturbed by resetting, with the long-time asymptotic form given by Eq. (130). In this situation both exponential functions from the third line of expression (40) contribute to the behavior, but in the limit of long times only one of them with the largest argument will survive because

$$\sigma^2 + 2\mu - r > \mu - r. \quad (62)$$

In the second subcase, when $|\mu - r|T \ll 1$ and $(\sigma^2 + 2\mu - r)T \gg 1$, the second exponential function in the third line of Eq. (40) can be neglected and, yet again, only a slightly resetting-perturbed growth of the variance at long times is predicted; see Eq. (132).

In the third subcase, when $|\mu - r|T \ll 1$ and $(\sigma^2 + 2\mu - r)T \ll 1$, we can expand both exponential functions in the general expression for the variance (40) in terms of their small arguments and obtain that the long-time behavior is identical to the short-time evolution (57), as given by Eq. (134).

In the fourth subcase, when $(\sigma^2 + 2\mu - r)T \gg 1$, the second exponential function in Eq. (40) can be neglected at long-enough times and the first exponential function dominates the growth of the variance in this subregime; see Eq. (136).

In the fifth subcase, when $-(\mu - r)T \gg 1$ and $|\sigma^2 + 2\mu - r|T \ll 1$, the first exponential function in the general expression (40) can be expanded for small arguments (in the entire interval of times), while the contribution of the second exponential function can be neglected. Then, provided the resetting process is intense enough, so that the condition $r \gg \mu$ holds, we arrive at a simple linear long-time asymptote in this subregime given by Eq. (138).

Finally, in the sixth subcase, for which the subregion of parameters is $-(\mu - r)T \gg 1$ and $-(\sigma^2 + 2\mu - r)T \gg 1$, the

resetting is frequent enough so that both exponential functions [related to the GBM growth] in Eq. (40) can be neglected and a plateau-like NESS-related behavior given by Eq. (140) is established, namely,

$$\langle (S(t) - \langle S(t) \rangle)^2 \rangle \approx S_0^2 \frac{r(\sigma^2 r + \mu^2)}{(r - \sigma^2 - 2\mu)(\mu - r)^2}. \quad (63)$$

In the limit of frequent resetting, such that $r \gg \mu$, we arrive from this expression at a simple result for drift-free reset GBM presented in Ref. [1], with the NESS-plateau given by

$$\langle (S(t) - \langle S(t) \rangle)^2 \rangle \approx S_0^2 \sigma^2 / (r - \sigma^2). \quad (64)$$

When the rate of resetting not only exceeds the drift $r \gg \mu$, but also $r \gg \sigma^2$, the long-time limits for the first and second moments are—due to extremely frequent resets to S_0 value—given by $\langle S(t) \rangle \rightarrow S_0$ (100) and $\langle S^2(t) \rangle \rightarrow S_0^2$ (116). For the variance, given by the respective difference (39), a small value

$$\langle (S(t) - \langle S(t) \rangle)^2 \rangle \approx S_0^2 \sigma^2 / r \ll S_0^2 \quad (65)$$

is obtained in this frequent-resetting limit from expression (140). Physically, frequent resetting (59) at long times rarely leads to random walks leaving the starting point far enough and, thus, the fluctuations of the particles' position from the mean—being quantified by the variance—tend to vanish accordingly; see Eqs. (65) and (140). All these characteristic behaviors are illustrated in Fig. 4.

D. TAMSD

With the help of the results for the two components $\langle \delta^2(\Delta) \rangle_\mu$ and $\langle \delta^2(\Delta) \rangle_{\sigma^2 + 2\mu}$ of the mean TAMSD in the limits of short and long lag times, in Table IV we present all possible asymptotes obtained from the final TAMSD result (48), that embodies the main result of the current study.

TABLE III. Asymptotes of the variance of reset GBM.

$\langle (S(t) - \langle S(t) \rangle)^2 \rangle / S_0^2$		Short time	Long time	
Regime 1 $\mu = r$	$+(\sigma^2 + r)T \gg 1$	$r \gg \sigma^2$	$\sigma^2 t$ (117)	$\frac{(\sigma^2 + 2r)e^{(\sigma^2 + r)t}}{\sigma^2 + r}$ (118)
		$r \ll \sigma^2$	$\sigma^2 t$ (119)	$2e^{rt}$ (120)
			$\sigma^2 t$ (121)	$e^{\sigma^2 t}$ (122)
			$\sigma^2 t$ (123)	$\sigma^2 t$ (124)
Regime 2 $\sigma^2 + 2\mu = r$	$ \mu - r T \ll 1$		$\sigma^2 t$ (125)	$\sigma^2 t$ (126)
	$-(\mu - r)T \gg 1$		$\sigma^2 t$ (127)	$rt + 1 - \frac{4r^2}{(\sigma^2 + r)^2}$ (128)
	$+(\mu - r)T \gg 1$	$+(\sigma^2 + 2\mu - r)T \gg 1$	$\sigma^2 t$ (129)	$\frac{(\sigma^2 + 2\mu)e^{(\sigma^2 + 2\mu - r)t}}{\sigma^2 + 2\mu - r}$ (130)
Regime 3 $\mu \neq r$ $\sigma^2 + 2\mu \neq r$	$ \mu - r T \ll 1$	$+(\sigma^2 + 2\mu - r)T \gg 1$	$\sigma^2 t$ (131)	$\frac{(\sigma^2 + 2\mu)e^{(\sigma^2 + 2\mu - r)t}}{\sigma^2 + 2\mu - r}$ (132)
		$ \sigma^2 + 2\mu - r T \ll 1$	$\sigma^2 t$ (133)	$\sigma^2 t$ (134)
		$+(\sigma^2 + 2\mu - r)T \gg 1$	$\sigma^2 t$ (135)	$\frac{(\sigma^2 + 2\mu)e^{(\sigma^2 + 2\mu - r)t}}{\sigma^2 + 2\mu - r}$ (136)
	$-(\mu - r)T \gg 1$	$ \sigma^2 + 2\mu - r T \ll 1$	$\sigma^2 t$ (137)	$(\sigma^2 + 2\mu)t$ (138)
		$-(\sigma^2 + 2\mu - r)T \gg 1$	$\sigma^2 t$ (139)	$\frac{r(\sigma^2 r + \mu^2)}{(r - \sigma^2 - 2\mu)(\mu - r)^2}$ (140)

We now describe all the regimes, subregimes, and explicit asymptotic behaviors realized for the mean TAMSD of the process of drift-containing reset GBM, as listed in Table IV. The description is done in the same order as for the same regions of parameters for the variance in Sec. VIC. The results for the mean TAMSD are presented in Figs. 17(a), 18(a), 5(a) and 17(b), 18(b), 5(b) for the domains of long and short lag times, correspondingly. Our starting expressions are the general result (48) as well as the particular expressions (42) and (44) for the first and second regime, correspondingly. Similar to the second moment and variance, the results for the mean TAMSD of reset GBM for the regime 1, regime 2, and regime 3 of typical behaviors are expressed in terms of their dependencies on $\{\sigma^2, r\}$, $\{\sigma^2, r\}$, and $\{\sigma^2, \mu, r\}$, correspondingly, with the model parameters being situated in the respective regions.

1. Regime 1

In the first regime, see Table IV summarising the TAMSD asymptotics, in the first subregion of the model parameters realized at $(\sigma^2 + r)T \gg 1$ in the limit of short lag times $(\sigma^2 + r)\Delta \ll 1$ one of the exponential functions in expression (42) defines the magnitude of the TAMSD, namely,

$$\overline{\langle \delta^2(\Delta) \rangle} \approx S_0^2 \frac{(\sigma^2 + 2r)}{(\sigma^2 + r)} \times e^{(\sigma^2 + r)T} \times \left(\frac{\Delta}{T}\right)^1. \quad (66)$$

This exponential function acts as a prefactor for the linear dependence of the mean TAMSD of reset GBM on the lag time, $\overline{\langle \delta^2(\Delta) \rangle} \propto \Delta$, as given by Eq. (141). This prefactor simplifies in the limit of strong/frequent (143) and weak/rare (145) resetting, whereas the latter coincides (not surprisingly) with the scaling relation (12) known for nonreset GBM [1,183–185]. The scaling relations (143) and (145) stemming from the general expression (141) correspond to the first subregion $(\sigma^2 + r)T \gg 1$, while the asymptote (147) is obtained under the second condition $|\sigma^2 + r|T \ll 1$. These two subcases are considered for the first region of model parameters.

For the long-time behavior in this subregion of parameters we find that at the very last point of the TAMSD trajectory, at $\Delta = T$, for the first subcase of the first regime, at $(\sigma^2 + r)T \gg 1$, the scaling relations (144) and (146) originating from the general expression (142) are found to be valid. The general relation (142) in this subregion of parameters illustrates the exponential increase of the end-point TAMSD magnitude as a function of the lag time for $(\sigma^2 + r)T \gg 1$,

$$\overline{\langle \delta^2(\Delta) \rangle} \approx S_0^2 \frac{(\sigma^2 + 2r)e^{(\sigma^2 + r)\Delta}}{\sigma^2 + r}. \quad (67)$$

As we clarified in Sec. VIC1 for the observed exponential growth of the second moment and variance at long times, for the mean TAMSD in this regime the argument of the exponential function in Eq. (142) [see the third line in Eq. (48)] is the reason for the exponential growth at $r \gg \sigma^2$. The NESS plateau of the TAMSD is only detected when both conditions— $r \gg \sigma^2$ and $r \gg \mu$ —are being satisfied, see Eq. (164) as well as the sixth subcase in Sec. VID3.

In the second subregion of model parameters, at $|\sigma^2 + r|T \ll 1$, the same exponential function can be expanded into the power series in the entire region of lag times

so that another linear-in-lag-time asymptotic expression for the TAMSD at short lag times $(\sigma^2 + r)\Delta \ll 1$ is obtained, namely, Eq. (147). We, again, obtain a linear-in-lag-time TAMSD dependence at short lag times, but with a functionally different prefactor, i.e.,

$$\overline{\langle \delta^2(\Delta) \rangle} \approx S_0^2(\sigma^2 - r^2T)\Delta^1. \quad (68)$$

For rare resetting (when $\sigma^2 \gg r^2T$) this expression, as expected, yields the result for the short-lag-time growth of the mean TAMSD of nonreset GBM, namely, $\overline{\langle \delta^2(\Delta) \rangle} \approx S_0^2\sigma^2\Delta$, that coincides with the result following from Eq. (43) at short lag times and for $\sigma^2T \ll 1$ (a condition for the model parameters similar to the one of the current subregion).

In the second subregion of parameters, at $|\sigma^2 + r|T \ll 1$, in the limit of long lag time the expression (148) is obtained. It describes the linear growth of the TAMSD with Δ for the parameter subregion $|\sigma^2 + r|T \ll 1$, namely,

$$\overline{\langle \delta^2(\Delta) \rangle} \approx S_0^2\sigma^2\Delta. \quad (69)$$

As one could have anticipated, at $|\sigma^2 + r|T \ll 1$ the number of resetting events for the entire trajectory is small and their effects are not salient: the long-lag-time growth of the mean TAMSD is (in the leading-order approximation) unperturbed by resetting. We, thus, detect two fundamentally different functional forms of the mean-TAMSD growth in the two subcases of the first regime: the exponential growth (67) in the first subcase and the linear growth (69) in the second subcase of regime 1, see also Fig. 17.

2. Regime 2

In the second region of parameters in Table IV we start with the simplified TAMSD expression (44). At short lag times in the first subregion of parameters, at $|\mu - r|T \ll 1$, the respective exponential functions involved in the TAMSD (44) can be expanded into the Taylor series such that a simple TAMSD asymptotic behavior (149) is obtained at short lag times for $|\mu - r|\Delta \ll 1$, namely,

$$\overline{\langle \delta^2(\Delta) \rangle} \approx S_0^2\sigma^2\Delta. \quad (70)$$

The asymptotic growth observed at long lag times in this subcase yields the very same linear dependence of the mean TAMSD on lag time, Eq. (150), i.e.,

$$\overline{\langle \delta^2(\Delta) \rangle} \approx S_0^2\sigma^2\Delta. \quad (71)$$

In the second subregion of parameters, at $-(\mu - r)T \gg 1$, at short lag times the exponential functions in expression (44) of the type $e^{(\mu - r)T}$ can be neglected, while the exponential function $e^{(\mu - r)\Delta}$ should be Taylor-series expanded. As a result, a linear-in-lag-time growth of the mean TAMSD is obtained, Eq. (151), that under the assumption of relatively frequent resetting—such that at $r \gg \sigma^2$ and for $rT \gg 1$ —yields a simple asymptotic expression $\overline{\langle \delta^2(\Delta) \rangle} \sim S_0^2r^2T \times \Delta$.

For the long-lag-time behavior in the second subcase of regime 2 we find expression (152) describing a constant-factor-offset linear growth of the mean TAMSD, with the leading dependence at $rT \gg 1$ being $\overline{\langle \delta^2(\Delta) \rangle} \sim S_0^2r\Delta$. We emphasize, however, that—for the values of the model parameters chosen in our simulations—additional next-order terms of the expansion presented in the short- and long-lag-time

TAMSD expressions (151) and (152) need to be taken into account to achieve a good, quantitative fit to the data extracted from the computer simulations, see Fig. 18.

3. Regime 3

In the third region of model parameters, the general expression (46) is utilized. For the first subregion of parameters, at $+(\mu - r)T \gg 1$ and $+(\sigma^2 + 2\mu - r)T \gg 1$, in the limit of short lag times—at $(\sigma^2 + 2\mu - r)\Delta \ll 1$ and $(\mu - r)\Delta \ll 1$ (and for condition $\Delta \ll T$ being additionally satisfied)—the exponential functions in expression (46) with short-lag-time arguments can be expanded, while the exponential functions containing the trace length as the argument serve as prefactors in the resulting mean-TAMSD asymptote showing a linear growth with the lag time, as given by Eq. (153), i.e.,

$$\overline{\langle \delta^2(\Delta) \rangle} \approx S_0^2 \frac{(\sigma^2 + 2\mu)(\sigma^2 + r)e^{(\sigma^2 + 2\mu - r)T}}{(\sigma^2 + 2\mu - r)^2} \left(\frac{\Delta}{T}\right)^1. \quad (72)$$

We emphasize here that in the case of positive drift (considered here) only one exponential function “survives” in the leading asymptotic order for long trajectories and short lag times in expression (72) (because $\sigma^2 + 2\mu - r > \mu - r$).

In the limit of long lag times of this subregion of parameters we observe the exponential growth of the mean TAMSD with the lag time, Eq. (154), namely,

$$\overline{\langle \delta^2(\Delta) \rangle} \approx S_0^2 \frac{(\sigma^2 + 2\mu)e^{(\sigma^2 + 2\mu - r)\Delta}}{\sigma^2 + 2\mu - r}. \quad (73)$$

In the second subcase of the third regime, at $|\mu - r|T \ll 1$ and $(\sigma^2 + 2\mu - r)T \gg 1$, the exponential function $e^{(\mu - r)t}$ can be expanded in the entire interval of times, while the exponential function $e^{(\sigma^2 + 2\mu - r)T}$ dominates the magnitude of the TAMSD. In this subregime, we again obtain a TAMSD asymptote growing linear with the lag time and featuring a characteristic exponential dependence on the total trajectory length as a prefactor, see Eq. (155). From this expression—identical to that of the first subcase given by Eq. (72)—in the limit of weak drift and rare resetting—i.e., at $\sigma^2 \gg \mu$ and $\sigma^2 \gg r$ —one naturally arrives at the short-time TAMSD for nonreset drift-free GBM, namely

$$\overline{\langle \delta^2(\Delta) \rangle} \approx S_0^2 e^{\sigma^2 T} \times (\Delta/T). \quad (74)$$

At long lag times in this subcase we, again, find the exponential growth of the mean TAMSD, with the actual expression being identical to that obtained in the first subcase of the third regime; see Eqs. (73) and (156).

In the third subcase of the third regime, at $|\mu - r|T \ll 1$ and $|\sigma^2 + 2\mu - r|T \ll 1$, all exponential functions of the general expression for the mean TAMSD of reset GBM, Eq. (46), can be expanded at small values of their arguments in the limit of short lag times Δ , i.e., at $|\mu - r|\Delta \ll 1$ and $|\sigma^2 + 2\mu - r|\Delta \ll 1$. As a result, after algebraic simplification, a very simple expression for short-lag-time TAMSD growth is found, with the TAMSD magnitude being independent on the trajectory length T , namely,

$$\overline{\langle \delta^2(\Delta) \rangle} \approx S_0^2 \sigma^2 \Delta, \quad (75)$$

as given by Eq. (157). We can thus conclude that the dynamics in this subregion of parameters is ergodic if considered in the

sense of the equivalence of the behaviors of the variance (57) and the mean TAMSD (75) at short (lag) times. The detailed description of (non)ergodicity is presented in Sec. VII A; the consideration of the ergodicity-breaking parameter of reset GBM is outlined additionally in Sec. VII B.

At long lag times, the very same asymptotic behavior of the TAMSD (75) is found in this subregion of model parameters; see Eq. (157).

In the fourth subcase of the third regime, at $-(\mu - r)T \gg 1$ and $(\sigma^2 + 2\mu - r)T \gg 1$, for the short-time behavior of the mean TAMSD of reset GBM the exponential function $e^{(\mu - r)T}$ can be neglected, while another exponential function $e^{(\sigma^2 + 2\mu - r)T}$ [yet again] dominates the TAMSD magnitude and provides the characteristic prefactor in the linear asymptotic growth of $\overline{\langle \delta^2(\Delta) \rangle}$ in this subcase, with the asymptotic TAMSD expression being identical to that obtained in the first and second subcases of the third regime; see Eqs. (72) and (159), respectively.

At long lag times the characteristic TAMSD behavior in this subregion of parameters is, likewise, identical to those found in the first and second subcases, see Eqs. (73) and (160).

In the fifth subcase of this third regime of the TAMSD scaling behavior, in the subregions of parameters $-(\mu - r)T \gg 1$ and $(\sigma^2 + 2\mu - r)T \ll 1$, after expanding all exponential functions in Eq. (46) [except $e^{(\mu - r)T}$ that can be neglected] in the allowed regimes of their arguments and after algebraic simplification of the terms, we arrive from Eq. (46) at a peculiar TAMSD asymptote (161), given (in the leading order) by

$$\overline{\langle \delta^2(\Delta) \rangle} \approx S_0^2 \left(\sigma^2 + \frac{2\mu r}{\mu - r} \right) \Delta. \quad (76)$$

This, yet again, gives a linear dependence of the TAMSD on the lag time, with the prefactor depending on all relevant model parameters in the set $\{\sigma^2, \mu, r\}$ and on the length of the trajectory T .

At long lag times the TAMSD behavior in this subcase obeys the asymptotic law

$$\overline{\langle \delta^2(\Delta) \rangle} \approx S_0^2 \left[(\sigma^2 + 2\mu)\Delta + \frac{2\mu}{\mu - r} \right]. \quad (77)$$

In this expression, typically, the first term is larger than the second one for small drift values and, therefore (yet again), a linear growth of the mean TAMSD with the lag time is realized in this subregion of model parameters.

Lastly, for the sixth subcase of regime 3 of the TAMSD behaviors, at $-(\mu - r)T \gg 1$ and $-(\sigma^2 + 2\mu - r)T \gg 1$, after neglecting the respective exponential functions $e^{(\mu - r)T}$ and $e^{(\sigma^2 + 2\mu - r)T}$ (vanishing asymptotically in this subregion of parameters), we obtain the asymptotic expression for the mean TAMSD of reset GBM given by Eq. (163),

$$\overline{\langle \delta^2(\Delta) \rangle} \approx S_0^2 \frac{2r(\mu^2 + \sigma^2 r)}{(\sigma^2 + 2\mu - r)(\mu - r)} \Delta. \quad (78)$$

In the limit of frequent resetting, at $r \gg \{\sigma^2, \mu\}$, it turns into $\overline{\langle \delta^2(\Delta) \rangle} \approx 2S_0^2 \sigma^2 \Delta$, already obtained for the frequently reset drift-free GBM process in our short communication [1].

At long lag times and in the limit of frequent resetting, when $r\Delta \gg 1$ but still in the domain $\Delta \ll T$, the TAMSD

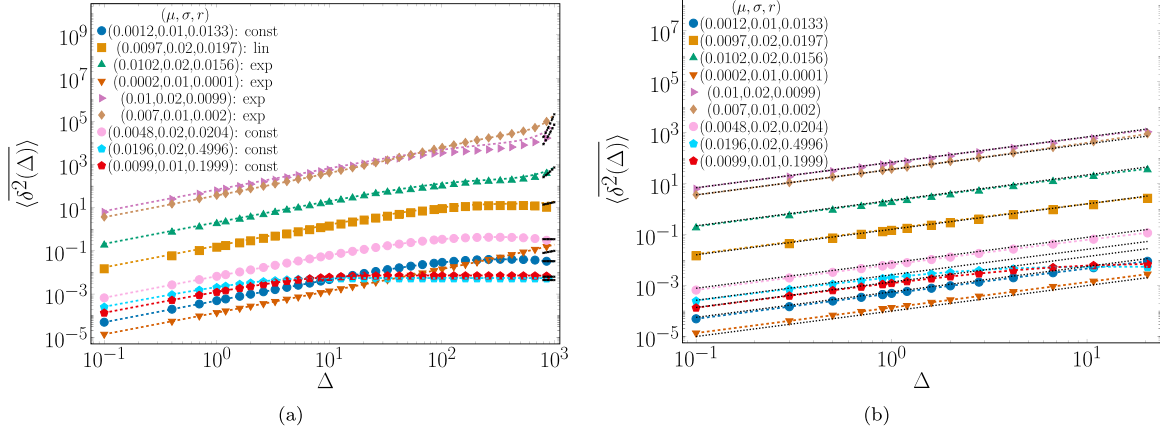


FIG. 5. The same as in Fig. 17 but the third region of parameters in Table IV. The parameters are the same as in Fig. 2. (a) The colored curves are according to Eq. (42), while the dashed asymptotes are plotted according to Eqs. (154), (156), (158), (160), (162), and (164). (b) The same as in Fig. 5(a) but presented at short times. The dashed linear are from Eqs. (153), (155), (157), (159), (161), and (163).

in this subcase reaches a plateau with the height given by expression (164), namely,

$$\overline{\langle \delta^2(\Delta) \rangle} \approx S_0^2 \frac{2r(\mu^2 + r\sigma^2)}{(r - \sigma^2 - 2\mu)(r - \mu)^2}. \quad (79)$$

This value is twice the plateau height of the variance in this NESS regime, as given by Eqs. (63) and (140), so that

$$\text{TAMSD}(\Delta) = 2 \times \text{Variance}(\Delta). \quad (80)$$

In the drift-free case, $\mu = 0$, clearly, the same relation (80) between the TAMSD and variance holds in the NESS, as follows from the TAMSD result

$$\overline{\langle \delta^2(\Delta) \rangle} \approx S_0^2 \frac{2\sigma^2}{r - \sigma^2} \quad (81)$$

and the result (64) for the variance (both obtained in Ref. [1]). We thus conclude that for the process of reset GBM featuring a nonzero first moment (33) the variance plays the same role as the MSD does for potential- and interval-confined processes with vanishing first moments. For the latter, the relation $\text{TAMSD} = 2 \times \text{MSD}$ holds in the plateau regime for the MSD and TAMSD, or in the quasistationary regime [202,203].

At the very last point of the trajectory, at $\Delta = T$, the mean-TAMSD magnitude of reset GBM attains in this subcase of regime 3 the value

$$\overline{\langle \delta^2(T) \rangle} \approx S_0^2 \frac{r\sigma^2 + \mu\sigma^2 + 2\mu^2}{(r - \sigma^2 - 2\mu)(r - \mu)}, \quad (82)$$

that is generally *not the same* as the variance at this point [still given by Eq. (64)]. The ratio of the two end-point quantities is

$$\frac{\overline{\langle \delta^2(T) \rangle}}{(\langle S(T) \rangle - \langle S(T) \rangle)^2} \approx \frac{r - \mu}{r} \frac{r\sigma^2 + \mu\sigma^2 + 2\mu^2}{\sigma^2 r + \mu^2}. \quad (83)$$

We stress here that in the drift-free reset-GBM scenario, in contrast, the TAMSD following from Eq. (82) has the same value as the variance (64) at the last point, so that one gets

$$\text{TAMSD}(T) = \text{Variance}(T). \quad (84)$$

This relation is, again, analogous to the $\text{TAMSD}(T) = \text{MSD}(T)$ equivalence found for confined stochastic processes with normal and anomalous dynamics, see, e.g., Refs. [202,203].

The graphical illustration of the mean-TAMSD evolution in this subregion of parameters, with a particular emphasis on the long-lag-time NESS regime, is shown in Figs. 6 and 7. As intuitively expected, at the highest rate of resetting the TAMSD plateau is most conspicuous and, as a result, the TAMSD-to-Variance ratio reaches strikingly the anticipated level of $\text{TAMSD}/\text{Variance}=2$ for this NESS regime. As Figs. 6 and 7 illustrate, the mean TAMSD at the last point drops in magnitude, see the colored dashed asymptotes on these plots.

For a drift-free frequently reset GBM the plateau expression (79) turns into twice the plateau of the variance for the same situation, as given by Eq. (64) and obtained by us in Ref. [1]. Note also that for such frequently reset

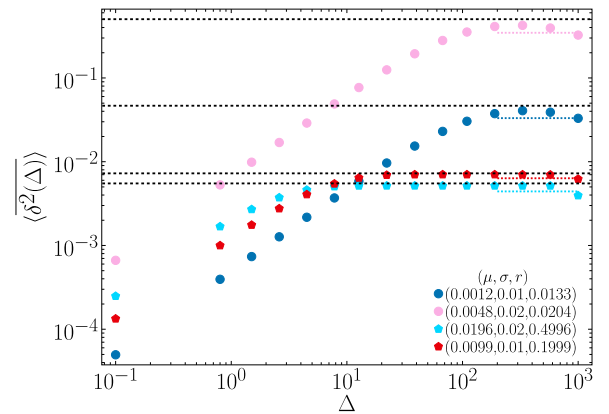


FIG. 6. Plateau magnitudes of the mean TAMSD in the frequent-resetting NESS-related regime (with the explicit parameters in this region indicated in the plot), as obtained from the results of computer simulations for the third regime. The theoretically expected relations (79) and (82) are indicated as the black and colored dotted asymptotes, correspondingly.

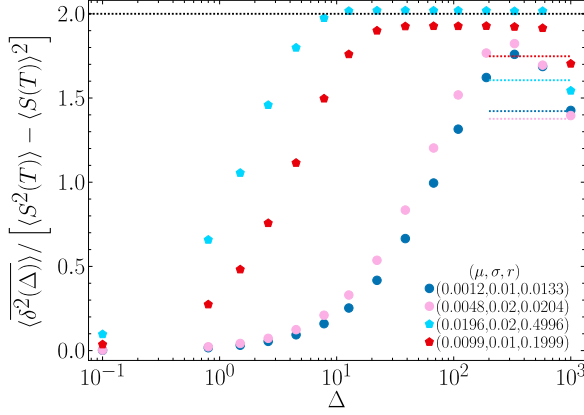


FIG. 7. Mean TAMSD, rescaled by the value of the variance computed at the last point of the trajectory, plotted for the third regime and for the parameters in the third region where the NESS is realized. Symbols are the results of computer simulations. The explicit values of relevant model parameters are given in the legend. The plateau level of TAMSD/Variance=2 given by Eq. (80) is the black line, while the theoretical expectations (83) are the colored dotted lines shown at large Δ values.

GBM at the very last point $\Delta = T$ the magnitude of the mean TAMSD (82) equals that of the variance (64). Such a behavior is reminiscent of the MSD-to-TAMSD relations unveiled, e.g., for FBM confined by parabolic potentials [202], for interval-bounded heterogeneous diffusion processes [203] as well as for the same two nonmultiplicative stochastic processes under Poissonian resetting considered by us in Refs. [71,98].

E. Summary of all regimes and asymptotic behaviors

Here, we present the detailed tables summarizing the asymptotic behaviors of the statistical quantifiers computed for all the regimes of behaviors in the respective regions of the model parameters, as considered above. The results for the first moment, the second moment, and variance, and the mean TAMSD are shown in Tables I, II, III, IV, correspondingly. The main findings of the current study are compared to the results of Ref. [1] for a simpler process of drift-free reset GBM in Table V.

VII. DISCUSSION AND CONCLUSIONS

A. Nonergodicity based on the MSD, variance, and TAMSD

We assess the nonergodicity of reset GBM based on the quantitative comparison of the short-time asymptotic laws of the second moment (and of the variance) to the short-lag-time behaviors of the mean TAMSD, see the corresponding columns of Tables II, III, and IV, respectively. We find that generally at short times the mean TAMSD *differs* from the second moment in all the regimes and from the variance in most of the regimes and, thus, the phenomenon of weak ergodicity breaking is observed for the process of Poisson-reset GBM. For drift-containing random walks, like the current ones, the variance—rather than the second moment—should be compared to the TAMSD to assess the ergodicity. The reason is that the first moment of both nonreset and reset GBM is, generally, nonzero.

We note that at short lag times the mean TAMSD always grows linearly in lag time. Comparing with the short-time behaviors of the second moment and variance we observe

TABLE IV. Asymptotes of the mean TAMSD for reset GBM.

$\overline{\langle \delta^2(\Delta) \rangle} / S_0^2$		Short lag times	Long lag times
		$\frac{(\sigma^2+2r)e^{(\sigma^2+r)T}}{(\sigma^2+r)T} \Delta$ (141)	$\frac{(\sigma^2+2r)e^{(\sigma^2+r)\Delta}}{\sigma^2+r}$ (142)
Regime 1		$2e^{rT} \Delta / T$ (143)	$2e^{r\Delta}$ (144)
$\mu = r$	$+(\sigma^2+r)T \gg 1$ $\begin{cases} r \gg \sigma^2 \\ r \ll \sigma^2 \end{cases}$	$e^{\sigma^2 T} \Delta / T$ (145)	$e^{\sigma^2 \Delta}$ (146)
	$ \sigma^2+r T \ll 1$	$(\sigma^2-r^2T)\Delta$ (147)	$\sigma^2 \Delta$ (148)
Regime 2	$ \mu-r T \ll 1$	$\sigma^2 \Delta$ (149)	$\sigma^2 \Delta$ (150)
$\sigma^2+2\mu=r$	$-(\mu-r)T \gg 1$	$(\frac{r(\sigma^2+r)T}{2} + \sigma^2 + 2r - \frac{4r^2}{\sigma^2+r})\Delta$ (151)	$2+rT - \frac{4r}{\sigma^2+r}$ (152)
Regime 3			
$\mu \neq r$	$+(\mu-r)T \gg 1$ $+(\sigma^2+2\mu-r)T \gg 1$	$\frac{(\sigma^2+2\mu)(\sigma^2+r)e^{(\sigma^2+2\mu-r)T}}{(\sigma^2+2\mu-r)^2T} \Delta$ (153)	$\frac{(\sigma^2+2\mu)e^{(\sigma^2+2\mu-r)\Delta}}{\sigma^2+2\mu-r}$ (154)
$\sigma^2+2\mu \neq r$	$ \mu-r T \ll 1$ $\begin{cases} +(\sigma^2+2\mu-r)T \gg 1 \\ \sigma^2+2\mu-r T \ll 1 \end{cases}$	$\frac{(\sigma^2+2\mu)(\sigma^2+r)e^{(\sigma^2+2\mu-r)T}}{(\sigma^2+2\mu-r)^2T} \Delta$ (155)	$\frac{(\sigma^2+2\mu)e^{(\sigma^2+2\mu-r)\Delta}}{\sigma^2+2\mu-r}$ (156)
		$\sigma^2 \Delta$ (157)	$\sigma^2 \Delta$ (158)
	$-(\mu-r)T \gg 1$ $\begin{cases} +(\sigma^2+2\mu-r)T \gg 1 \\ \sigma^2+2\mu-r T \ll 1 \\ -(\sigma^2+2\mu-r)T \gg 1 \end{cases}$	$\frac{(\sigma^2+2\mu)(\sigma^2+r)e^{(\sigma^2+2\mu-r)T}}{(\sigma^2+2\mu-r)^2T} \Delta$ (159)	$\frac{(\sigma^2+2\mu)e^{(\sigma^2+2\mu-r)\Delta}}{\sigma^2+2\mu-r}$ (160)
		$(\sigma^2 + \frac{2\mu r}{\mu-r} + \frac{(\sigma^2+2\mu)(\sigma^2+r)T}{2})\Delta$ (161)	$(\sigma^2+2\mu)\Delta + \frac{2\mu}{\mu-r}$ (162)
		$\frac{2r(\mu^2+\sigma^2r)}{(\sigma^2+2\mu-r)(\mu-r)} \Delta$ (163)	$\frac{2r(\mu^2+r\sigma^2)}{(r-\sigma^2-2\mu)(r-\mu)^2}$ (164)

TABLE V. Main differences of the long-time results for reset GBM obtained in Ref. [1] with zero drift (middle column, designated by the wavy-underlined results [to be compared to the respective double-underlined results in the right column]) and in the current study for a nonzero drift (right column), both for the conditions of frequent resetting. The expressions are presented for the first two moments, the variance, and the TAMSD (all normalized to the initial value of the process, as shown). The relative standard deviation—or the coefficient of variation—squared gives the EB parameter for the distribution of different TAMSD realizations, shown in the last row of the table. For drift-free reset GBM treated in Ref. [1] in the limit of frequent resetting and for long trajectories the first two moments, the variance, and the mean TAMSD all assume constant values and the NESS is thus realized. For drift-containing GBM, under similar conditions imposed onto the model parameters, in regime 3 all these statistical quantifiers also have constant values at long time, modified as compared to those derived in Ref. [1] due to nonzero drift, see the current and all the previous Tables. The situation changes drastically in regimes 1 and 2. Namely, in regime 2 only the first moment is constant, whereas the second moment, the variance, and the mean TAMSD feature terms growing linearly with time or with the trace length. Finally, in regime 1 already the first moment contains a linearly-in-time growing term, whereas the second moment, the variance, and the mean TAMSD are all growing rapidly—namely, exponentially—with the diffusion time or with the lag time. Thus, in the limit of long times no NESS is realized in regime 1 of reset GBM with a nonzero drift.

Statistical quantifiers	Reset GBM with $\mu = 0$	Reset GBM with $\mu > 0$
First moment, $\langle S(t) \rangle / S_0$	1, at $r \gg \sigma^2, rT \gg 1$	Regime 3: $\frac{r}{r-\mu}$, Eq. (100), at $r \gg 2\mu + \sigma^2, (r - \mu)T \gg 1$ Regime 2: 2, Eq. (92), at $(r - \mu)T \gg 1, r \gg \sigma^2$ Regime 1: $1 + rt$, Eq. (86), at all t
Second moment, $\langle S^2(t) \rangle / S_0^2$	$\frac{r}{r-\sigma^2}$, Eq. (7) of Ref. [1], at $r \gg \sigma^2, (r - \sigma^2)T \gg 1$	Regime 3: $\frac{r}{r-\sigma^2-2\mu}$, Eq. (116), at $(r - \mu)T \gg 1, (r - \sigma^2 - 2\mu)T \gg 1$ Regime 2: $1 + rt$, Eq. (110), at all t Regime 1: $2e^{rt}$, Eq. (104), at $(\sigma^2 + r)T \gg 1, r \gg \sigma^2$
Variance, $\langle (S(t) - \langle S(t) \rangle)^2 \rangle / S_0^2$	$\frac{\sigma^2}{r-\sigma^2}$, Eq. (10) of Ref. [1], at $r \gg \sigma^2, (r - \sigma^2)T \gg 1$	Regime 3: $\frac{r(\sigma^2+r+\mu^2)}{(r-\sigma^2-2\mu)(\mu-r)^2}$, Eq. (140), at $(r - \mu)T \gg 1, (r - \sigma^2 - 2\mu)T \gg 1$ Regime 2: $rt + 1 - \frac{4r^2}{(\sigma^2+r)^2}$, Eq. (128), at $(r - \mu)T \gg 1$ Regime 1: $2e^{rt}$, Eq. (120), at $(\sigma^2 + r)T \gg 1, r \gg \sigma^2$
TAMSD, $\overline{\langle \delta^2(\Delta) \rangle} / S_0^2$	$\frac{2\sigma^2}{r-\sigma^2}$, Eq. (15) of Ref. [1], at $r \gg \sigma^2, rT \gg 1$	Regime 3: $\frac{2r(\mu^2+r\sigma^2)}{(r-\sigma^2-2\mu)(r-\mu)^2}$, Eq. (164), at $(r - \mu)T \gg 1, (r - \sigma^2 - 2\mu)T \gg 1$ Regime 2: $2 + rT - \frac{4r}{\sigma^2+r}$, Eq. (152), at $(r - \mu)T \gg 1$ Regime 1: $2e^{r\Delta}$, Eq. (144), at $(\sigma^2 + r)T \gg 1, r \gg \sigma^2$
EB parameter, $\frac{\overline{\langle (\delta^2(\Delta) - \langle \delta^2(\Delta) \rangle)^2 \rangle}}{(\overline{\langle \delta^2(\Delta) \rangle})^2}$	$\propto \frac{1}{rT}$, Fig. 10 of Ref. [1], at $r \gg \sigma^2, rT \gg 1$	Regime 3: $\frac{\sigma^2}{(r-\sigma^2-2\mu)T}$, Fig. 10, at $(r - \mu)T \gg 1, (r - \sigma^2 - 2\mu)T \gg 1$ Regime 2: grows with $(r - \mu)$ and T , at $(r - \mu)T \gg 1$ Regime 1: grows with $(\sigma^2 + r)$ and T , at $r \ll (\sigma^2 + r)$

their general nonequivalence and, thus, the existence of weak ergodicity breaking for Poisson-reset GBM. This conclusion has already been communicated in our short study [1].

In some particular subcases, however, the equivalence of the TAMSD and the variance at short (lag) times is found. These are the situations of (a) the second subcase of the first regime in the limit $\sigma^2 \gg r^2T$, (b) the first subcase of the

second regime (producing ergodic dynamics irrespective of specific values of model parameters), (c) the third subcase of the third regime which is also always ergodic, and (d) the fifth subcase of the third regime in the limit of vanishing drift $\mu = 0$ and at $\sigma^2T \ll 1$. In these situations of “intermediate resetting” the process of reset GBM loses the typical exponential growth and becomes effectively ergodic.

For other subcases/subregimes in other subregions of the model parameters characterizing the process of reset GBM we observed so-called *ultraweak* ergodicity breaking [204]—when the corresponding mean TAMSD and the variance possess the same short-time functional dependence and only differ by a constant multiplicative factor. Note that for a number of subcases and scenarios this factor is, however, a quickly (exponentially) varying function of the trajectory length T leading to large differences in magnitude of these two quantifiers. Note also that for the case of frequent resetting, at $r \gg \sigma^2$ and $r \gg \mu$, for the sixth subcase of the third regime at short (lag) times the mean TAMSD is simply twice the variance in the same region of parameters and time domain.

We refer the reader to the short-time columns of Tables II and IV which demonstrate the (second moment)-to-TAMSD nonequivalence and to the respective columns of Tables III and IV for the variance-TAMSD comparison (as well as for the examination of variance-TAMSD ultraweak ergodicity breaking) for all possible subregions of the model parameters.

Several remarks are in place here. Firstly, we emphasize that the consideration of the increment-MSD—we introduced in the recent study [98],

$$\text{iMSD}(t_1, \Delta) = \langle (S(t_1 + \Delta) - S(t_1))^2 \rangle, \quad (165)$$

as an “improvement” of the standard MSD(Δ) for general power-law-like anomalous-diffusion processes—leads to the “restoration of ergodicity” in terms of the iMSD-to-TAMSD equivalence if the increments are examined for time instances t_1 late enough in the quasistationary NESS regime.

Secondly, we stress that the ensemble-based averages have been computed above as the standard arithmetic means for a set of available realizations. Averaging procedures based on the geometric mean have, however, also been used in some single-particle tracking experiments [205,206]. We refer the reader, e.g., to the recent studies [207,208] for the general functional expected-value Kolmogorov-Nagumo procedure [209,210], discussed also for a class of multiplicative processes by Kirkwood in Ref. [211] and by Samuelson in Ref. [212], as well as to the concepts of “optimal” averaging by Chisini (see Refs. [213,214]). The most physically appropriate mathematical definition for the “functional average” for computing the means and the “generalized” TAMSDs—with the subsequent assessment of nonergodicity in terms of these redefined ensemble- and time-based averages—for a general drift-containing stochastic process is *a priori* not clear. For instance, different generalized means might be appropriate for processes with a power-law, exponential, or logarithmic growth of the MSD. This issue, being beyond the scope of the current study, deserves a separate investigation.

Thirdly, another modification for drift-containing nonzero-mean processes can be proposed. Namely, in addition to Eq. (2), the “increment-TAMSD” definition $\overline{\delta\delta^2(\Delta)}$ is also tantalizing [187],

$$\overline{\delta\delta^2(\Delta)} = \frac{\int_0^{T-\Delta} [S(t+\Delta) - S(t) - \langle S(t+\Delta) - S(t) \rangle]^2 dt}{T - \Delta}. \quad (166)$$

This way, the deviation of the increments from the mean value of the increments is considered as the integrand of this increment-TAMSD. A similar “recalibration” of the MSD can be performed too, see Refs. [98,215], to remove the effects of drift and of the initial conditions imposed. We mention here also the recent approach [216] aimed at redefining the MSD and the TAMSD functionals for stochastic processes with a space-dependent dynamics [203,217,218], yielding a homogeneous-in-space and ultimately ergodic dynamics in terms of the transformed ensemble- and time-averaged quantities. For simplicity, we restricted ourselves above to the standard definitions of the MSD and TAMSD given by Eqs. (1) and (2), respectively.

B. Nonergodicity based on the EB parameter

After the calculations of Ref. [1] were finished, we became aware of an alternative study [73] aimed at assessing nonergodicity of reset GBM. The fundamental difference of the analysis [73] from our short study [1] as well as from the current calculations is the process-universal definition of nonergodicity we are pursuing in terms of the nonequivalence of the MSD and the (mean) TAMSD [152]. The degree of nonergodicity can be quantified via the value and the decay properties of the so-called ergodicity-breaking parameter [150–152,219],

$$\text{EB}(\Delta) = \langle (\overline{\delta^2(\Delta)})^2 \rangle / \overline{\delta^2(\Delta)}^2 - 1, \quad (167)$$

as a function of normalized lag time, $\text{EB}(\Delta/T)$.

The EB parameter quantifies the dispersion of individual TAMSD trajectories near their mean, obtained upon using different realizations of noise for a time series of a stochastic process. Individual TAMSD traces are, thus, endogenously fluctuating quantities [151,152], even for the [most] ergodic stochastic process of paradigmatic Brownian motion. At short lag times and for long trajectories, at $\Delta/T \ll 1$, the behavior of EB for a given stochastic process is often compared to that known for Brownian motion [152,178,220],

$$\text{EB}(\Delta) \approx 4\Delta/(3T). \quad (168)$$

In the limit $\Delta/T \rightarrow 0$ the statements based on assessing the values of EB and its functional dependence on the lag time and trajectory length are known to be statistically most reliable [152]; we thus focus on this regime in the description below. A special consideration will be devoted to calculations of EB for reset and pure GBM in a future analytical study [221], to complement the results of computer simulations for the EB evolution presented below and in Ref. [183].

The results of our computer simulations for drift-free reset GBM indicate that as an [on average] exponentially growing process of GBM is being reset progressively more often, the spread of individual $\overline{\delta^2(\Delta)}$ trajectories gets generally reduced. This effect takes place both at short and long lag times; see Fig. 9 of Ref. [1] as well as the situation of frequent resetting in Fig. 8 representing the TAMSD spread for the third region of model parameters. We show $N = 20$ individual traces for each parameter choice for the first, second, and third regime of functional behaviors of reset GBM in Figs. 8, 19, and 20, respectively. The results of EB simulations for nonreset GBM were presented in Ref. [183]. For Poisson-reset drift-free

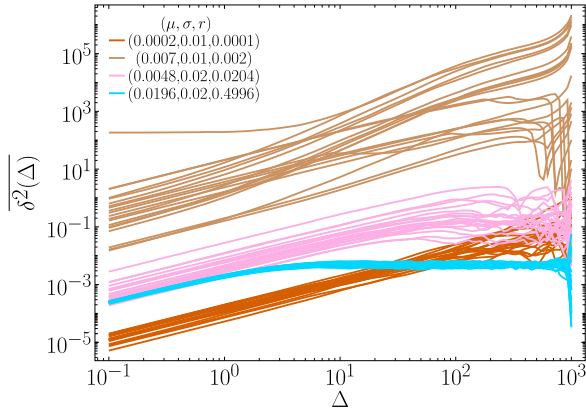


FIG. 8. The same as in Fig. 19 but for the third regime of model parameters and of TAMSD variation. The triplets of values of drift, volatility, and reset rate used in the computations are provided in the legend. Other parameters are the same as in Fig. 2.

GBM the EB(Δ) results were presented in Ref. [1], while for the drift-containing scenario they are shown in Figs. 9, 21, and 22, respectively for regimes 1, 2, and 3 of model parameters. To illustrate the scale of the obtained EB values, each of the latter EB plots we supplement with the Brownian-motion asymptote (168).

For the drift-free reset-GBM scenario, the analysis of EB(Δ_1) variation at short lag times $\Delta = \Delta_1 = \Delta t$ with the reset rate r also unveils that for the conditions of frequent resetting, at $r \gg \sigma^2$, in the long-time NESS we observed [1]

$$EB(\Delta_1) \approx 1/(rT). \quad (169)$$

Remarkably, a robust nonmonotonic variation of the EB-plateau values at short lag times for drift-free reset GBM as a function of r was found, with a peak of EB at intermediate reset rates, see Fig. 10 in Ref. [1]. Note that other reset random walks—such as, e.g., nonmultiplicative reset FBM and heterogeneous diffusion processes under Poissonian

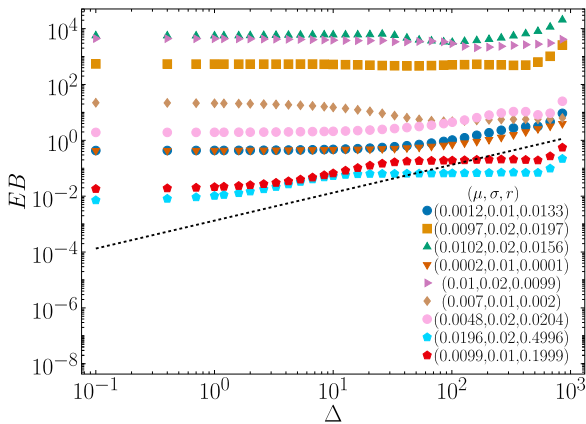


FIG. 9. The same as in Fig. 21 but in the third regime of model parameters. Multiple triplets of drift, volatility, and reset rates are listed in the legend. The parameters are the same as in Fig. 2. The dashed line is the Brownian-motion asymptote (168).

resetting, as we demonstrated recently [71]—also feature this peculiar nonmonotonic EB(Δ_1, r)-versus- r dependence. We remind the reader that the NESS features a time-independent PDF of particle displacements; see Sec. III B.

We describe now the variation of EB(Δ) and of EB(Δ_1, r) for the three regions of parameters of reset GBM with a nonzero drift. We observe that often the EB parameter in the limit $\Delta \rightarrow 0$ has a nearly lag-time-insensitive behavior, with much higher levels than the EB values at the same [short] lag times for Brownian motion, as shown in Figs. 9, 21, and 22. This behavior—valid for all three regions of model parameters—supports the statement that both pure [183] and reset [1] GBM are generally nonergodic processes.

Note that for frequently reset GBM, the plateau of EB at intermediate-to-long lag times can be considerably smaller than the value (88). We emphasize here also that the shape of EB(Δ)-dependence for reset GBM is similar to that detected in the recent analysis of other reset [71] and potential-confined [222] random walks.

We describe now the variation of EB parameter with the lag time for three regimes of model parameters, as presented in Figs. 21, 22, and 9, respectively.

1. Regime 1

In the first region of model parameters, we find that the overall values of EB typically increase with σ^2 ; see Fig. 21. Also, for a fixed σ^2 value the magnitude of the EB parameter computed at short lag times increases with growing values of $\mu = r$; see Fig. 21. This increasing trend persists for large r values. The drift-free asymptotic law (169) for EB versus r dependence is however *not followed* [results not shown (see, however, Table V)]. The reason for a drastically different behavior of EB(Δ_1, r) is a “compensation” of resetting by drift in virtue of $\mu = r$ condition in this regime of variation.

2. Regime 2

In the second region of parameters, similar to the first one, a nonmonotonic dependence of the EB parameter with lag time is observed for some combinations of the model parameters; see Fig. 22. The EB parameter varies from a plateau-like behavior at short lag times, to a drop at intermediate Δ , and, finally, to a region of increasing EB at long lag times, up to $\Delta \rightarrow T$. Also, similarly to the behavior in the first regime, we find the overall increase of EB values at short lag times with σ^2 and an “inverted” dependence of EB(Δ_1, r) on the reset rate (results not shown, see Table V).

3. Regime 3

For the third regime of EB behavior, the reset rate is not conditionally coupled to the values of drift and volatility (as compared to the other two regions of parameters) and r can be varied independently. Reset rates can reach large values assuring the existence of the NESS in this regime of model parameters. Frequent restarts, in turn, make the process of reset GBM more reproducible in the sense of a reduced spread of TAMSDs and more ergodic in the sense of smaller values of the ergodicity-breaking parameter, EB. These dependencies

are presented, respectively, in Figs. 8 and 9 for the model parameters in the same third regime (as for all other figures in the main text). For frequent-reset conditions in this region of parameters—denoted by the red and cyan pentagonal symbols in Fig. 9—after an increase of EB at short lag times (at $\Delta \ll r$) a plateau of EB at long lag times is being detected. These plateau time-domains correspond to the plateaus of the mean TAMSD for the same parameters in this regime, compare Fig. 6 versus Fig. 9, but the EB plateaus are realized at somewhat longer lag times (compare the same pentagonal symbols for the same parameters in Figs. 6, 7, and 9).

Similarly to the frequent-reset regime of drift-free GBM [1], the EB parameters at short lag times—as well as the EB plateaus at intermediate-to-long lag times—exhibit a non-monotonic dependence on r , with a maximum at intermediate reset rates. As GBM is a rapidly growing process, at intermediate reset rates the impact of large increments of the process induced at the points of reset appears to be maximized in terms of the largest resulting EB values. The process of reset GBM itself departs far enough from the starting price and the occurring reset jumps perturb the TAMSD values and the uncertainty of the TAMSD trajectories strongly enough so that the maximum of the EB parameter emerges at intermediate r values.

At very large reset rates, on the contrary, the process is being interrupted too frequently so that such reset GBM has not yet grown enough in value (starting from the reset price S_0) before the next reset event takes place. As a consequence, typically both the magnitude of the TAMSDs and their trajectory-to-trajectory fluctuations decrease at larger r , thus causing the EB value to drop for the conditions of very frequent resetting. This behavior is only observed in the third regime in the long-time NESS-related scenario, when the moments, the variance, the TAMSD, and (to a certain extent) the EB parameter are bounded.

In the parameter region $r \gg \{\mu, \sigma^2\}$, the short-lag-time EB values decrease with r similarly to expression (169), namely,

$$EB(\Delta_1) \propto f(\sigma^2, \mu)/r, \tag{170}$$

where the prefactor $f(\sigma^2, \mu)$ is a function of the strength of randomness and the drift magnitude; see Fig. 10. The reduction of EB values computed at short lag times with reset rate r indicates smaller fluctuations of “price displacements” in the trajectories of such reset drift-containing GBM, yielding a more reproducible and more ergodic process in terms of the EB magnitude. The effective “reset-rate parameter” replacing r in this third regime is the reset rate renormalized by drift and randomness parameters, namely,

$$\tilde{r} = r - 2\mu - \sigma^2, \tag{171}$$

as used for the abscissa coordinate in Fig. 10. The NESS thus emerges at long times for large values of \tilde{r} .⁶ We refer the reader to Table V for the summary of the long-time behaviors

⁶Here, a remark is in place regarding the time-discreteness effects occurring in simulations, Δt . We have recently examined the implications of such effects on the ergodic properties of pure [178] and Poisson-reset [71] FBM. We found—both analytically and via performing stochastic computer simulations—that for the ordinary,

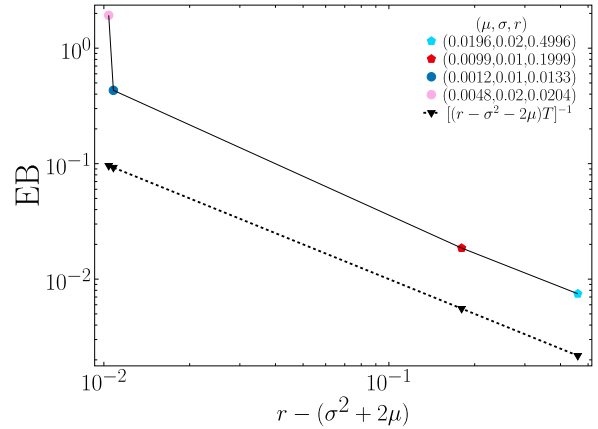


FIG. 10. Variation of the EB parameter at short lag times $\Delta = \Delta_1$ versus the “effective” rate of reset computed for the model parameters in the third region (see the legend; with $r = \sigma^2 + 2\mu$ defining the border of this parameter region). Other parameters are the same as in Fig. 2. The dashed-line asymptote portrays the EB decay law (168).

of the EB parameter—as well of the moments, variance, and TAMSD—in all three regions of the model parameters.

We note that for reset FBM a dependence similar to Eqs. (169) and (170) was detected [71], $EB(\delta t) \propto f(H)/(rT)$, with the prefactor $f(H)$ depending on the Hurst exponent H ; see Fig. 4 in Ref. [178]. A similar characteristic decay of the EB values at high reset rates—indicative of progressively more ergodic dynamics—was also found for the “hybrid” reset process of FBM and heterogeneous-diffusion process in Ref. [178]. We stress here, however, that for reset FBM the trend $EB \propto 1/r$ stops at extremely high reset rates, when $r \times \delta t \sim 1$. In this limit, the reset events take place almost every time step and the assumptions of the Poissonian statistics can be violated. As a result, the EB parameter of frequently reset FBM does not actually vanish at $r \rightarrow \infty$ but reveals a more intricate behavior, see Fig. 5 of Ref. [178] for details. We do not reach such extreme reset rates in the current simulations of reset drift-containing GBM, see Fig. 10 where (as in all other plots) the simulation time-step was 0.1.

C. Nonergodicity in economics

Recently, the problems of nonergodicity in economics (both within the GBM-based models and well beyond it) [199,223–226], wealth inequality [74,120,227–230], nonergodicity in psychological and biological science [162,231] as well as in decision-making models [232] were discussed in the literature.

Specifically, in the alternative approach to the nonergodicity of reset GBM proposed in Ref. [73]—we became

free FBM process the value of EB at short lag times reveals a time-step-dependent plateau, $EB(\Delta_1 = \Delta t) \propto \Delta t/T$. The manifestations of varying Δt onto the EB parameter for GBM in the same domain of short lag times remains to be examined and understood [221].

aware of after finishing the main calculations of Ref. [1]—no process-invariant rigorous and universal criteria based on the MSD-vs-TAMSD equivalence [152] and on certain decay properties of the ergodicity-breaking parameter $EB(\Delta, T)$ [152,222,233] were implemented. Instead, as proposed for the analysis of nonergodicity of nonreset GBM [224], a convenient but nonunique characteristic of the logarithmic growth rate was employed in Ref. [73] (see also recent Ref. [231] for different “ergodic descriptors”). This quantifier effectively “removes” the exponential growth-trend of GBM, so that the time-variation of the natural logarithm of a “finite-sample” average trajectory is considered [73,198,224], namely,

$$g(t, N) = \frac{\delta}{\delta t} \log \left[\frac{1}{N} \sum_{i=1}^N S_i(t) \right]. \quad (172)$$

The noncommutativity of the ensemble average $\langle g(t) \rangle = \lim_{N \rightarrow \infty} g(t, N)$ computed for an infinite sample of trajectories and the “time average” of the growth rate in the limit of infinite time [for a fixed number of traces N]—denoted by the wide tilde as $\widetilde{g(N)} = \lim_{t \rightarrow \infty} g(t, N)$ as in Ref. [1] [to distinguish from the sliding-window time-averaging procedure (2)]—was attributed to nonergodicity for both pure [199,224] and reset [73] GBM.

Note that the best strategy of portfolio growth based on optimizing the geometric mean and respective returns in long sequences of investment events and the Kelly criterion, see Refs. [117,212,234,235], has a long history (going back to Bernoulli [236–238]). The same concept of maximizing the geometric-growth-rate is utilized in the population dynamics, with a subpopulation featuring the best “fitness” (defined this way) turning dominant in the long term in an ensemble of subpopulations which are simultaneously growing (exponentially) with various traits; see, e.g., Refs. [148,239,240].

We stress, however, that frequently reset GBM is not growing exponentially: it is rather a stalling diffusion process, thus questioning the use of a logarithm of the growth rates, such as that in Eq. (172). Note also that the same quantifier (172) was recently used to assess nonergodicity in the wealth-growth dynamics and the associated reallocating-GBM process [74]. The latter process mimics the redistribution of taxes collected from a richer fraction in a collective of individuals among all of them (see, e.g., Ref. [120] for a review on income distribution and inequality dynamics).

Instead of a growth-rate-based signature of nonergodicity (172), in Ref. [1] and here we followed the universal approach employed over the last decade—by us and in the wide stat-phys community—to quantify the degree of nonergodicity of a plethora of anomalous-diffusion processes highly variable in their stochastic “nature” [152]. The list of such (non)ergodicity analyses includes the studies of continuous-time random walks [150,187,241], Lévy walks [204,242,243], FBM [220,244,245] (also in the underdamped case [246,247]), standard [248–252] and ultraslow [253] scaled Brownian motion, exponential and logarithmic (under- and overdamped) scaled Brownian motion [233], heterogeneous diffusion processes [217,218,254,255], scaled Brownian motion in the presence of heterogeneous diffusion [256], diffusing-diffusivity process for Brownian [176,177] and for scaled Brownian [257,258] motion, FBM with the

diffusing-diffusivity process [178], FBM with heterogeneous diffusion processes [71,259], FBM with scaled Brownian motion [260] (as well as multiple variants of these processes in the presence of external potentials, under interval-based confinement, ageing conditions, etc.).

We emphasize here once again that a descriptor of nonergodicity not involving the time-averaging concept and the TAMSD *per se* cannot be considered as a rigorous statistical measure of nonergodicity. In a well-established sense, the long-time equivalence of the time-averaged quantities to their probabilistic ensemble-based averages is the prerequisite of an ergodic behavior [151,152,154,160]. Moreover, the quantitative analysis of pertinent functional behaviors of the ergodicity-breaking parameters of reset GBM as a function of lag time, trace length, and reset rate delivers additional important insights on the actual *degree of ergodicity*, enabling a tractable EB-based comparison of “realizations” of a system at different values of its parameters. The analytical analysis of the EB evolution for pure and reset GBM will be the subject of a separate investigation [221]. The epistemology and usefulness of the two ergodicity-assessment approaches (with their totally different underlying concepts) to the problems of financial mathematics, to the analysis of option-pricing data, as well as to the general problems of wealth distribution [261] and of economic growth in a society remain to be understood.

D. Summary of the main results

This study extends the investigation of the time-averaged and ergodic properties of the process of Poisson-reset GBM, decisively generalizing the results of the simplest driftless reset-GBM ($\mu = 0$) we presented recently as a short communication [1]. We here quantified in detail the asymptotic behaviors of the first and second moments of reset GBM, the variance, the PDF, and—most importantly and most mathematically involved—the mean TAMSD in all regions of model parameters. The analytical results obtained in all the regimes are in excellent agreement with the findings of stochastic computer simulations. Additionally, the results of *in silico* simulations for the behavior of the EB parameter in all the regimes were examined.

Nonzero drift has dramatically enhanced the number of possible asymptotic regimes of all the above-mentioned displacement-related quantifiers, both at short and long times, as compared to their behaviors for drift-free reset GBM [1]. For reset GBM with a nonzero drift the asymptotic behaviors in the regimes of rare ($r \ll \{\sigma^2, \mu\}$) and frequent ($r \gg \{\sigma^2, \mu\}$) resetting were obtained and systematically examined. We obtained that the second moment from ensemble-based-averaging as well as the variance of the process generally differ from the trajectory-based-averaging quantified by the TAMSD and, therefore, reset GBM with a drift is one more example of a stochastic process featuring weak ergodicity breaking [151,152].

The main differences in the characteristic behaviors of the main statistical quantifiers of the drift-containing process—as compared to those of drift-free reset GBM with the parameter space $\{\sigma^2, r\}$ [1]—are summarized in Table V and shortly overviewed below. The existence of multiple regions in the space of parameters $\{\sigma^2, \mu, r\}$ redefines the conditions for the

existence of the NESS. Namely, while for the drift-free reset GBM [1] the NESS is observed at $r \gg \sigma^2$, for reset GBM with a nonzero drift the NESS is realized in regime 3 (the third region of parameters) at $r \gg 2\mu + \sigma^2$ in the limit of a large number of reset events occurring within a trajectory. The PDF of particle displacements in the NESS is stationary: a plateau-like or converging behavior of the first two moments—as well as of the variance and of the TAMSD—is a prerequisite of the NESS at long times in this regime of model parameters. We focus in Table V on the long-time behavior and on the NESS conditions in the scenarios $\mu = 0$ (Ref. [1]) and $\mu \neq 0$ (regime 3 of this study) of the process of reset GBM, while all scaling behaviors in the limits of short- and long times and for various conditions on the three main model parameters are overviewed in Tables I, II, III, and IV.

The conditions for the existence of converging first and second moments (26) define the two boundaries in the three-dimensional space of model parameters $\{\sigma^2, \mu, r\}$ of reset GBM with a nonzero drift. At these boundaries the first two moments, the variance, the TAMSD, and the EB parameter all differ decisively in their characteristic dependencies compared to those in Ref. [1]; see the right and middle column of Table V, correspondingly. Specifically, while in the third regime of the current study the functional scaling relations for all these statistical quantifiers turn in the limit of zero drift, for frequent-resetting conditions, and for long trajectories (with many reset events) into those obtained by us previously in the similarly constructed NESS regime in Ref. [1], the behaviors in regimes 2 and 1 are entirely different.

Concretely, in regime 2 the first moment attains a constant value, whereas the second moment, the variance, and the TAMSD grow with time—or trajectory length—linearly; see Table V. In regime 1 the first moment is already not a constant but rather a linearly growing function of time, whereas the second moment, the variance, and the TAMSD grow exponentially with time (or lag time). We stress here that the asymptotic behavior for the first moment in regime 1 and of the second moment in regime 2 are valid for all diffusion times t and do not require any additional conditions for the model parameters to be satisfied. There are no subcases in the above-mentioned subcases and regimes: the “effective” strength of resetting is $r - \mu = 0$ for the first moment for regime 1 and it is $r - \sigma^2 - 2\mu = 0$ for the second moment for regime 2.

The EB parameter at short lag times in the NESS for regime 3 considered here and for the results of Ref. [1] decreases linearly with the [effective] rate of reset, namely, as $\propto 1/[(r - \sigma^2 - 2\mu)T]$ and $\propto 1/(rT)$, respectively; see Table V. The dependence of EB on r in regions 2 and 1—with the moments not converging at long time (see above)—is totally different. Here, the process of reset GBM does not become increasingly ergodic as r increases: the respective EB parameter at short lag times does not decrease for more frequently occurring resetting events.

For the EB parameter, in regime 1 only the limit of weak resetting in terms of the effective reset rate $r - \sigma^2 - 2\mu$ exists. The EB values grow in this case [roughly as $\propto rT$] as $\sigma^2 + 2\mu - r \approx \sigma^2 + r$ increases (results not shown). For EB in regime 2 only the limit of strong resetting in terms of $r - \mu$ exists: the EB values grow as $r - \mu$ increases (again roughly

as $\propto rT$, results not shown). The EB parameter in regime 3 has both the limits of strong and weak resetting in terms of the effective reset rate $r - \sigma^2 - 2\mu$. In the weak-resetting limit EB at short lag times seems to scale roughly as $\propto rT$, while for strong resetting we clearly observe the dependence $\propto 1/[(r - \sigma^2 + 2\mu)T]$, see Table V.

The latter dependence—being the most essential result of the current analysis of the EB behavior—turns into the results of Ref. [1] for drift-free reset GBM. Further analytical investigations are needed to understand the details of the intricate behavior of the EB parameter of both nonreset and reset GBM in the general scenario with a nonzero drift. This can certainly be the subject of future investigations [221]. The quantitative application of the MSD, TAMSD and EB results of reset GBM to the analysis of real financial data (e.g., for time series of some reset- or barrier-option prices) is of immediate relevance. This is, however, also beyond the scope of the current study. Here, in particular, the importance of including a nonzero drift to the process of reset GBM (as an underlying mathematical model) as well as a possibility of drawing certain predictions—based, e.g., on the trends of the approach of reset GBM to the NESS—can be of practical interest.

E. Perspectives

Reset-GBM-like stochastic processes can describe the growth dynamics of stock-market prices subject to stochastically(?) occurring bubble-bursting events and economic crashes [261–264] (with the magnitude of an index drop reflecting the impact of a crisis), the spreading dynamics of infection in a population subjected to strict lockdown measures (aimed at eradicating the disease), as well as the telephone queues featuring a log-normal distribution of required service times [265–267], with long waiting times amenable to mitigation via Poissonian resetting [87]. Several examples of log-normal distribution [268] in human behavior were addressed in Ref. [269] (see also Ref. [270] for a historical perspective). Models of catastrophic events in queuing systems were also developed [271,272], including the analysis of steady-state probabilities [271].

Reflecting back on the path-dependent and reset options mentioned Sec. IA, our current TAMSD-based analysis potentially enables to extract the model parameters μ , σ^2 and r from the analysis of the time series of real reset-type options (see Ref. [183] for the respective numerical procedures). The quantitative comparison of the theoretical predictions of the current study and the behavior of reset- and barrier-type options (describable by GBM with a bankruptcy risk [273]), in particular from the perspective of the TAMSD, is potentially promising. A quantitative examination of the threshold-crossing statistics of the time series of barrier- and reset-type options could provide valuable information regarding the applicability of the Poissonian statistics for a reset GBM in such situations and also to suggest possible modifications pertinent to the quantitative description of the statistics of jumps for these options. Data-driven time-series analyses of this kind deserve a separate investigation (beyond the scope of the current theoretical study); this can be of interest also for option-trading practitioners.

Note also that the *modus operandi* of barrier options—with the two levels limiting the process evolution—involves large deviations [274,275], extreme-value statistics [276–282] (also with a nonzero drift [283]), and the max-min distributions [284] to unveil the barrier-crossing characteristics (for both up- and downwards jumps occurring in the time series). The ultimate goal would be to envisage/forecast whether the crossings of a preset price level will occur within a preset time-span [285]. This goal reaches to the “holy grail” of financial mathematics—see the recent perspectives [286–288], also on the “pandemic economics” [289,290]—

often involving multiplicative, hardly predictable stochastic processes.

ACKNOWLEDGMENTS

A.G.C. is grateful to Humboldt University of Berlin for hospitality and support. A.G.C. thanks H. Safdari, J. Shin, S. Thapa, and W. Wang for providing rare and inaccessible articles. We thank G. Oshanin for making us aware of Ref. [129]. R.M. acknowledges support from the Deutsche Forschungsgemeinschaft (DFG Grant No. ME 1535/12-1).

APPENDIX A: DERIVATION OF THE RESET TAMSD

The mean TAMSD of reset GBM is calculated using Eq. (2), which can be expanded into three terms as

$$\langle \overline{\delta^2(\Delta)} \rangle = \underbrace{\frac{1}{T-\Delta} \int_0^{T-\Delta} dt \langle S^2(t+\Delta) \rangle}_{I_1} + \underbrace{\frac{1}{T-\Delta} \int_0^{T-\Delta} dt \langle S^2(t) \rangle}_{I_2} - 2 \underbrace{\frac{1}{T-\Delta} \int_0^{T-\Delta} dt \langle S(t)S(t+\Delta) \rangle}_{I_3}. \quad (\text{A1})$$

The mean TAMSD was split into I_1 , I_2 , and I_3 terms for ease of calculation. This “standard” splitting procedure produces two standard TAMSD terms and one term with the time-shifted correlator of the process. The latter term (with its integral) is notoriously—as also the current case—much more complicated to compute analytically.

Using the expression for the second moment (36) at time $(t+\Delta)$ and performing the integration, we get for I_1 that

$$I_1 = S_0^2 \begin{cases} \frac{1}{T-\Delta} \frac{(\sigma^2+2\mu)(e^{(\sigma^2+2\mu-r)T} - e^{(\sigma^2+2\mu-r)\Delta})}{(\sigma^2+2\mu-r)^2} - \frac{r}{\sigma^2+2\mu-r}, & \sigma^2 + 2\mu \neq r, \\ 1 + \frac{r}{2}(T+\Delta), & \sigma^2 + 2\mu = r. \end{cases} \quad (\text{A2})$$

The term I_2 is similar, with the only difference being at time t , therefore

$$I_2 = S_0^2 \begin{cases} \frac{1}{T-\Delta} \frac{(\sigma^2+2\mu)(e^{(\sigma^2+2\mu-r)(T-\Delta)} - 1)}{(\sigma^2+2\mu-r)^2} - \frac{r}{\sigma^2+2\mu-r}, & \sigma^2 + 2\mu \neq r, \\ 1 + \frac{r}{2}(T-\Delta), & \sigma^2 + 2\mu = r. \end{cases} \quad (\text{A3})$$

The calculation of the term I_3 in Eq. (A1) is considerably more involved and the required autocorrelation function is calculated via classifying possible trajectories of the reset process based on the occurrence of resetting events at different times. We, thus, extend the arguments of Ref. [45], applicable to any resetting process with a finite reset time, including the process of Poisson-reset GBM. We calculate I_3 in the interval $[t, t+\Delta]$ and the classification of resetting events is based on the same time domain.

There exist three classes of trajectories (with reset events) contributing differently to the autocorrelation function. For the first class, no reset event till time $(t+\Delta)$ has occurred. These are essentially traces of a nonreset stochastic process, denoted as $X(t)$. With the Poisson-distributed times of resetting events, the probability of such an event is $e^{-r(t+\Delta)}$ [the general expression via the reset-waiting-time density is $\int_{t+\Delta}^{\infty} \psi(z) dz$]. In combination, the contribution of the first class of trajectories is

$$e^{-r(t+\Delta)} \langle X(t)X(t+\Delta) \rangle. \quad (\text{A4})$$

The second class comprises the trajectories for which the last resetting event occurred before the interval of interest, i.e., at times $z < t$. These trajectories behave as a stochastic process with no resetting starting at time z , so that the autocorrelation is $\langle X(t-z)X(t-z+\Delta) \rangle$. The probability

associated with such a trajectory is $re^{-r(t+\Delta-z)} dz$ [generally, $\psi(t+\Delta-z) dz$]. The contribution of the second class of trajectories to the autocorrelation accounts for all such traces with $z < t$, namely,

$$\int_0^t re^{-r(t+\Delta-z)} \langle X(t-z)X(t-z+\Delta) \rangle dz. \quad (\text{A5})$$

Using the transformation of variables $\tau = t-z$ we find

$$e^{-r\Delta} \int_0^t d\tau re^{-r\tau} \langle X(\tau)X(\tau+\Delta) \rangle. \quad (\text{A6})$$

For the third class of trajectories a resetting event occurs in the interval of interest, i.e., at a time $z > t$. For such trajectories $S(t)$ and $S(t+\Delta)$ are uncorrelated because they are separated by one or more resetting events. The autocorrelation function splits into the respective expectation values, with $\langle S(t) \rangle$ and $S(t+\Delta)$ being a stochastic process with no resetting starting at z with the expectation value $\langle X(t+\Delta-z) \rangle$ [the general expression is $\psi(t+\Delta-z) dz$]. Using the probability associated with such trajectories, $re^{-r(t+\Delta-z)} dz$, the contribution from all of them amounts to

$$\int_t^{t+\Delta} re^{-r(t+\Delta-z)} \langle S(t) \rangle \langle X(t+\Delta-z) \rangle dz. \quad (\text{A7})$$

Using the variable transformation $\tau = t + \Delta - z$ we get

$$\langle S(t) \rangle \int_0^\Delta d\tau r e^{-r\tau} \langle X(\tau) \rangle. \quad (\text{A8})$$

The entire autocorrelation function is then found by combining expressions (A4), (A6), and (A8) in the form

$$\langle S(t)S(t + \Delta) \rangle = \underbrace{e^{-r\Delta} \left[e^{-rt} \langle X(t)X(t + \Delta) \rangle + \int_0^t d\tau r e^{-r\tau} \langle X(\tau)X(\tau + \Delta) \rangle \right]}_{C_1} + \underbrace{\langle S(t) \rangle \int_0^\Delta d\tau r e^{-r\tau} \langle X(\tau) \rangle}_{C_2}. \quad (\text{A9})$$

For a general form of the waiting-time distribution of resetting events, $\psi(\tau)$, we obtain

$$\begin{aligned} \langle S(t)S(t + \Delta) \rangle &= \langle X(t)X(t + \Delta) \rangle \int_{t+\Delta}^\infty \psi(\tau) d\tau \\ &+ \int_0^t d\tau \psi(\tau) \langle X(\tau)X(\tau + \Delta) \rangle \\ &+ \langle S(t) \rangle \int_0^\Delta d\tau \psi(\tau) \langle X(\tau) \rangle. \end{aligned} \quad (\text{A10})$$

To calculate the first two terms in Eq. (A9) we use the autocorrelation of nonreset GBM. We start with the property that the increments of the underlying pure Brownian motion, denoted below by $B(t)$, are independent. This yields

$$\begin{aligned} \langle X(t)X(t + \Delta) \rangle &= S_0^2 \langle e^{B(t+\Delta)} e^{B(t)} \rangle \\ &= S_0^2 \langle e^{B(t+\Delta)-B(t)} e^{B(t)+B(t)} \rangle = S_0^2 \langle e^{B(t+\Delta)-B(t)} \rangle \langle e^{2B(t)} \rangle. \end{aligned} \quad (\text{A11})$$

The first term in the last expression contains the exponentiation of the underlying process,

$$W(\Delta) = B(t + \Delta) - B(t), \quad (\text{A12})$$

a Wiener process with the variance $\sigma^2\Delta$ and mean $(\mu - \sigma^2/2)\Delta$. It simplifies to

$$\langle e^{B(t+\Delta)-B(t)} \rangle = \langle e^{W(\Delta)} \rangle = e^{\mu\Delta}. \quad (\text{A13})$$

The second term in the product of Eq. (A11) is the second moment of nonreset GBM given by Eq. (9),

$$\langle e^{2B(t)} \rangle = \langle X^2(t) \rangle = e^{(\sigma^2+2\mu)t}. \quad (\text{A14})$$

Substituting Eqs. (A13) and (A14) into Eq. (A11) we find

$$\langle X(t)X(t + \Delta) \rangle = S_0^2 e^{\mu\Delta} e^{(\sigma^2+2\mu)t}. \quad (\text{A15})$$

The expressions for C_1 in Eq. (A9) can thus be simplified to

$$C_1 = S_0^2 e^{\mu\Delta} e^{-r\Delta} \left[e^{(\sigma^2+2\mu-r)t} + \int_0^t d\tau r e^{(\sigma^2+2\mu-r)\tau} \right], \quad (\text{A16})$$

and after the integration—for the respective regions of the three main model parameters—we get

$$C_1 = S_0^2 \begin{cases} \frac{e^{(\mu-r)\Delta} \left((\sigma^2+2\mu)e^{(\sigma^2+2\mu-r)t} - r \right)}{\sigma^2+2\mu-r}, & \sigma^2 + 2\mu \neq r, \\ e^{(\mu-r)\Delta} (1 + rt), & \sigma^2 + 2\mu = r. \end{cases} \quad (\text{A17})$$

The term C_2 in Eq. (A9) can be computed using the first moments, Eqs. (8) and (33), that after the integration gives

$$C_2 = S_0^2 \begin{cases} \frac{r[\mu e^{(\mu-r)t} - r][e^{(\mu-r)\Delta} - 1]}{(\mu-r)^2}, & \mu \neq r, \\ [1 + rt]r\Delta, & \mu = r. \end{cases} \quad (\text{A18})$$

Combining expressions (A17) and (A18) yields the full autocorrelation function of Poisson-reset GBM in the form

$$\langle S(t)S(t + \Delta) \rangle = S_0^2 \begin{cases} [1 + rt]r\Delta + \frac{[(\sigma^2+2r)e^{(\sigma^2+r)t} - r]}{\sigma^2+r}, & \mu = r, \\ \frac{r}{(\mu-r)^2} [\mu e^{(\mu-r)t} - r][e^{(\mu-r)\Delta} - 1] + e^{(\mu-r)\Delta} (1 + rt), & \sigma^2 + 2\mu = r, \\ \frac{r}{(\mu-r)^2} [\mu e^{(\mu-r)t} - r][e^{(\mu-r)\Delta} - 1] + \frac{e^{(\mu-r)\Delta} [(\sigma^2+2\mu)e^{(\sigma^2+2\mu-r)t} - r]}{\sigma^2+2\mu-r}, & \mu \neq r, \sigma^2 + 2\mu \neq r. \end{cases} \quad (\text{A19})$$

The term I_3 in Eq. (A1) is calculated with the help of Eq. (A19) by integration as

$$I_3 = \underbrace{\frac{1}{T - \Delta} \int_0^{T-\Delta} dt C_1}_{D_1} + \underbrace{\frac{1}{T - \Delta} \int_0^{T-\Delta} dt C_2}_{D_2}, \quad (\text{A20})$$

where the first and second terms are given by (in their regions of model parameters), respectively,

$$D_1 = S_0^2 \begin{cases} e^{(\mu-r)\Delta} \left[\frac{(\sigma^2+2\mu)(e^{(\sigma^2+2\mu-r)(T-\Delta)} - 1)}{(\sigma^2+2\mu-r)^2(T-\Delta)} - \frac{r}{\sigma^2+2\mu-r} \right], & \sigma^2 + 2\mu \neq r, \\ e^{(\mu-r)\Delta} \left[1 + \frac{r}{2}(T - \Delta) \right], & \sigma^2 + 2\mu = r, \end{cases} \quad (\text{A21})$$

and

$$D_2 = S_0^2 \begin{cases} [e^{(\mu-r)\Delta} - 1] r \frac{[\mu(e^{(\mu-r)(T-\Delta)} - 1) - r(\mu-r)(T-\Delta)]}{(\mu-r)^3(T-\Delta)}, & \mu \neq r, \\ r\Delta [1 + r \frac{(T-\Delta)}{2}], & \mu = r. \end{cases} \quad (\text{A22})$$

Now, we assemble these expressions into the final result for the mean TAMSD of drift-containing reset GBM. For expressions (A2), (A3), (A21), and (A22) we see that I_1 , I_2 , and D_1 have the same parameter regions as the second moment (36) with a “branching point” at $\sigma^2 + 2\mu = r$, whereas D_2 has the same parameter regimes as the first moment (33) with a branching point at $\mu = r$. We, therefore, group the first set of terms into one component of the mean TAMSD, while the other terms form another component.

The first component of the mean TAMSD solely contains D_2 from Eq. (A22) and it is denoted $\langle \overline{\delta^2(\Delta)} \rangle_\mu$ (after the branching point at $\mu = r$), namely,

$$\langle \overline{\delta^2(\Delta)} \rangle_\mu = S_0^2 \begin{cases} (e^{(\mu-r)\Delta} - 1) r \frac{[\mu(e^{(\mu-r)(T-\Delta)} - 1) - r(\mu-r)(T-\Delta)]}{(\mu-r)^3(T-\Delta)}, & \mu \neq r, \\ r\Delta [1 + r \frac{(T-\Delta)}{2}], & \mu = r. \end{cases} \quad (\text{A23})$$

After grouping I_1 , I_2 , and D_1 from expressions (A2), (A3), and (A21), respectively, we get the second component of the mean TAMSD, $\langle \overline{\delta^2(\Delta)} \rangle_{\sigma^2+2\mu}$ —with the index reflecting the branching point at $\sigma^2 + 2\mu = r$ —as

$$\langle \overline{\delta^2(\Delta)} \rangle_{\sigma^2+2\mu} = S_0^2 \begin{cases} \frac{(\sigma^2+2\mu)(1+e^{(\sigma^2+2\mu-r)\Delta} - 2e^{(\mu-r)\Delta})(e^{(\sigma^2+2\mu-r)(T-\Delta)} - 1)}{(\sigma^2+2\mu-r)^2(T-\Delta)} + \frac{2r}{\sigma^2+2\mu-r} [e^{(\mu-r)\Delta} - 1], & \sigma^2 + 2\mu \neq r, \\ (2+rT)(1 - e^{(\mu-r)\Delta}) + e^{(\mu-r)\Delta} r\Delta, & \sigma^2 + 2\mu = r. \end{cases} \quad (\text{A24})$$

The total mean TAMSD is then given by

$$\langle \overline{\delta^2(\Delta)} \rangle = \langle \overline{\delta^2(\Delta)} \rangle_{\sigma^2+2\mu} - 2 \langle \overline{\delta^2(\Delta)} \rangle_\mu, \quad (\text{A25})$$

with the term $\langle \overline{\delta^2(\Delta)} \rangle_\mu$ stemming from integrating the term $\langle S(t)S(t+\Delta) \rangle$ given by Eq. (A19) in expression (A1). As for the variance in Eq. (40), combining the two components of the mean TAMSD in two different parameter regions yields three

different regimes for the mean TAMSD, as detailed in Sec. VI of the main text.

APPENDIX B: SUPPLEMENTARY FIGURES

This Appendix contains auxiliary Figs. 11–22 supporting the claims in the main text.

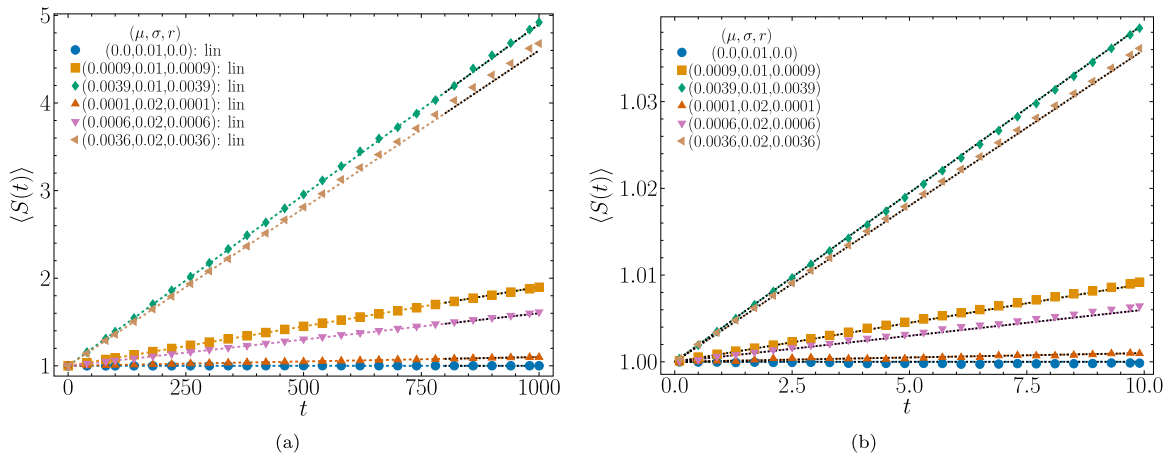


FIG. 11. Variation of the first moment of Poisson-reset GBM in the first regime in Table I. The explicit values of the model parameters in this region used in computer simulations are: $S_0 = 1$, $\delta t = 10^{-1}$, $T = 10^3$, $N = 3 \times 10^4$ (see also the legend). (a) The colored curves are according to the full analytical expression given by Eq. (33), while the dashed asymptotes are Eq. (86). The details are provided in Sec. VI A and in Table I. In panel (a) of this figure and all later related plots we add in the legend the “exp,” “lin,” and “const” indicators to emphasize the corresponding exponential, linear, and constant behaviors of the respective quantities at long times. For the values of model parameters where no such asymptotes are clear we neither show the dotted black asymptotes at long times nor list the “exp,” “lin,” and “const” indicators in the legends. For the parameter values in the legends, as the numbers used in computations were of base 2, the floating-point numbers were rounded to four decimal digits (machine precision). (b) The same as in Fig. 11(a), for the same parameters, shown in the short-time region. The dashed asymptotes are given by Eq. (85).

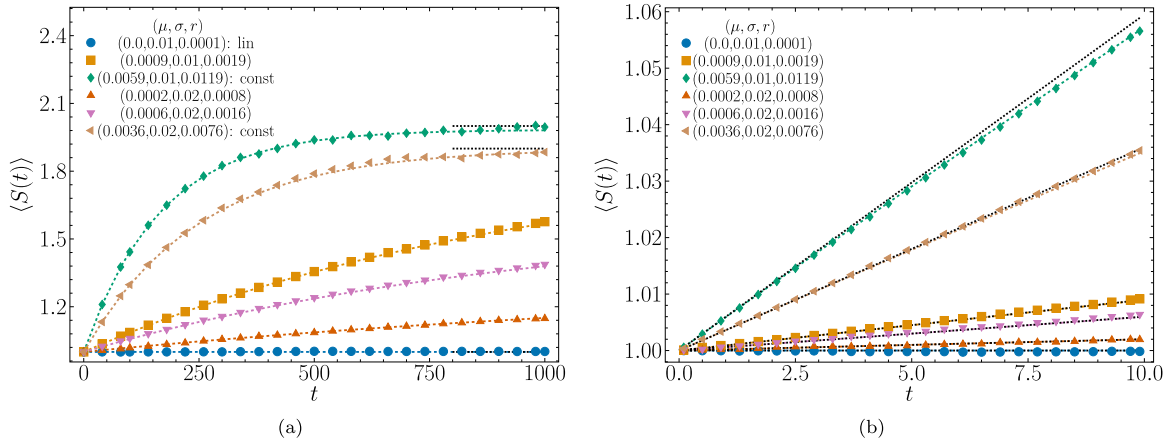


FIG. 12. The same as in Fig. 11 but in the second region of parameters in Table I. (a) The colored curves are according to Eq. (33), while the dashed asymptotes are Eqs. (88), (90), and (92). Parameters are provided in the legend. (b) The same as in Fig. 12(a), for the same values of the model parameters, shown at short times. The dashed asymptotes shown are Eqs. (87), (89), and (91).

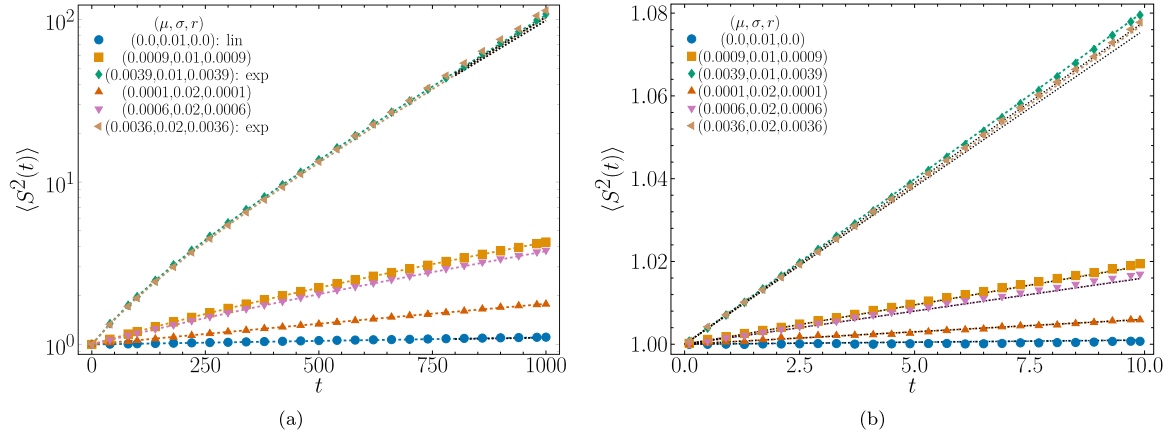


FIG. 13. The second moment of reset GBM, for the first region of parameters in Table II, for the same parameters as in Fig. 11. (a) The colored curves are according to the exact analytical result given by Eq. (36), while the dashed asymptotes are plotted according to Eqs. (102), (104), and (108). The details can be found in Sec. VIB and in Table II. (b) The same as in Fig. 13(a) but at short times. The asymptotes shown as black dashed lines are according to Eqs. (101), (103), and (107).

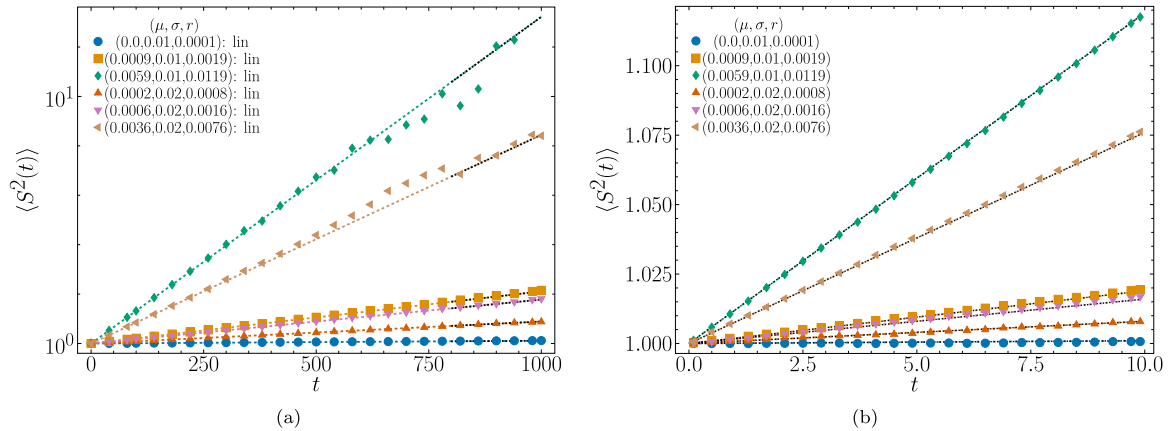


FIG. 14. The same as in Fig. 13, but for the second regime in Table II. The parameters are the same as in Fig. 12. (a) The colored curves are according to Eq. (36), while the dashed asymptotes are plotted according to Eq. (110). (b) The same as in Fig. 14(a) but plotted at short times. The colored curves are according to Eq. (36), while the dashed asymptotes are plotted according to Eq. (109).

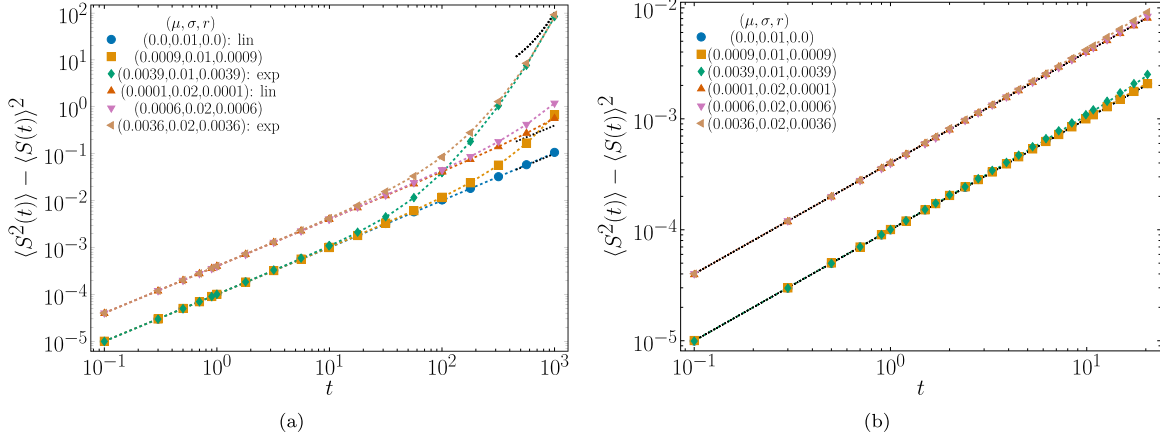


FIG. 15. The variance of reset GBM, for the first region of parameters, for the parameters of Fig. 11. (a) The colored curves are according to the exact analytical result (40), while the dashed asymptotes are plotted according to Eqs. (118), (120), and (124). The details are provided in Sec. VIC and in Table III. (b) The same as in Fig. 15(a) but at short times. The dashed asymptotes are Eqs. (117) and (119).

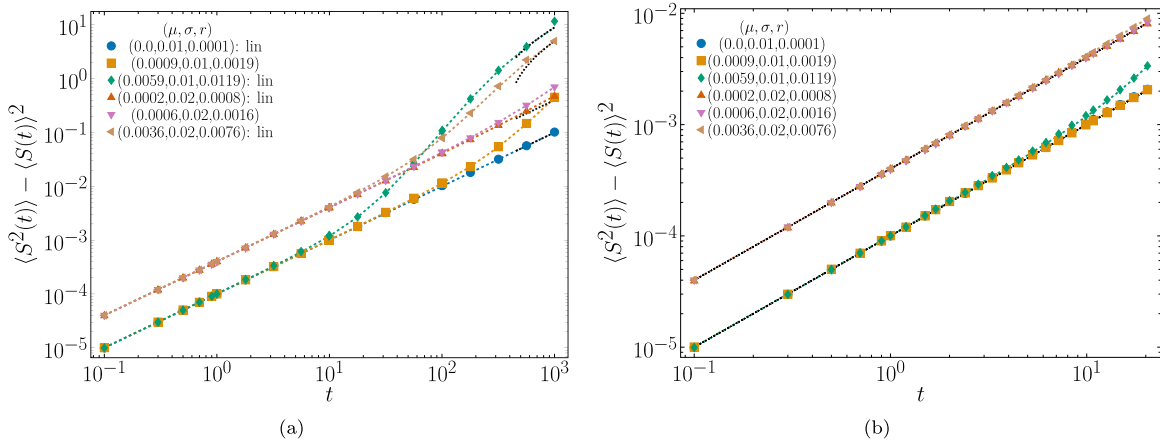


FIG. 16. The same as in Fig. 15, but computed in the second region of parameters as listed in Table III. The model parameters are the same as used in Fig. 12. (a) The colored curves are according to Eq. (40), while the dashed asymptotes are Eqs. (126) and (128). Log-log scale emphasizes the linear growth of the variance both at short and long times. (b) The same as in Fig. 16(a) but presented at short times. The dashed asymptotes are Eqs. (125) and (127).

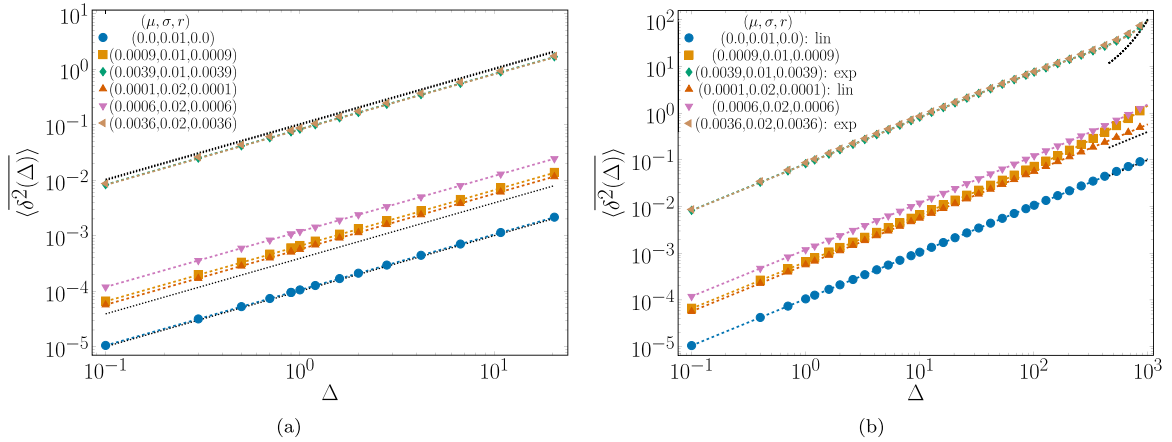


FIG. 17. The mean TAMSD of reset GBM, for the first region of model parameters. The results are plotted for the parameters of Fig. 11. (a) The colored curves represent the exact analytical result of Eq. (42) and the black lines are asymptotes from Eqs. (142), (144), and (148). For details we refer the reader to Sec. VID and in Table IV. While the *short-lag-time* behaviors of the mean TAMSD of reset GBM is always linear, for the respective model parameters used in the computations we indicate in this and later TAMSD panel (a) plots the asymptotics of $\langle \delta^2(\Delta) \rangle$ at *long* lag times in the legends by “exp,” “lin,” and “const” indicators. (b) The same as in Fig. 17(a) but presented at *short* lag times, in the region where the mean-TAMSD behavior is always linear. The dashed lines represent Eqs. (141), (143), and (147).

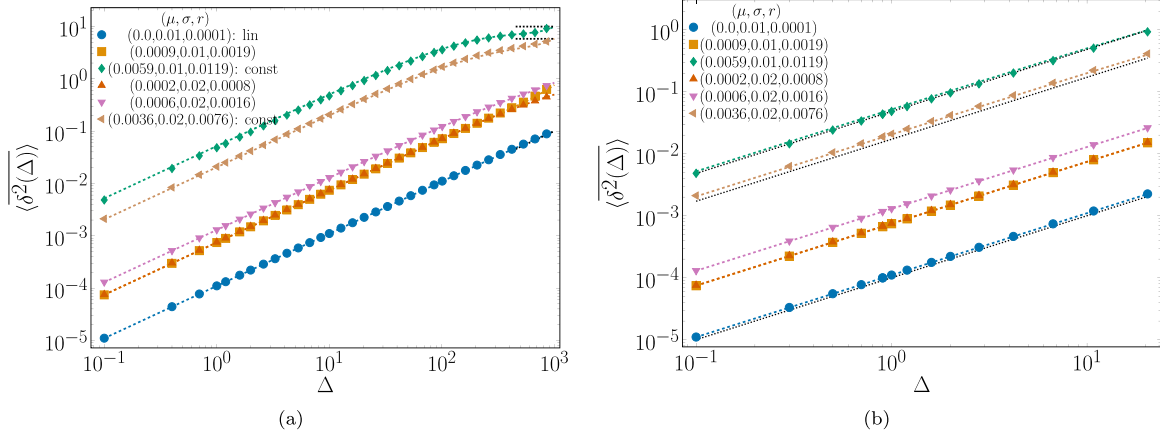


FIG. 18. The same as in Fig. 17 but for the second regime in Table IV and plotted for the parameters of Fig. 12. (a) The colored curves are according to Eq. (42), while the dashed asymptotes are according to Eqs. (150) and (152). (b) The same as in Fig. 18(a) but presented at short times. The dashed lines are plotted according to Eqs. (149) and (151).

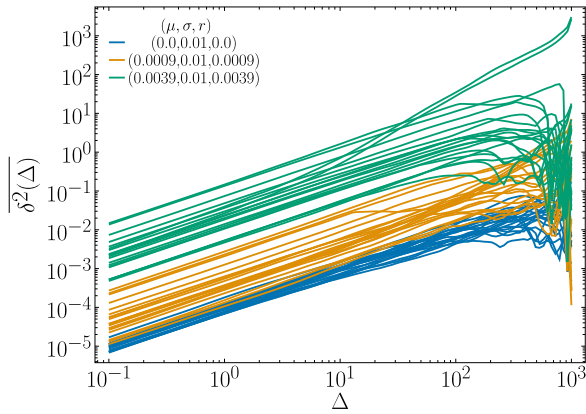


FIG. 19. Spread of TAMSD trajectories in the first regime of model parameters computed for three distinct sets of values of drift, volatility, and reset rate. The other parameters are as in Fig. 11.

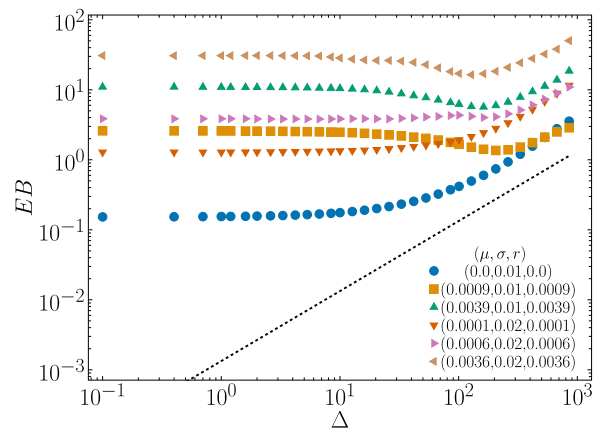


FIG. 21. Variation of the ergodicity-breaking parameter EB as a function of lag time Δ , computed for the first regime of model parameters. The dashed line is the Brownian-motion asymptote (168). The parameters are the same as in Fig. 11.

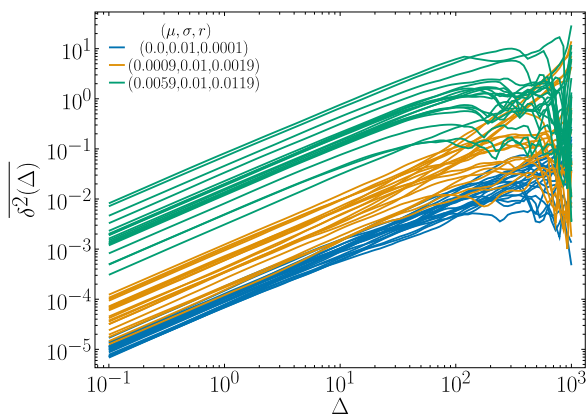


FIG. 20. The same as in Fig. 19 but for the second region of parameters. Other parameters are as in Fig. 12.

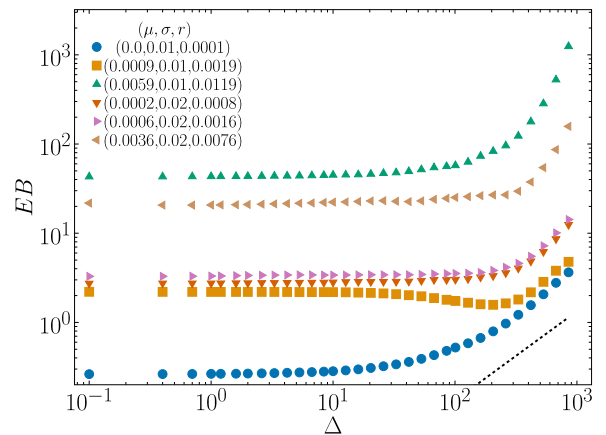


FIG. 22. The same as in Fig. 21 but for the behaviors in the second regime of model parameters as in Fig. 12. The dashed line is the Brownian-motion asymptote (168).

APPENDIX C: ABBREVIATIONS

Geometric Brownian motion, GBM; fractional Brownian motion, FBM; probability-density function, PDF; mean-

squared displacement, MSD; time-averaged MSD, TAMSD; nonequilibrium stationary state, NESS.

-
- [1] D. Vinod, A. G. Cherstvy, W. Wang, R. Metzler, and I. M. Sokolov, Nonergodicity of reset geometric Brownian motion, *Phys. Rev. E* **105**, L012106 (2022).
- [2] R. C. Merton, Theory of rational option pricing, *Bell J. Econ. Manage. Sci.* **4**, 141 (1973).
- [3] M. B. Goldman, H. B. Sosin, and M. A. Gatto, Path dependent options: “Buy at the low, sell at the high”, *J. Finance* **34**, 1111 (1979).
- [4] A. Conze and S. Viswanathan, Path dependent options: The case of lookback options, *J. Finance* **46**, 1893 (1991).
- [5] M. Rubinstein and E. Reiner, Breaking down the barriers, *Risk* **4**, 28 (1991).
- [6] N. Kunitomo and M. Ikeda, Pricing options with curved boundaries I, *Math. Financ.* **2**, 275 (1992).
- [7] H. Geman and M. Yor, Pricing and hedging double-barrier options: A probabilistic approach, *Math. Financ.* **6**, 365 (1996).
- [8] N. N. Taleb, *Dynamic Hedging: Managing Vanilla and Exotic Options* (Wiley, New York, NY, 1997).
- [9] S. F. Gray and R. E. Whaley, Valuing S&P 500 bear market warrants with a periodic reset, *J. Derivatives* **5**, 99 (1997).
- [10] H. He, W. P. Keirstead, and J. Rebholz, Double lookbacks, *Math. Financ.* **8**, 201 (1998).
- [11] S. F. Gray and R. E. Whaley, Reset put options: Valuation, risk characteristics, and an application, *Austral. J. Manag.* **24**, 1 (1999).
- [12] M. Broadie, P. Glasserman, and S.-G. Kou, Connecting discrete and continuous path-dependent options, *Finance Stochast.* **3**, 55 (1999).
- [13] P. P. Boyle, Y. Tian *et al.*, Pricing lookback and barrier options under the CEV process, *J. Financ. Quant. Anal.* **34**, 241 (1999).
- [14] Wai-Yan Cheng and Shuguang Zhang, The analytics of reset options, *J. Deriv.* **8**, 59 (2000).
- [15] M. Yor, *Exponential Functionals of Brownian Motion and Related Processes* (Springer Science & Business Media, Berlin, 2001).
- [16] D. Davydov and V. Linetsky, Pricing and hedging path-dependent options under the CEV process, *Manag. Sci.* **47**, 949 (2001).
- [17] S.-G. Kou, A jump-diffusion model for option pricing, *Manag. Sci.* **48**, 1086 (2002).
- [18] S.-G. Kou and H. Wang, First passage times of a jump diffusion process, *Adv. Appl. Probab.* **35**, 504 (2003).
- [19] S.-G. Kou and H. Wang, Option pricing under a double exponential jump diffusion model, *Manag. Sci.* **50**, 1178 (2004).
- [20] G. Petrella and S. Kou, Numerical pricing of discrete barrier and lookback options via laplace transforms, *J. Comput. Finance* **8**, 1 (2004).
- [21] V. Linetsky, Lookback options and diffusion hitting times: A spectral expansion approach, *Finance Stochast.* **8**, 373 (2004).
- [22] L. Feng and V. Linetsky, Pricing options in jump-diffusion models: An extrapolation approach, *Oper. Res.* **56**, 304 (2008).
- [23] G. Fusai, Lookback options, in *Encyclopedia of Quantitative Finance* (John Wiley & Sons, New York, NY, 2010).
- [24] G. Fusai, G. Germano, and D. Marazzina, Spitzer identity, Wiener-Hopf factorization and pricing of discretely monitored exotic options, *Eur. J. Oper. Res.* **251**, 124 (2016).
- [25] Y.-S. Hsu and C.-H. Wu, Extended Black and Scholes model under bankruptcy risk, *J. Math. Anal. Appl.* **482**, 123564 (2020).
- [26] G. Krzyżanowski and M. Magdziarz, A computational weighted finite difference method for American and barrier options in subdiffusive Black–Scholes model, *Commun. Nonlin. Sci. Numer. Simulat.* **96**, 105676 (2021).
- [27] L. Bachelier, Théorie de la spéculation, *Annales scientifiques de l’École Normale Supérieure, Série 3* **17**, 21 (1900).
- [28] V. Bronzin, *Theorie der Prämien-geschäfte* (Leipzig und Wien, Verlag Franz Deticke, 1908).
- [29] C. M. Sprenkle, Warrant prices as indicators of expectations and preferences, *Yale economic essays*, **1**, 179 (1961).
- [30] P. A. Samuelson, Rational theory of warrant pricing, *Industr. Manage. Rev.* **6**, 13 (1965).
- [31] E. O. Thorp, Optimal gambling systems for favorable games, *Rev. Int. Stat. Inst.* **37**, 273 (1969).
- [32] F. Black and M. Scholes, The pricing of options and corporate liabilities, *J. Politic. Econ.* **81**, 637 (1973).
- [33] R. C. Merton, An intertemporal capital asset pricing model, *Econometrica* **41**, 867 (1973).
- [34] R. C. Merton, Option pricing when underlying stock returns are discontinuous, *J. Financ. Econ.* **3**, 125 (1976).
- [35] J. C. Cox and S. A. Ross, The valuation of options for alternative stochastic processes, *J. Financ. Econ.* **3**, 145 (1976).
- [36] J. C. Cox, S. A. Ross, and M. Rubinstein, Option pricing: A simplified approach, *J. Financ. Econ.* **7**, 229 (1979).
- [37] A. G. Hawkes, Hawkes processes and their applications to finance: A review, *Quant. Financ.* **18**, 193 (2018).
- [38] A. G. Hawkes, Hawkes jump-diffusions and finance: A brief history and review, *Eur. J. Finance* **28**, 627 (2020).
- [39] S. C. Manrubia and D. H. Zanette, Stochastic multiplicative processes with reset events, *Phys. Rev. E* **59**, 4945 (1999).
- [40] M. Nirei and W. Souma, Income distribution and stochastic multiplicative process with reset event, in *The Complex Dynamics of Economic Interaction*, edited by Mauro Gallegati, Alan P. Kirman, and Matteo Marsili, Lecture Notes in Economics and Mathematical Systems (Springer, Berlin, 2004).
- [41] A. Montanari and R. Zecchina, Optimizing Searches via Rare Events, *Phys. Rev. Lett.* **88**, 178701 (2002).
- [42] M. R. Evans and S. N. Majumdar, Diffusion with Stochastic Resetting, *Phys. Rev. Lett.* **106**, 160601 (2011).
- [43] D. H. Zanette and S. C. Manrubia, Fat tails and black swans: Exact results for multiplicative processes with resets, *Chaos* **30**, 033104 (2020).

- [44] É. Roldán and S. Gupta, Path-integral formalism for stochastic resetting: Exactly solved examples and shortcuts to confinement, *Phys. Rev. E* **96**, 022130 (2017).
- [45] S. N. Majumdar and G. Oshanin, Spectral content of fractional Brownian motion with stochastic reset, *J. Phys. A* **51**, 435001 (2018).
- [46] A. V. Chechkin and I. M. Sokolov, Random Search with Resetting: A Unified Renewal Approach, *Phys. Rev. Lett.* **121**, 050601 (2018).
- [47] S. Belan, Restart Could Optimize the Probability of Success in a Bernoulli Trial, *Phys. Rev. Lett.* **120**, 080601 (2018).
- [48] J. Masoliver, Telegraphic processes with stochastic resetting, *Phys. Rev. E* **99**, 012121 (2019).
- [49] J. Masoliver and M. Montero, Anomalous diffusion under stochastic resettings: A general approach, *Phys. Rev. E* **100**, 042103 (2019).
- [50] M. dos Santos, Fractional Prabhakar derivative in diffusion equation with non-static stochastic resetting, *Physics* **1**, 40 (2019).
- [51] U. Basu, A. Kundu, and A. Pal, Symmetric exclusion process under stochastic resetting, *Phys. Rev. E* **100**, 032136 (2019).
- [52] A. Pal, Ł. Kuśmierz, and S. Reuveni, Invariants of motion with stochastic resetting and space-time coupled returns, *New J. Phys.* **21**, 113024 (2019).
- [53] D. Gupta, Stochastic resetting in underdamped Brownian motion, *J. Stat. Mech.* (2019) 033212.
- [54] A. Pal, I. Eliazar, and S. Reuveni, First Passage under Restart with Branching, *Phys. Rev. Lett.* **122**, 020602 (2019).
- [55] A. Pal, R. Chatterjee, S. Reuveni, and A. Kundu, Local time of diffusion with stochastic resetting, *J. Phys. A* **52**, 264002 (2019).
- [56] X. Durang, S. Lee, L. Lizana, and J.-H. Jeon, First-passage statistics under stochastic resetting in bounded domains, *J. Phys. A* **52**, 224001 (2019).
- [57] M. R. Evans, S. N. Majumdar, and G. Schehr, Stochastic resetting and applications, *J. Phys. A* **53**, 193001 (2020).
- [58] M. Antonio Faustino dos Santos, Comb model with non-static stochastic resetting and anomalous diffusion, *Fractal Fract.* **4**, 28 (2020).
- [59] V. Domazetoski, A. Masó-Puigdellosas, T. Sandev, V. Méndez, A. Iomin, and L. Kocarev, Stochastic resetting on comblike structures, *Phys. Rev. Res.* **2**, 033027 (2020).
- [60] A. S. Bodrova, A. V. Chechkin, and I. M. Sokolov, Nonrenewal resetting of scaled Brownian motion, *Phys. Rev. E* **100**, 012119 (2019).
- [61] A. S. Bodrova, A. V. Chechkin, and I. M. Sokolov, Scaled Brownian motion with renewal resetting, *Phys. Rev. E* **100**, 012120 (2019).
- [62] A. S. Bodrova and I. M. Sokolov, Resetting processes with noninstantaneous return, *Phys. Rev. E* **101**, 052130 (2020).
- [63] I. Eliazar and S. Reuveni, Mean-performance of sharp restart I: Statistical roadmap, *J. Phys. A* **53**, 405004 (2020).
- [64] R. K. Singh, R. Metzler, and T. Sandev, Resetting dynamics in a confining potential, *J. Phys. A* **53**, 505003 (2020).
- [65] B. De Bruyne, J. Randon-Furling, and S. Redner, Optimization in First-Passage Resetting, *Phys. Rev. Lett.* **125**, 050602 (2020).
- [66] C. A. Plata, D. Gupta, and S. Azaele, Asymmetric stochastic resetting: Modeling catastrophic events, *Phys. Rev. E* **102**, 052116 (2020).
- [67] P. Singh, Random acceleration process under stochastic resetting, *J. Phys. A* **53**, 405005 (2020).
- [68] O. Tal-Friedman, A. Pal, A. Sekhon, S. Reuveni, and Y. Roichman, Experimental realization of diffusion with stochastic resetting, *J. Phys. Chem. Lett.* **11**, 7350 (2020).
- [69] A. M. Ramoso, J. A. Magalang, D. Sanchez-Taltavull, J. P. Esguerra, and É. Roldán, Stochastic resetting antiviral therapies prevent drug resistance development, *Europhys. Lett.* **132**, 50003 (2020).
- [70] A. Miron and S. Reuveni, Diffusion with local resetting and exclusion, *Phys. Rev. Res.* **3**, L012023 (2021).
- [71] W. Wang, A. G. Cherstvy, H. Kantz, R. Metzler, and I. M. Sokolov, Time averaging and emerging nonergodicity upon resetting of fractional Brownian motion and heterogeneous diffusion processes, *Phys. Rev. E* **104**, 024105 (2021).
- [72] B. De Bruyne, J. Randon-Furling, and S. Redner, *J. Stat. Mech.* (2021) 013203.
- [73] V. Stojkoski, T. Sandev, L. Kocarev, and A. Pal, Geometric Brownian motion under stochastic resetting: A stationary yet nonergodic process, *Phys. Rev. E* **104**, 014121 (2021).
- [74] V. Stojkoski, P. Jolakoski, A. Pal, T. Sandev, L. Kocarev, and R. Metzler, Income inequality and mobility in geometric Brownian motion with stochastic resetting: Theoretical results and empirical evidence of non-ergodicity, *Phil. Trans. R. Soc. A* **380**, 20210157 (2022).
- [75] P. C. Bressloff, Switching diffusions and stochastic resetting, *J. Phys. A* **53**, 275003 (2020).
- [76] G. Mercado-Vásquez and D. Boyer, Search of stochastically gated targets with diffusive particles under resetting, *J. Phys. A* **54**, 444002 (2021).
- [77] I. Eliazar and S. Reuveni, Mean-performance of sharp restart: II. Inequality roadmap, *J. Phys. A* **54**, 355001 (2021).
- [78] V. Méndez, A. Masó-Puigdellosas, T. Sandev, and D. Campos, Continuous time random walks under Markovian resetting, *Phys. Rev. E* **103**, 022103 (2021).
- [79] I. T. Gómez Garay and D. H. Zanette, Collective behavior of coupled multiplicative processes with stochastic resetting, *J. Phys. Complex.* **2**, 035020 (2021).
- [80] M. Dahlenburg, A. V. Chechkin, R. Schumer, and R. Metzler, Stochastic resetting by a random amplitude, *Phys. Rev. E* **103**, 052123 (2021).
- [81] D. M. Busiello, D. Gupta, and A. Maritan, Inducing and optimizing Markovian Mpemba effect with stochastic reset, *New J. Phys.* **23**, 103012 (2021).
- [82] J. Villarroel, M. Montero, and J. A. Vega, A semi-deterministic random walk with resetting, *Entropy* **23**, 825 (2021).
- [83] T. T. da Silva and M. D. Fragoso, Diffusion with stochastic resetting of interacting particles emerging from a model of population genetics, *J. Phys. A* **55**, 014003 (2022).
- [84] G. R. Calvert and M. R. Evans, Searching for clusters of targets under stochastic resetting, *Eur. Phys. J. B* **94**, 228 (2021).
- [85] R. D. Schumm and P. C. Bressloff, Search processes with stochastic resetting and partially absorbing targets, *J. Phys. A* **54**, 404004 (2021).
- [86] S. Ray and S. Reuveni, Resetting transition is governed by an interplay between thermal and potential energy, *J. Chem. Phys.* **154**, 171103 (2021).
- [87] O. L. Bonomo, A. Pal, and S. Reuveni, Mitigating long queues and waiting times with service resetting, *PNAS Nexus* **1**, pgac070 (2022).

- [88] M. Radice, One-dimensional telegraphic process with non-instantaneous stochastic resetting, *Phys. Rev. E* **104**, 044126 (2021).
- [89] K. Goswami and R. Chakrabarti, Stochastic resetting and first arrival subjected to Gaussian noise and Poisson white noise, *Phys. Rev. E* **104**, 034113 (2021).
- [90] P. C. Bressloff, Accumulation time of stochastic processes with resetting, *J. Phys. A* **54**, 354001 (2021).
- [91] B. De Bruyne and F. Mori, Resetting in stochastic optimal control, [arXiv:2112.11416](https://arxiv.org/abs/2112.11416).
- [92] A. Stanislavsky and A. Weron, Optimal non-Gaussian search with stochastic resetting, *Phys. Rev. E* **104**, 014125 (2021).
- [93] S. N. Majumdar, P. Mounaix, S. Sabhapandit, and G. Schehr, Record statistics for random walks and Lévy flights with resetting, *J. Phys. A* **55**, 034002 (2022).
- [94] M. Radice, Diffusion processes with Gamma-distributed resetting and non-instantaneous returns, *J. Phys. A* **55**, 224002 (2022).
- [95] A. Pal, S. Kostinski, and S. Reuveni, The inspection paradox in stochastic resetting, *J. Phys. A* **55**, 021001 (2022).
- [96] M. K. Lenzi, E. K. Lenzi, L. M. S. Guilherme, L. R. Evangelista, and H. V. Ribeiro, Transient anomalous diffusion in heterogeneous media with stochastic resetting, *Physica A* **588**, 126560 (2022).
- [97] T. Sandev, V. Domazetovski, L. Kocarev, R. Metzler, and A. V. Chechkin, Heterogeneous diffusion with stochastic resetting, *J. Phys. A* **55**, 074003 (2022).
- [98] W. Wang, A. G. Cherstvy, R. Metzler, and I. M. Sokolov, Restoring ergodicity of stochastically reset anomalous-diffusion processes, *Phys. Rev. Res.* **4**, 013161 (2022).
- [99] N. R. Smith and S. N. Majumdar, Condensation transition in large deviations of self-similar Gaussian processes with stochastic resetting, *J. Stat. Mech.* (2022) 053212.
- [100] B. De Bruyne, S. N. Majumdar, and G. Schehr, Optimal Resetting Brownian Bridges, *Phys. Rev. Lett.* **128**, 200603 (2022).
- [101] P. Xu, T. Zhou, R. Metzler, and W. Deng, Stochastic harmonic trapping of a Levy walk: Transport and first-passage dynamics under soft resetting strategies, *New J. Phys.* **24**, 033003 (2022).
- [102] I. Santra, Effect of tax dynamics on linearly growing processes under stochastic resetting: A possible economic model, *Europhys. Lett.* **137**, 52001 (2022).
- [103] M. R. Evans, S. N. Majumdar, and G. Schehr, An exactly solvable predator prey model with resetting, *J. Phys. A* **55**, 274005 (2022).
- [104] S. Gupta and A. M. Jayannavar, Stochastic resetting: A (very) brief review, *Front. Phys.* **10**, 789097 (2022).
- [105] B. Mukherjee, K. Sengupta, and S. N. Majumdar, Quantum dynamics with stochastic reset, *Phys. Rev. B* **98**, 104309 (2018).
- [106] D. C. Rose, H. Touchette, I. Lesanovsky, and J. P. Garrahan, Spectral properties of simple classical and quantum reset processes, *Phys. Rev. E* **98**, 022129 (2018).
- [107] A. Riera-Campenya, J. Ollé, and A. Masó-Puigdellosas, Measurement-induced resetting in open quantum systems, [arXiv:2011.04403](https://arxiv.org/abs/2011.04403).
- [108] S. Wald and L. Böttcher, From classical to quantum walks with stochastic resetting on networks, *Phys. Rev. E* **103**, 012122 (2021).
- [109] G. Peretto, F. Carollo, M. Magoni, and I. Lesanovsky, Designing nonequilibrium states of quantum matter through stochastic resetting, *Phys. Rev. B* **104**, L180302 (2021).
- [110] G. Peretto, F. Carollo, and I. Lesanovsky, Thermodynamics of quantum-jump trajectories of open quantum systems subject to stochastic resetting, [arXiv:2112.05078](https://arxiv.org/abs/2112.05078).
- [111] M. Magdziarz and W. Szczotka, Lévy walks with rests: Long-time analysis, *Phys. Rev. E* **105**, 014114 (2022).
- [112] N. D. Kondratieff, Die langen Wellen der Konjunktur, *Archiv für Sozialwissenschaft und Sozialpolitik* **56**, 573 (1926).
- [113] G. Garvy, Kondratieff's theory of long cycles, *Rev. Econ. Stat.* **25**, 203 (1943).
- [114] A. V. Korotayev and S. V. Tsirel, A spectral analysis of world GDP dynamics: Kondratieff waves, Kuznets swings, Juglar and Kitchin cycles in global economic development, and the 2008–2009 economic crisis, *Structure and Dynamics*, Vol. 4, Issue no. 1 (UC Irvine, Irvine, CA, 2010).
- [115] S. Hsu, *Financial Crises, 1929 to the Present*, 2nd ed. (Edward Elgar Publishing, Cheltenham, UK, 2017).
- [116] H. M. Markowitz, *Portfolio Selection: Efficient Diversification of Investments* (Yale University Press, New Haven, CT, 1968).
- [117] E. O. Thorp, Portfolio choice and the Kelly criterion, in *Stochastic Optimization Models in Finance*, edited by W. T. Ziemba and R. G. Vickson (Academic Press, San Diego, CA, 1975), pp. 599–619.
- [118] S. Browne and W. Whitt, Portfolio choice and the Bayesian Kelly criterion, *Adv. Appl. Probab.* **28**, 1145 (1996).
- [119] M. B. Goldman, H. B. Sosin, and L. A. Shepp, On contingent claims that insure ex-post optimal stock market timing, *J. Finance* **34**, 401 (1979).
- [120] X. Gabaix, J.-M. Lasry, P.-L. Lions, and B. Moll, The dynamics of inequality, *Econometrica* **84**, 2071 (2016).
- [121] J. L. Lebowitz and S. I. Rubinow, A theory for the age and generation time distribution of a microbial population, *J. Math. Biol.* **1**, 17 (1974).
- [122] S. Iyer-Biswas, C. S. Wright, J. T. Henry, K. Lo, S. Burov, Y. Lin, G. E. Crooks, S. Crosson, A. R. Dinner, and N. F. Scherer, Scaling laws governing stochastic growth and division of single bacterial cells, *Proc. Natl. Acad. Sci. USA* **111**, 15912 (2014).
- [123] N. Q. Balaban, S. Helaine, K. Lewis, M. Ackermann, B. Aldridge, D. I. Andersson, M. P. Brynildsen, D. Bumann, A. Camilli, J. J. Collins, C. Dehio, S. Fortune, J.-M. Ghigo, W.-D. Hardt, A. Harms, M. Heinemann, D. T. Hung, U. Jenal, B. R. Levin, J. Michiels *et al.*, Definitions and guidelines for research on antibiotic persistence, *Nat. Rev. Microbiol.* **17**, 441 (2019).
- [124] S. M. Roy, V. Garg, S. Barman, C. Ghosh, A. R. Maity, and S. K. Ghosh, Kinetics of nanomedicine in tumor spheroid as an *in vitro* model system for efficient tumor-targeted drug delivery with insights from mathematical models, *Front. Bioeng. Biotechnol.* **9**, 1117 (2021).
- [125] D. Basak and S. Deb, Sensitivity of SARS-CoV-2 towards alcohols: Potential for alcohol-related toxicity in humans, *Life* **11**, 1334 (2021).
- [126] R. Villanueva and M. Epstein, Vibrations of Euler's disk, *Phys. Rev. E* **71**, 066609 (2005).
- [127] W. Thomson, XVI. On a self-acting apparatus for multiplying and maintaining electric charges, with applications to illustrate the voltaic theory, *Proc. R. Soc. London* **16**, 67 (1868).

- [128] D. R. Cox, Some statistical methods connected with series of events, *J. Roy. Stat. Soc.* **17**, 129 (1955).
- [129] I. M. Gel'fand and M. L. Tsetlin, Some methods of control for complex systems, *Russian Math. Surveys* **17**, 95 (1962).
- [130] S. Dharmaraja, A. Di Crescenzo, V. Giorno, and A. G. Nobile, A continuous-time Ehrenfest model with catastrophes and its jump-diffusion approximation, *J. Stat. Phys.* **161**, 326 (2015).
- [131] A. G. Pakes, On the age distribution of a Markov chain, *J. Appl. Probab.* **15**, 65 (1978).
- [132] F. B. Hanson and H. C. Tuckwell, Logistic growth with random density independent disasters, *Theoret. Pop. Biol.* **19**, 1 (1981).
- [133] P. J. Brockwell, J. Gani, and S. I. Resnick, Birth, immigration and catastrophe processes, *Adv. Appl. Probab.* **14**, 709 (1982).
- [134] G. Gripenberg, A stationary distribution for the growth of a population subject to random catastrophes, *J. Math. Biol.* **17**, 371 (1983).
- [135] P. J. Brockwell, The extinction time of a birth, death and catastrophe process and of a related diffusion model, *Adv. Appl. Probab.* **17**, 42 (1985).
- [136] P. J. Brockwell, The extinction time of a general birth and death process with catastrophes, *J. Appl. Probab.* **23**, 851 (1986).
- [137] A. G. Pakes, The Markov branching-catastrophe process, *Stochast. Process. Appl.* **23**, 1 (1986).
- [138] A. G. Pakes, Limit theorems for the population size of a birth and death process allowing catastrophes, *J. Math. Biol.* **25**, 307 (1987).
- [139] R. Bartoszyński, W. J. Bühler, W. Chan, and D. K. Pearl, Population processes under the influence of disasters occurring independently of population size, *J. Math. Biol.* **27**, 167 (1989).
- [140] R. Lande, Risks of population extinction from demographic and environmental stochasticity and random catastrophes, *Am. Nat.* **142**, 911 (1993).
- [141] E. G. Kyriakidis, Stationary probabilities for a simple immigration-birth-death process under the influence of total catastrophes, *Stat. Probabil. Lett.* **20**, 239 (1994).
- [142] S. M. Berman and F. Halina, Distributions associated with Markov processes with killing, *Commun. Statistics. Stochast. Models* **12**, 367 (1996).
- [143] G. Bakshi, C. Cao, and Z. Chen, Empirical performance of alternative option pricing models, *J. Finance* **52**, 2003 (1997).
- [144] A. G. Pakes, Killing and resurrection of Markov processes, *Commun. Stat. Stochast. Models* **13**, 255 (1997).
- [145] F. B. Hanson and H. C. Tuckwell, Population growth with randomly distributed jumps, *J. Math. Biol.* **36**, 169 (1997).
- [146] E. A. van Doorn and A. I. Zeifman, Extinction probability in a birth-death process with killing, *J. Appl. Probab.* **42**, 185 (2005).
- [147] A. Di Crescenzo, V. Giorno, A. G. Nobile, and L. M. Ricciardi, A note on birth-death processes with catastrophes, *Statist. Probabil. Lett.* **78**, 2248 (2008).
- [148] R. C. Lewontin and D. Cohen, On population growth in a randomly varying environment, *Proc. Natl. Acad. Sci. USA* **62**, 1056 (1969).
- [149] M. I. G. Daepf, M. J. Hamilton, G. B. West, and L. M. A. Bettencourt, The mortality of companies, *J. R. Soc. Interface* **12**, 20150120 (2015).
- [150] Y. He, S. Burov, R. Metzler, and E. Barkai, Random Timescale Invariant Diffusion and Transport Coefficients, *Phys. Rev. Lett.* **101**, 058101 (2008).
- [151] S. Burov, J.-H. Jeon, R. Metzler, and E. Barkai, Single particle tracking in systems showing anomalous diffusion: The role of weak ergodicity breaking, *Phys. Chem. Chem. Phys.* **13**, 1800 (2011).
- [152] R. Metzler, J.-H. Jeon, A. G. Cherstvy, and E. Barkai, Anomalous diffusion models and their properties: Nonstationarity, nonergodicity, and ageing at the centenary of single particle tracking, *Phys. Chem. Chem. Phys.* **16**, 24128 (2014).
- [153] C. Manzo and M. F. Garcia-Parajo, A review of progress in single particle tracking: From methods to biophysical insights, *Rep. Prog. Phys.* **78**, 124601 (2015).
- [154] L. Boltzmann, Ueber die Eigenschaften monocyclischer und anderer damit verwandter Systeme, *Journal für die reine und angewandte Mathematik* **98**, 68 (1885).
- [155] P. Ehrenfest and T. Ehrenfest, Art. 32. Begriffliche Grundlagen der statistischen Auffassung in der Mechanik, *Encyclopädie der mathematischen Wissenschaften, Band IV: Mechanik, 4. Teilband*, edited by F. Klein and C. Müller (Springer Fachmedien Wiesbaden, 1907–1914), pp. 3–90.
- [156] G. D. Birkhoff, Proof of the ergodic theorem, *Proc. Natl. Acad. Sci. USA* **17**, 656 (1931).
- [157] J. von Neumann, Proof of the quasi-ergodic hypothesis, *Proc. Natl. Acad. Sci. USA* **18**, 70 (1932).
- [158] J. L. Lebowitz and O. Penrose, Modern ergodic theory, *Phys. Today* **26**, 23 (1973).
- [159] O. Penrose, Foundations of statistical mechanics, *Rep. Prog. Phys.* **42**, 1937 (1979).
- [160] C. C. Moore, Ergodic theorem, ergodic theory, and statistical mechanics, *Proc. Natl. Acad. Sci. USA* **112**, 1907 (2015).
- [161] Y. Meroz and I. M. Sokolov, A toolbox for determining subdiffusive mechanisms, *Phys. Rep.* **573**, 1 (2015).
- [162] M. Mangalam and D. G. Kelty-Stephen, Point estimates, Simpson's paradox, and nonergodicity in biological sciences, *Neurosci. Biobehav. Rev.* **125**, 98 (2021).
- [163] P. Palacios, *Ehrenfest and Ehrenfest-Afanassjewa on the Ergodic Hypothesis* (Springer International Publishing, Cham, 2021), pp. 101–120.
- [164] O. Vasicek, An equilibrium characterization of the term structure, *J. Financ. Econ.* **5**, 177 (1977).
- [165] J. C. Cox, J. E. Ingersoll, and S. A. Ross, A theory of the term structure of interest rates, *Econometrica* **53**, 385 (1985).
- [166] J. Hull and A. White, The pricing of options on assets with stochastic volatilities, *J. Finance* **42**, 281 (1987).
- [167] H. Johnson and D. Shanno, Option pricing when the variance is changing, *J. Financ. Quant. Anal.* **22**, 143 (1987).
- [168] E. M. Stein and J. C. Stein, Stock price distributions with stochastic volatility: An analytic approach, *Rev. Financ. Stud.* **4**, 727 (1991).
- [169] S. L. Heston, A closed-form solution for options with stochastic volatility with applications to bond and currency options, *Rev. Financ. Studies* **6**, 327 (1993).
- [170] E. Ghysels, A. C. Harvey, and E. Renault, Stochastic volatility, *Statistical Methods in Finance, Handbook of Statistics*, Vol. 14 (Elsevier Science B.V., Amsterdam, 1996), pp. 119–191.
- [171] J. C. Cox, The constant elasticity of variance option pricing model, *J. Portfolio Manag.* **23**, 15 (1997).

- [172] F. Comte and E. Renault, Long memory in continuous-time stochastic volatility models, *Math. Financ.* **8**, 291 (1998).
- [173] A. A. Dragulescu and V. M. Yakovenko, Probability distribution of returns in the Heston model with stochastic volatility, *Quant. Financ.* **2**, 443 (2002).
- [174] A. Gulisashvili, F. Viens, and X. Zhang, Small-time asymptotics for Gaussian self-similar stochastic volatility models, *Appl. Math. Optim.* **82**, 183 (2020).
- [175] M. V. Chubynsky and G. W. Slater, Diffusing Diffusivity: A Model for Anomalous, Yet Brownian, Diffusion, *Phys. Rev. Lett.* **113**, 098302 (2014).
- [176] A. V. Chechkin, F. Seno, R. Metzler, and I. M. Sokolov, Brownian Yet Non-Gaussian Diffusion: From Superstatistics to Subordination of Diffusing Diffusivities, *Phys. Rev. X* **7**, 021002 (2017).
- [177] W. Wang, F. Seno, I. M. Sokolov, A. V. Chechkin, and R. Metzler, Unexpected crossovers in correlated random-diffusivity processes, *New J. Phys.* **22**, 083041 (2020).
- [178] W. Wang, A. G. Cherstvy, A. V. Chechkin, S. Thapa, F. Seno, X. Liu, and R. Metzler, Fractional Brownian motion with random diffusivity: Emerging residual nonergodicity below the correlation time, *J. Phys. A* **53**, 474001 (2020).
- [179] E. Gurarie, J. J. Anderson, and R. W. Zabel, Continuous models of population-level heterogeneity inform analysis of animal dispersal and migration, *Ecology* **90**, 2233 (2009).
- [180] S. Hapca, J. W. Crawford, and I. M. Young, Anomalous diffusion of heterogeneous populations characterized by normal diffusion at the individual level, *J. R. Soc. Interface* **6**, 111 (2009).
- [181] S. Petrovskii and A. Morozov, Dispersal in a statistically structured population: Fat tails revisited, *Am. Nat.* **173**, 278 (2009).
- [182] I. M. Sokolov, Ito, Stratonovich, Hänggi and all the rest: The thermodynamics of interpretation, *Chem. Phys.* **375**, 359 (2010).
- [183] S. Ritschel, A. G. Cherstvy, and R. Metzler, Universality of delay-time averages for financial time series: Analytical results, computer simulations, and analysis of historical stock-market prices, *J. Phys. Complex.* **2**, 045003 (2021).
- [184] A. G. Cherstvy, D. Vinod, E. Aghion, I. M. Sokolov, and R. Metzler, Scaled geometric Brownian motion features sub- or superexponential ensemble-averaged, but linear time-averaged mean-squared displacements, *Phys. Rev. E* **103**, 062127 (2021).
- [185] A. G. Cherstvy, D. Vinod, E. Aghion, A. V. Chechkin, and R. Metzler, Time averaging, ageing, and delay analysis of financial time series, *New J. Phys.* **19**, 063045 (2017).
- [186] K. G. Wang, Long-time-correlation effects and biased anomalous diffusion, *Phys. Rev. A* **45**, 833 (1992).
- [187] R. Hou, A. G. Cherstvy, R. Metzler, and T. Akimoto, Biased continuous-time random walks for ordinary and equilibrium cases: Facilitation of diffusion, ergodicity breaking and ageing, *Phys. Chem. Chem. Phys.* **20**, 20827 (2018).
- [188] Y. Chen, X. Wang, and W. Deng, Subdiffusion in an external force field, *Phys. Rev. E* **99**, 042125 (2019).
- [189] T. Akimoto and K. Saito, Trace of anomalous diffusion in a biased quenched trap model, *Phys. Rev. E* **101**, 042133 (2020).
- [190] J. Liu, C. Zhang, J.-D. Bao, and X. Chen, Correlated continuous-time random walk in the velocity field: The role of velocity and weak asymptotics, *Soft Matter* **17**, 9786 (2021).
- [191] M. Montero and J. Villarroel, Directed random walk with random restarts: The Sisyphus random walk, *Phys. Rev. E* **94**, 032132 (2016).
- [192] M. Watorek, S. Drozd, J. Kwapien, L. Minati, P. Oswiecimka, and M. Stanuszek, Multiscale characteristics of the emerging global cryptocurrency market, *Phys. Rep.* **901**, 1 (2021).
- [193] D. Boyer and C. Solis-Salas, Random Walks with Preferential Relocations to Places Visited in the Past and Their Application to Biology, *Phys. Rev. Lett.* **112**, 240601 (2014).
- [194] S. N. Majumdar, S. Sabhapandit, and G. Schehr, Random walk with random resetting to the maximum position, *Phys. Rev. E* **92**, 052126 (2015).
- [195] G. M. Schütz and S. Trimper, Elephants can always remember: Exact long-range memory effects in a non-Markovian random walk, *Phys. Rev. E* **70**, 045101(R) (2004).
- [196] M. Antonio Alves da Silva, J. C. Cressoni, G. M. Schütz, G. M. Viswanathan, and S. Trimper, Non-Gaussian propagator for elephant random walks, *Phys. Rev. E* **88**, 022115 (2013).
- [197] E. Baur and J. Bertoin, Elephant random walks and their connection to Pólya-type urns, *Phys. Rev. E* **94**, 052134 (2016).
- [198] A. Adamou and O. Peters, Dynamics of inequality, *Significance* **13**, 32 (2016).
- [199] Ergodicity TV, <https://www.youtube.com/c/ErgodicityTV>.
- [200] V. Stojkoski and M. Karbevski, Ergodicity breaking in wealth dynamics: The case of reallocating geometric Brownian motion, *Phys. Rev. E* **105**, 024107 (2022).
- [201] V. Stojkoski, T. Sandev, L. Basnarkov, L. Kocarev, and R. Metzler, Generalised geometric Brownian motion: Theory and applications to option pricing, *Entropy* **22**, 1432 (2020).
- [202] J.-H. Jeon and R. Metzler, Inequivalence of time and ensemble averages in ergodic systems: Exponential versus power-law relaxation in confinement, *Phys. Rev. E* **85**, 021147 (2012).
- [203] A. G. Cherstvy, A. V. Chechkin, and R. Metzler, Ageing and confinement in non-ergodic heterogeneous diffusion processes, *J. Phys. A* **47**, 485002 (2014).
- [204] A. Godec and R. Metzler, Finite-Time Effects and Ultraweak Ergodicity Breaking in Superdiffusive Dynamics, *Phys. Rev. Lett.* **110**, 020603 (2013).
- [205] Y. Golan and E. Sherman, Resolving mixed mechanisms of protein subdiffusion at the T cell plasma membrane, *Nat. Commun.* **8**, 15851 (2017).
- [206] A. Sabri, X. Xu, D. Krapf, and M. Weiss, Elucidating the Origin of Heterogeneous Anomalous Diffusion in the Cytoplasm of Mammalian Cells, *Phys. Rev. Lett.* **125**, 058101 (2020).
- [207] M. de Carvalho, Mean, what do you mean? *Amer. Stat.* **70**, 270 (2016).
- [208] N. D. Singpurwalla and B. Lai, What does the “mean” really mean? [arXiv:2003.01973](https://arxiv.org/abs/2003.01973).
- [209] A. N. Kolmogorov, *Sur La Notion De La Moyenne* (G. Bardi, tip. della R. Accad. dei Lincei, 1930).
- [210] M. Nagumo, Ueber eine Klasse der Mittelwerte, *Japan. J. Math.* **7**, 71 (1930).
- [211] T. B. L. Kirkwood, Geometric means and measures of dispersion, *Biometrics* **35**, 908 (1979).
- [212] P. A. Samuelson, The “fallacy” of maximizing the geometric mean in long sequences of investing or gambling, *Proc. Natl. Acad. Sci. USA* **68**, 2493 (1971).

- [213] O. Chisini, Sul concetto di media, *Periodico di Matematiche* **2**, 106 (1929).
- [214] R. Graziani and P. Veronese, How to compute a mean? the Chisini approach and its applications, *Amer. Stat.* **63**, 33 (2009).
- [215] Y. Mardoukhi, A. V. Chechkin, and R. Metzler, Spurious ergodicity breaking in normal and fractional Ornstein-Uhlenbeck process, *New J. Phys.* **22**, 073012 (2020).
- [216] K. S. Fa, Attaining ergodicity in a Langevin equation with heterogeneous media, *Chaos, Solitons Fractals* **160**, 112263 (2022).
- [217] A. G. Cherstvy, A. V. Chechkin, and R. Metzler, Anomalous diffusion and ergodicity breaking in heterogeneous diffusion processes, *New J. Phys.* **15**, 083039 (2013).
- [218] A. G. Cherstvy and R. Metzler, Nonergodicity, fluctuations, and criticality in heterogeneous diffusion processes, *Phys. Rev. E* **90**, 012134 (2014).
- [219] S. M. Rytov, Y. A. Kravtsov, and V. I. Tatarskii, *Principles of Statistical Radiophysics 1: Elements of Random Process Theory* (Springer, Heidelberg, 1987).
- [220] W. Deng and E. Barkai, Ergodic properties of fractional Brownian-Langevin motion, *Phys. Rev. E* **79**, 011112 (2009).
- [221] A. G. Cherstvy *et al.*, Ergodicity breaking parameter of geometric Brownian motion (unpublished).
- [222] A. G. Cherstvy, S. Thapa, Y. Mardoukhi, A. V. Chechkin, and R. Metzler, Time averages and their statistical variation for the Ornstein-Uhlenbeck process: Role of initial particle distributions and relaxation to stationarity, *Phys. Rev. E* **98**, 022134 (2018).
- [223] O. Peters, Optimal leverage from non-ergodicity, *Quant. Financ.* **11**, 1593 (2011).
- [224] O. Peters and W. Klein, Ergodicity Breaking in Geometric Brownian Motion, *Phys. Rev. Lett.* **110**, 100603 (2013).
- [225] O. Peters, The ergodicity problem in economics, *Nat. Phys.* **15**, 1216 (2019).
- [226] J. N. Doctor, P. P. Wakker, and T. V. Wang, Economists' views on the ergodicity problem, *Nat. Phys.* **16**, 1168 (2020).
- [227] J.-P. Bouchaud and M. Mézard, Wealth condensation in a simple model of economy, *Physica A* **282**, 536 (2000).
- [228] X. Gabaix, Power laws in economics and finance, *Annu. Rev. Econ.* **1**, 255 (2009).
- [229] B. K. Chakrabarti, A. Chakraborti, S. R. Chakravarty, and A. Chatterjee, *Econophysics of Income and Wealth Distributions* (Cambridge University Press, Cambridge, UK, 2013).
- [230] R. Farmer and J.-P. Bouchaud, *Self-fulfilling prophecies, quasi non-ergodicity and wealth inequality*, Working Paper 28261 (National Bureau of Economic Research, 2020).
- [231] M. Mangalam and D. G. Kelty-Stephen, Ergodic descriptors of nonergodic stochastic processes, [arXiv:2202.01091](https://arxiv.org/abs/2202.01091).
- [232] D. Meder, F. Rabe, T. Morville, K. H. Madsen, M. T. Koudahl, R. J. Dolan, H. R. Siebner, and O. J. Hulme, Ergodicity-breaking reveals time optimal decision making in humans, *PLoS Comput. Biol.* **17**, e1009217 (2021).
- [233] A. G. Cherstvy, H. Safdari, and R. Metzler, Anomalous diffusion, nonergodicity, and ageing for exponentially and logarithmically time-dependent diffusivity: Striking differences for massive versus massless particles, *J. Phys. D* **54**, 195401 (2021).
- [234] J. L. Kelly Jr., A new interpretation of information rate, *Bell Syst. Tech. J.* **35**, 917 (1956).
- [235] L. Breiman, Investment policies for expanding businesses optimal in a long-run sense, *Naval Res. Logist. Quart.* **7**, 647 (1960).
- [236] D. Bernoulli, Specimen theoriae novae de mensura sortis, *Commentarii Academiae Scientiarum Imperialis Petropolitanae, Tomus V [Papers of the Imperial Academy of Sciences in Petersburg, Vol. V]*, **5**, 175 (1738).
- [237] D. Bernoulli, Exposition of a new theory on the measurement of risk, *Econometrica* **22**, 23 (1954).
- [238] S. C. Stearns, Daniel Bernoulli (1738): Evolution and economics under risk, *J. Biosci.* **25**, 221 (2000).
- [239] H. A. Orr, Fitness and its role in evolutionary genetics, *Nat. Rev. Genet.* **10**, 531 (2009).
- [240] O. Rivoire and S. Leibler, The value of information for populations in varying environments, *J. Stat. Phys.* **142**, 1124 (2011).
- [241] T. Neusius, I. M. Sokolov, and J. C. Smith, Subdiffusion in time-averaged, confined random walks, *Phys. Rev. E* **80**, 011109 (2009).
- [242] T. Albers and G. Radons, Exact Results for the Nonergodicity of d -Dimensional Generalized Lévy Walks, *Phys. Rev. Lett.* **120**, 104501 (2018).
- [243] T. Albers and G. Radons, Nonergodicity of d -dimensional generalized Lévy walks and their relation to other space-time coupled models, *Phys. Rev. E* **105**, 014113 (2022).
- [244] M. Schwarzl, A. Godec, and R. Metzler, Quantifying non-ergodicity of anomalous diffusion with higher order moments, *Sci. Rep.* **7**, 3878 (2017).
- [245] F. Thiel and I. M. Sokolov, Weak ergodicity breaking in an anomalous diffusion process of mixed origins, *Phys. Rev. E* **89**, 012136 (2014).
- [246] A. G. Cherstvy, W. Wang, R. Metzler, and I. M. Sokolov, Inertia triggers nonergodicity of fractional Brownian motion, *Phys. Rev. E* **104**, 024115 (2021).
- [247] Y. Chen and X. Wang, Novel anomalous diffusion phenomena of underdamped Langevin equation with random parameters, *New J. Phys.* **23**, 123024 (2021).
- [248] J.-H. Jeon, A. V. Chechkin, and R. Metzler, Scaled Brownian motion: a paradoxical process with a time dependent diffusivity for the description of anomalous diffusion, *Phys. Chem. Chem. Phys.* **16**, 15811 (2014).
- [249] F. Thiel and I. M. Sokolov, Scaled Brownian motion as a mean-field model for continuous-time random walks, *Phys. Rev. E* **89**, 012115 (2014).
- [250] H. Safdari, A. G. Cherstvy, A. V. Chechkin, F. Thiel, I. M. Sokolov, and R. Metzler, Quantifying the non-ergodicity of scaled Brownian motion, *J. Phys. A* **48**, 375002 (2015).
- [251] A. Bodrova, A. V. Chechkin, A. G. Cherstvy, and R. Metzler, Quantifying non-ergodic dynamics of force-free granular gases, *Phys. Chem. Chem. Phys.* **17**, 21791 (2015).
- [252] H. Safdari, A. G. Cherstvy, A. V. Chechkin, A. Bodrova, and R. Metzler, Aging underdamped scaled Brownian motion: Ensemble- and time-averaged particle displacements, nonergodicity, and the failure of the overdamping approximation, *Phys. Rev. E* **95**, 012120 (2017).
- [253] A. S. Bodrova, A. V. Chechkin, A. G. Cherstvy, and R. Metzler, Ultraslow scaled Brownian motion, *New J. Phys.* **17**, 063038 (2015).
- [254] X. Wang, W. Deng, and Y. Chen, Ergodic properties of heterogeneous diffusion processes in a potential well, *J. Chem. Phys.* **150**, 164121 (2019).

- [255] M. A. F. dos Santos and L. M. Junior, Log-normal superstatistics for Brownian particles in a heterogeneous environment, *Physics* **2**, 571 (2020).
- [256] A. G. Cherstvy and R. Metzler, Ergodicity breaking, ageing, and confinement in generalized diffusion processes with position and time dependent diffusivity, *J. Stat. Mech.* (2015) P05010.
- [257] A. G. Cherstvy and R. Metzler, Anomalous diffusion in time-fluctuating non-stationary diffusivity landscapes, *Phys. Chem. Chem. Phys.* **18**, 23840 (2016).
- [258] X. Wang and Y. Chen, Ergodic property of random diffusivity system with trapping events, *Phys. Rev. E* **105**, 014106 (2022).
- [259] W. Wang, A. G. Cherstvy, X. Liu, and R. Metzler, Anomalous diffusion and nonergodicity for heterogeneous diffusion processes with fractional Gaussian noise, *Phys. Rev. E* **102**, 012146 (2020).
- [260] W. Wang, R. Metzler, and A. G. Cherstvy, Anomalous diffusion, aging, and nonergodicity of scaled Brownian motion with fractional Gaussian noise: Overview of related experimental observations and models, *Phys. Chem. Chem. Phys.* **24**, 18482 (2022).
- [261] N. N. Taleb, *The Black Swan: The Impact of the Highly Improbable*, 1st ed. (Random House, New York, NY, 2007).
- [262] T. Lux, Herd behaviour, bubbles and crashes, *Econ. J.* **105**, 881 (1995).
- [263] D. Sornette, Critical market crashes, *Phys. Rep.* **378**, 1 (2003).
- [264] D. Sornette, *Why Stock Markets Crash: Critical Events in Complex Financial Systems* (Princeton University Press, Princeton, NJ, 2017).
- [265] N. Gans, G. Koole, and A. Mandelbaum, Telephone call centers: Tutorial, review, and research prospects, *Manufact. Serv. Oper. Manage.* **5**, 79 (2003).
- [266] L. Brown, N. Gans, A. Mandelbaum, A. Sakov, H. Shen, S. Zeltyn, and L. Zhao, Statistical analysis of a telephone call center, *J. Am. Stat. Assoc.* **100**, 36 (2005).
- [267] S. Gualandi and G. Toscani, Call center service times are log-normal: A Fokker-Planck description, *Math. Models Methods Appl. Sci.* **28**, 1513 (2018).
- [268] John Aitchison and James Alexander Campbell Brown, *The Lognormal Distribution: With Special Reference to Its Uses in Economics* (Cambridge University Press, Cambridge, UK, 1957).
- [269] S. Gualandi and G. Toscani, Human behavior and lognormal distribution: A kinetic description, *Math. Models Methods Appl. Sci.* **29**, 717 (2019).
- [270] M. Mitzenmacher, A brief history of generative models for power law and lognormal distributions, *Internet Math.* **1**, 226 (2004).
- [271] Balasubramaniam Krishna Kumar and Deivasigamani Arivudainambi, Transient solution of an M/M/1 queue with catastrophes, *Comput. Math. Appl.* **40**, 1233 (2000).
- [272] A. Di Crescenzo, V. Giorno, A. G. Nobile, and L. M. Ricciardi, On the M/M/1 queue with catastrophes and its continuous approximation, *Queue. Syst.* **43**, 329 (2003).
- [273] Y.-S. Hsu, P.-C. Chen, and C.-H. Wu, Double-barrier option pricing equations under extended geometric Brownian motion with bankruptcy risk, *Stat. Probabil. Lett.* **184**, 109383 (2022).
- [274] H. Touchette, The large deviation approach to statistical mechanics, *Phys. Rep.* **478**, 1 (2009).
- [275] J. Feng and T. G. Kurtz, *Large Deviations for Stochastic Processes*, Vol. 131 of *Mathematical Surveys and Monographs* (AMS, Providence, RI, 2006).
- [276] P. Embrechts, S. I. Resnick, and G. Samorodnitsky, Extreme value theory as a risk management tool, *North Amer. Actuar. J.* **3**, 30 (1999).
- [277] M. R. Leadbetter, G. Lindgren, and H. Rootzen, *Extremes and Related Properties of Random Sequences and Processes*, Springer Series in Statistics (Springer, New York, 2012).
- [278] J.-Y. Fortin and M. Clusel, Applications of extreme value statistics in physics, *J. Phys. A* **48**, 183001 (2015).
- [279] S. N. Majumdar, A. Pal, and G. Schehr, Extreme value statistics of correlated random variables: A pedagogical review, *Phys. Rep.* **840**, 1 (2020).
- [280] A. Hansen, The three extreme value distributions: An introductory review, *Front. Phys.* **8**, 533 (2020).
- [281] J. Fan, J. Meng, Y. Liu, A. A. Saberi, J. Kurths, and J. Nagler, Universal gap scaling in percolation, *Nat. Phys.* **16**, 455 (2020).
- [282] S. Thapa, A. Wyłomańska, G. Sikora, C. E. Wagner, D. Krapf, H. Kantz, A. V. Chechkin, and R. Metzler, Leveraging large-deviation statistics to decipher the stochastic properties of measured trajectories, *New J. Phys.* **23**, 013008 (2021).
- [283] M. Arutkin, B. Walter, and K. J. Wiese, Extreme events for fractional Brownian motion with drift: Theory and numerical validation, *Phys. Rev. E* **102**, 022102 (2020).
- [284] F. Mori, S. N. Majumdar, and G. Schehr, Distribution of the time of the maximum for stationary processes, *Europhys. Lett.* **135**, 30003 (2021).
- [285] I. Simonsen, M. H. Jensen, and A. Johansen, Optimal investment horizons, *Eur. Phys. J. B* **27**, 583 (2002).
- [286] J. Blackledge and M. Lamphiere, A review of the fractal market hypothesis for trading and market price prediction, *Mathematics* **10**, 117 (2022).
- [287] W. B. Arthur, Foundations of complexity economics, *Nat. Rev. Phys.* **3**, 136 (2021).
- [288] V. Brătian, A.-M. Acu, D. M. Mihaiu, and R.-A. Serban, Geometric Brownian Motion (GBM) of stock indexes and financial market uncertainty in the context of non-crisis and financial crisis scenarios, *Mathematics* **10**, 309 (2022).
- [289] E. Gibney, This physicist-turned-economist is modelling the pandemic's financial fallout, *Nature (London)* **581**, 131 (2020).
- [290] V. Stojkoski, Z. Utkovski, P. Jolakoski, D. Tevdovski, and L. Kocarev, The socio-economic determinants of the coronavirus disease (COVID-19) pandemic, *SSRN Electronic Journal* (2020), retrieved from <https://papers.ssrn.com/sol3/papers.cfm?abstractid=3576037>.